Computer design and optimisation of holographic phase elements.

Sergei Samus

Submitted for the degree of PhD.

Department of Physics

The University of Edinburgh

1995

Abstract.

Computer generated phase holograms are essential components in many modern optical systems including optical parallel computing, image processing, optical interconnects, and optical neural networks. This study enhances the flexibility and power of computer generated holograms by improving the existing algorithms and methods of hologram design and also introducing new algorithms. The main aim was to increase the speed of the design of holograms and their efficiency.

The theoretical basis of the binary and multi-phase holograms is presented in this thesis. The global strategy for the binary and multi-phase holograms design is developed. The methods to increase the computational speed of the design are developed, explained and implemented. This technique is extended to give an iterative design method for an electrically switchable novel liquid crystal fan-out connected hologram using a constrained growing technique that ensures electrical conductivity.

The technique for pseudo four level sandwich holograms is described and extended. Sandwich holograms which are tolerant to misalignment are developed. Various types of structured overlays for sandwich holograms including overlays for error diffusion are developed and described.

A novel algorithm ("missing pixel holograms") is developed for varying the intensity of a small number of output spots by taking combinations of predesigned primitive holograms with additional filling of the non-overlapped areas. The intensities of the output spots can be changed quickly and without further design of the holograms.

The "combined holograms" method for fast design of fully optimised holograms of small fan-out is presented. The design is realised by applying autocorrelation and binarisation operations to the combination of simple gratings. In addition the potential of phase holograms for laser beam scanning and optical interconnects is examined.

Most of the simulations were either implemented as etched binary phase only gratings or as binary phase-only spatial light modulators. The optical results show very good agreement with the simulations.

Finally this thesis introduces the unique software package "Holomaster 1", that implements the visual methods developed in this study. The software package incorporates many methods of hologram design described in the thesis.

To Tania Samus.

Acknowledgements.

I wish to thank to all of those who have contributed to this work. I am very grateful to my supervisor William Hossack for his support and guidance. I appreciate the freedom and peace of mind he gave me during these years.

I would like to thank Peter McOwan whose interest in my work and valuable discussions were very encouraging to me. Many thanks to James Gourlay for his friendship and help.

I also would like to thank Callum Gray who generously lended me his own laser printer for a few months.

Finally, thanks are due to the Science and Engineering Research Council for funding this work.

Most of all I would like to thank my wife Tania whose love and care were the main source of encouragement. I dedicate this thesis to her.

Chapter 1. The theoretical basis of the phase holographic beam splitters.

Introduction.

Holograms designed by a computer allow generation of wavefronts of any desired distribution of phase and intensities [17]. This makes computer generated holograms (CGH) essential components in many optical systems such as optical interconnects [46], neural networks [2,6,70], image processing [42], beam scanning [17] and others. Just as for conventional holograms CGHs can be classified as image holograms, Fourier transform holograms or Fresnel holograms depending on the wavefront recorded in the hologram [36]. My work is devoted to Fourier transform phase holographic elements, mostly laser beam splitters [7,8].

The main feature of holographic beam splitters is to realise an optical fan-out i.e. separate a laser beam into a number of beams of uniform or different intensities so to create a structured pattern of dots in the output plane of the optical system. This

feature makes such holograms indispensable components in the optical systems where redistribution or multiplexing of the optical information is required. The most natural areas for using of holographic beam splitters are laser beam scanning, optical communications, and neural networks.

The two basic set-ups for Fourier holograms are shown on fig. 1.1 and 1.2. The first one is a traditional setup where the collimated beam goes through the hologram and then is Fourier transformed by a lens. The holographic structure is usually highly replicated for better image reconstruction. Experiments show that it is enough to illuminate 8 or more periods of a hologram to obtain a high quality output. This scheme allows one to obtain an efficient and uniform fan-out. The disadvantage of this setup is that the distances between dots of the output pattern are fixed and depend on the parameters of lenses and holograms. This may cause some difficulties when matching the components of a real optical system together. An alternative setup, which is more flexible has the hologram placed behind the lens. By moving the holographic plate along the optical axes we can change the size of the output. The scheme works well as long as a beam covers a large enough area of the holographic plate (8 periods or more).

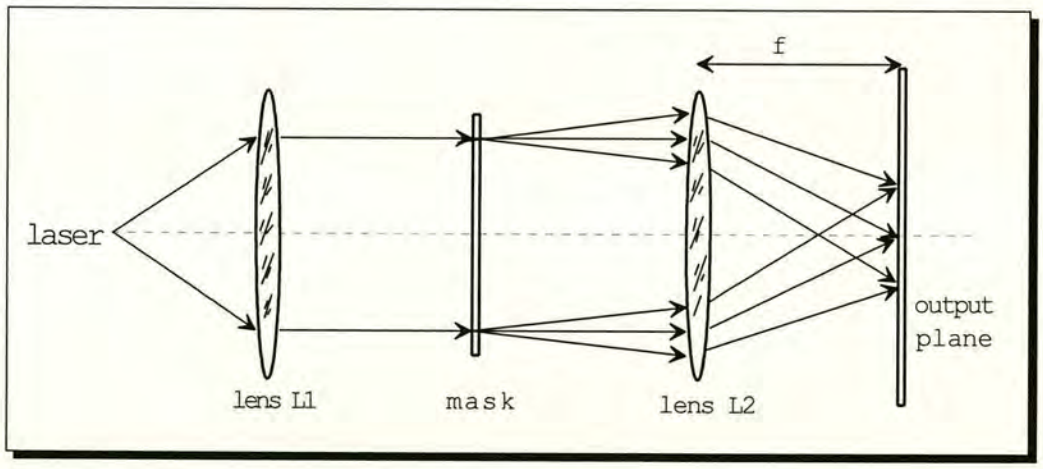

Fig. 1.1 Traditional setup for Fourier holograms

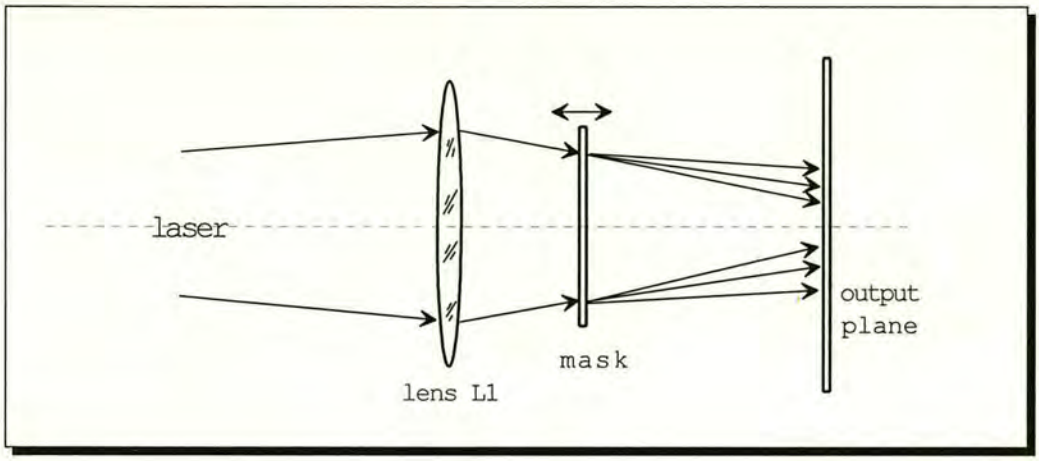

Fig. 1.2 Flexible setup for Fourier holograms.

The conventional methods of CGH design can be divided into two major steps:

- Calculate the complex amplitude of the object wave at the hologram plane. This is usually the Fourier transform of the complex amplitude in the object plane.
- Compute the actual holographic mask using the calculated values.

While it is possible to create amplitude holographic elements with continuous grey scale capabilities or multiple phase elements the area of great interest has always been to create holograms with only two amplitude or phase levels. It makes the fabrication of holographic elements considerably easier. Such holograms are called binary holograms.

Brown and Lohmann detour-phase holograms.

This approach was introduced in 1966 by Brown and Lohmann in their detour-phase holograms [5]. To produce such a hologram, the output format covered by a plotter is divided into NxN cells, which correspond to the NxN

Fig. 1.3 Brown and Lohmann method. Firstly the hologram is sampled into evenly spaced square regions. Then the complex signal is represented in any square as a transparent rectangle with height proportional to amplitude and position proportional to phase.

coefficients of the discrete Fourier transform of the complex amplitude in the object plane. Each complex Fourier coefficient is represented by a rectangular area within a cell whose size corresponds to the modulus of the Fourier coefficient and position within the cell is determined by the phase of the Fourier coefficient. This hologram encoding method is shown on Fig.1.3. Many improvements and variations on this method have been developed but all of them have used the same principles [36, 43].

Kinoform.

One major variant which leads to highly efficient on-axis holograms is the "kinoform" [37]; a smooth phase structure with a theoretical conversion efficiency close to 100%. A kinoform can be fabricated using different methods, for example, in photoresist by laser beam writing lithography [65] or on a photographic plate.

Ignoring the amplitude, it is possible to produce a transmission $e^{i\phi}_{m,n}$ in the cell at position (m, n) in the hologram. The transmission of a bleached photographic plate is given by

$$T_D = e^{i\alpha D}$$

where α is a constant for a given emulsion and processing procedure. Thus to create the desired transmission the following should be done:

Expose to achieve a density $D_{m,n} = \phi_{m,n}/\alpha$ in cell (m,n).

Bleach.

This is a complex process which requires a lot of experience but it allows the achievement of values of very high efficiency. Multilevel or binary phase holographic structures can be viewed as discrete phase kinoforms .

An error diffusion method

An error diffusion or pulse density modulation method, introduced by Hauck and Bryngdahl [18], is an alternative approach to the detour-phase holograms. In this method, the complex amplitude is coded as a real positive transmission function. Each addressable sampling point of the output device is regarded as a single pulse. The brightness of the image is coded in the arrangement of the spatial density of these pulses. The process is illustrated in fig.1.4. This one dimensional representation shows the function to be coded with its spread of transmission values. The value of the function is compared with a threshold value 0.5 here, and the corresponding pixel set to 1 only if the function value is greater than the threshold. The error, that is the difference between the actual function value and the plotted pixel value (0 or 1), is calculated and this value is passed on to the next unprocessed pixel position. The error is added to the function value and this new value compared with the threshold again. The pixel value is determined, as before, by the new

function value relative to the threshold. The error is again calculated dependent on the pixel value set and the process repeated at all pixels in the hologram.

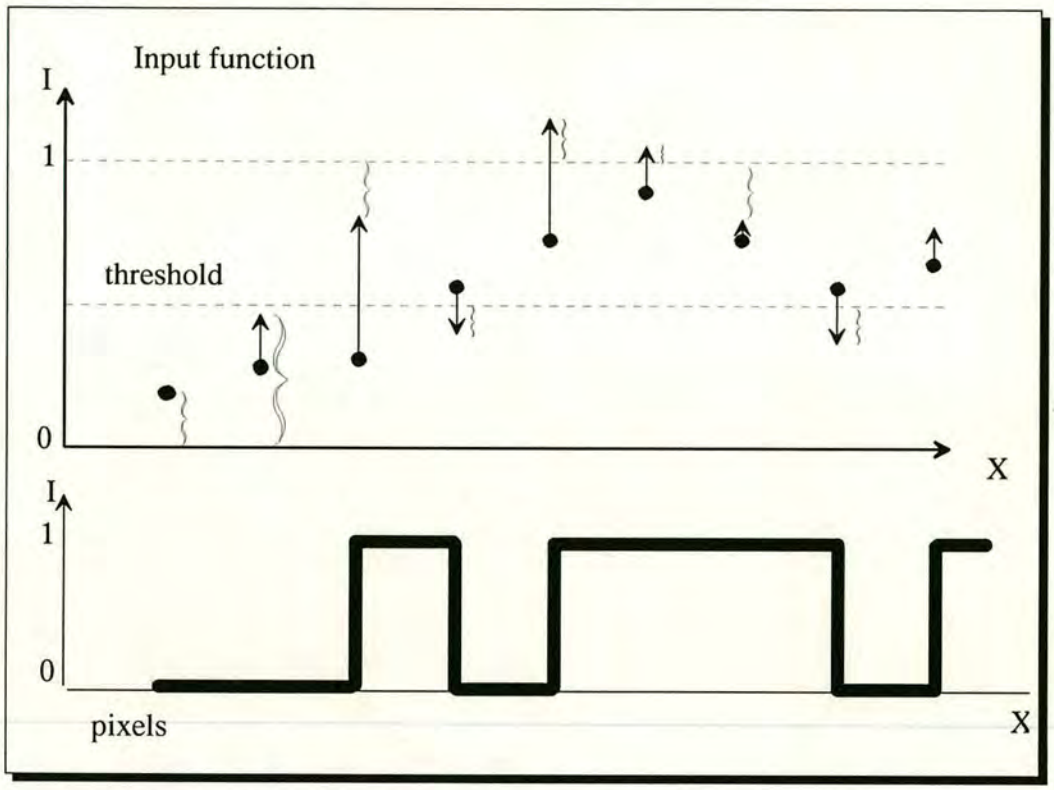

Fig. 1.4 Pulse density modulation coding principles.

This method allows to shift away from desired regions in the reconstruction unavoidable errors obtained during the binarization process. In general, however, this method results in sub-optimal solutions, particularly with respect to diffraction efficiency. Another work [1] has applied optimisation methods to produce a set of diffusion coefficients to implement a more efficient method of distributing the error.

All the hologram design methods derived from the Brown and Lohmann method [1,67] have two big disadvantages: the calculated binary holograms have very low efficiency (less than 10%) and do not work on-axis [36]. Although the pulse density modulation method has several advantages such as redistribution of unwanted replications in the controlled error clouds still the efficiency can only be less than 10% and these holograms can not be implemented on-axis.

Alternative methods of optical fan-out.

Multiple spots can also be produced by large arrays of refractive microlenses [22,25] or Fresnel lenses [11]. There are some advantages in using microlenses. They are not as sensitive to wavelength variations as holographic elements. They also can produce the outputs of different configurations not limited to the rectangular shape. However the arrays of microlenses have some serious disadvantages [7]. The quality of the output is not very high because microlenses cut up the illuminating beam. Usually the distance between the microlens array and the output is restricted by the small focus distance of the lenses. Also there is a significant interference between output spots.

Another approach to the design of CGH is to find optimal binary (or multi- phase) patterns that are not directly representing the complex amplitude of the object in Fourier space but some different solution. How do we find these optimised solutions then if we do not know what they look like? One of the answers is using optimisation algorithms. This approach requires considerable computational power. As computers become more and more powerful the realisation of such tasks is becoming quite realistic.

Dammann gratings.

Dammann gratings are binary phase gratings that can be used to generate a 1-D or 2-D array of equal intensity spots. The idea of using a special type of diffraction grating for this purpose originated with Dammann and Gortler in 1971 [9]. The use of Dammann gratings is based on Fraunhofer diffraction. The amplitude of the diffraction pattern is given mathematically by the Fourier transform of the complex amplitude transmittance of the grating. This pattern is described by a binary function G(x,y). If the output array is separable in the x- and y-directions, g(x,y) is also separable. Therefore, it may be written as the product of two 1-D functions:

$$g(x,y) = g_1(x)g_2(y)$$

A binary phase grating is a periodic structure which has only two different values of phase. This approach helped reduce the problem of finding g(x,y) of the phase-only form

$$g(x, y) = e^{-i\varphi(x,y)} ,$$

the Fourier transform of which yields a given G(u,v) to a one dimensional task.
It is possible to solve this optimisation problem analytically only in the case of a three-beam phase grating [62]. For more complex tasks the optimisation techniques are required . Fig. 1.5 shows a typical Dammann grating for (16x16) fan-out.

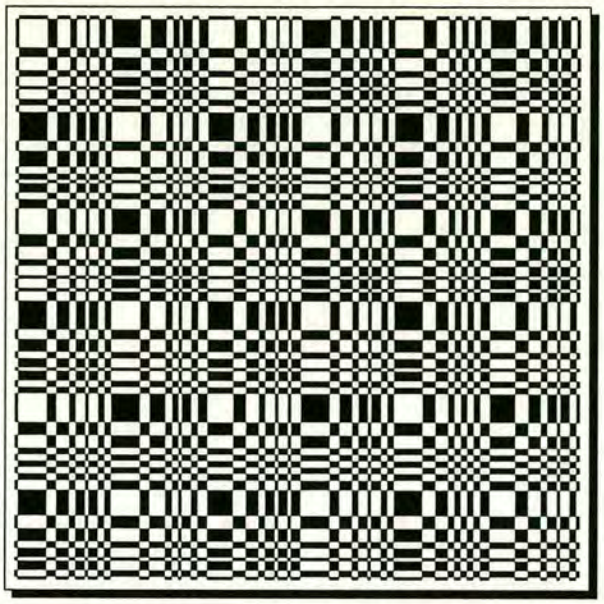

Fig. 1.5 A Dammann grating for 16x16 beam splitter.

The Dammann gratings offer significant increase of efficiency comparing to detour-phase type of holograms. The typical efficiencies obtained for 1-D binary phase Dammann gratings is between 70 and 80%. The remainder of the light is diffracted into the unused orders. When a 2-D grating is formed, by crossing this pattern with itself, the efficiency is squared. It then falls to ~50-65%.

By using the advanced fabrication methods such as controlled etching [56], electron beam lithography [64] or controlled plasma etching of fused silica [43] it is possible to almost avoid the DC spot in the centre of the output. Thus Dammann gratings may be implemented on-axis. However the output is restricted to producing only rectangular arrays of spots which restricts the usage of such holograms.

Iterative reverse methods.

Direct binary search and other techniques.

As we said before, Dammann grating structures have many limitations. In the late 80s many iterative methods for the design of optimised non-separable holograms were reported [26]. In 1987 Seldowitz et al [55] proposed a new technique which they called direct binary search (DBS). This technique included all the elements for the design of optimised phase holograms. This iterative search algorithm minimised an error criterion by directly manipulating the binary hologram and observing the effect on the output plane. The paper contained all main principles for iterative algorithms, which were successfully used later by other authors:

- The hologram is sampled into the small elements. The state of one such element is changed with each iteration.
- In order to reduce the computational complexity, instead of the calculating of the reconstruction with each iteration, only the update in the reconstruction is found.
- The technique of simulated annealing [33] (see appendices) allows it to escape from local optima to reach a global, or nearly global, optimum.
- The error measure is based on only the magnitude of the reconstruction instead of its complex amplitude, as in many applications only the intensity of the reconstructed image is of interest.

They did not achieve optimal results however because of their methods of regulated scanning of a hologram (instead of random scanning) with very small number of iterations.

In 1989 M.Feldman and C.Guest [10] reported their iterative encoding (IDO) method for high-efficiency multiple beam holograms. The method contained an iterative optimisation routine based on simulated annealing to determine the binary phase state of each sampled cell and the value of the phase difference between cells

of different states. The efficiency of their 3x3 hologram was close to optimal (73-74%). However the method worked extremely slowly.

Successful results were also reported by Wyrowski [71] in 1990. His technique for iterative calculation of quantized, blazed phase structures produced very efficient binary and multi-phase level holographic structures. This method suffered from the same drawback of very long time required for the algorithm to converge.

In 1990 Just and Ling suggested using neural networks for binary holograms design [28]. This approach led to nearly optimal solutions but required even more computer resources than other iterative methods.

Two-dimensional surface relief holograms.

The technique proposed by Dames et al in 1991 [7] partly overcame the problem of low computational speed. It was very similar to the DBS with the main difference that scanning of the mask was done randomly and the algorithm run through large number of iterations. Some speed increase was also achieved by using the symmetry features of holograms. This method is now widely used for binary and multiple phase holograms design. As my work is also based on this technique I will discuss it in detail later in chapter 2.

Fast holograms.

Fast holograms is a new approach to the fast design of holograms of small fan-out which we developed during the last year. There are two methods: missing pixel holograms and combined holograms. These two methods are capable of producing optimal or nearly optimal solutions by combining simple predesigned holograms or

gratings which are calculated analytically [48, 52 ,53]. I will describe these methods in chapter 4.

A modified error diffusion method for efficient design of binary holograms.

This method was introduced by Kirk et al in 1992 [29]. This is an alternative approach to inverse design methods. It generalises the error diffusion algorithm by considering a filter for binarization errors in the reconstruction plane as an error diffusion mask in the hologram plane.

The method is capable to produce output of any configuration. The efficiency of the method is slightly less than the efficiency of Dames's surface relief gratings but it can be compared to Dammann gratings (efficiency up to 73.7% has been reported). For small problems the algorithm does not perform as well as inverse techniques. However for large tasks the reverse methods require much greater computer resources. The Dammann gratings and surface relief holograms have some advantage in terms of the ease of fabrication. The holograms designed by error diffusion is characterised by a halftoned pixelated appearance which is difficult to accurately fabricate due to the proximity effect which results in isolated pixels being obliterated.

Objectives.

The objectives of this work were to:

1. Repeat and improve the existing results and methods of hologram design.

2. Develop new types of holograms and new algorithms.
3. Develop principally new fast methods of holograms design for their implementation in totally dynamic systems.
4. Develop a multi-purpose software package to integrate most of the known techniques and implement novel visual methods of holograms design.

Thesis outline.

In chapter 2, I concentrate on different types of holograms based on Dammann gratings [8,9] and the later two-dimensional surface relief approach proposed by Dames et al [7]. I show how simulated annealing technique can be implemented for the design of Dammann gratings to optimise one dimensional solutions. Then I introduce two-dimensional relief holograms and methods to increase their efficiency and speed of design including visual methods. In this chapter I also present a novel type of continuous or connected hologram as ultra fast switching devices. Then follows a brief introduction of four phase holograms, the main feature of which is the ability of producing non symmetrical fan-out. This feature is essential in many applications especially in beam steering and optical interconnects. As four phase holograms are difficult to fabricate and implement in dynamic optical systems, I considered pseudo four phase sandwich technique [67] and developed new types of overlays to implement various desired features of sandwich holograms such as high tolerance to misalignment, better contrast ratio, reconfiguration of output field and total tolerance to misalignment.

Chapter 3 gives a brief overview of fabrication methods of phase holographic beam splitters and then concentrates on the implementation of holograms on an SLM. I review the advantages and disadvantages of SLM devices as a media for hologram display and develop a hypothetical 25% fill factor SLM model to present a technique of spreading the error towards the edges of the replay field. The following subjects of this chapter are laser beam steering and optical interconnects. As these

applications require implementations of dynamic holograms, I present an investigation of the reliability of SLM device as a media for such structures. In the end of chapter 3 I present the results of holographic animations for demonstration purposes.

In chapter 4, I introduce my totally new approach to the design of holograms of limited fan-out that increases the design speed by a factor of 100-1000. I present a missing pixel technique that uses some predesigned holograms to create synthetic holograms for analogue weighted fan-outs and the combined holograms technique for instant design of holograms for outputs of up to 8 dots. These two techniques represent a break-through, in terms of overcoming the two main weaknesses of holographic elements in optical dynamic systems; which are the long computing time and the need for their predesign. Both techniques are approved by optical results obtained with 256x256 SLM.

Chapter 5 presents a unique software package called "Holomaster 1" which I created in order to integrate all the essential techniques of holograms design. This program is capable of making five different types of phase holographic beam splitters. The visual methods described in chapter 2 can only be implemented using software with professionally programmed GUI (Graphical User Interface). The "Holomaster 1" is an example of such software. It also simplifies the predesign of multiple holograms often required for dynamic optical systems.

Finally in the chapter 6, I discuss the possible improvements of fast holograms design and future work in the promising field of dynamic holography.

Chapter 2. Methods and results.

Types of holograms.

Introduction.

In this chapter I present the results of my research in conventional methods of holograms design such as Dammann gratings and surface relief holograms. I also introduce some novel types of holograms, connected and pseudo four phase structures.

Dammann gratings.

For the design of Dammann gratings, I used the approach based on the work of Turunen et al [62]. This is briefly described below. The idea was to use the simulated annealing technique to find one of the acceptable local minima for the transition

points positions. Another improvement was made by developing a technique for minimizing the number of transition points.

A binary phase grating is a periodic structure which has only two different values of phase. The grating and its spectrum are completely determined by the set $\{a_l, b_l\}$, l = 1..,L, of transition point positions of f(x) (see Fig. 2.1).

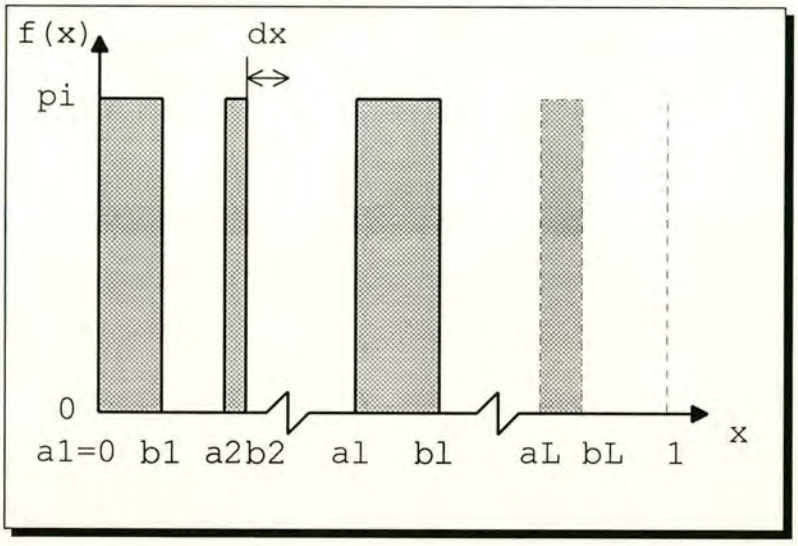

Fig. 2.1 One dimensional Dammann grating

If f(x) is periodic, it can be represented in the form of a Fourier series,

$$f = \sum_{m=-\infty}^{\infty} F(m)\, e^{2\pi i m x}$$

The power spectrum P(m) is defined as

$$P(m) = |F(m)|^2$$

The goal is to find a set {a, b}, l = 1, ..., L, of transition point positions in such a way that the power spectrum P(m), |m| = 0, ..., M, closely approximates some desired power spectrum $\hat{P}(m)$, with good diffraction efficiency P_E.

$$P_E = P(0) + \sum_{m=1}^{M} P(m)$$

If even numbered fan-out is required only the odd orders are included and the even orders, including zeroth order, are set to 0.
The uniformity of the output is calculated as:

$$\eta = \max_{m} \left\{ \left| 1 - \frac{P(m)}{P_E \hat{P}(m)} \right| \right\}$$

The Fourier coefficients of the grating structure are found in terms of the transition point positions:

$$f(0) = \sum_{l=1}^{L} (b_l - a_l),$$

for order m = 0 and

$$F(m) = \frac{1}{2\pi m}[F_R(m) + iF_I(m)]$$

for higher orders. It is possible to solve analytically this optimisation problem only in the case of a three-beam phase grating [62]. For more complex tasks the optimisation techniques are required.

Design technique. Incorporation of simulated annealing into Dammann gratings.

The optimisation method described in [62] works well if we need to find a local minimum, but it does not work for the global minima search. Therefore the routine to find an acceptable local minimum becomes quite a tedious task. In order to compare the results I tried to follow the design technique proposed by Turunnen et al as closely as possible. Therefore, I considered their rather complex cost function as a measure of the progress of optimisation:

$$\Delta C = \alpha\left\{[P(0) - P_E\hat{P}(0)]^2 + 2\sum_{m=1}^{M}[P(m) - P_E\hat{P}(m)]^2\right\} + (1-\alpha)(1-P_E)^2,$$

Where α is a parameter within the range [0, 1]. For the optimisation technique I chose the Fast Simulating Annealing technique (FSA). Simulated annealing is a stochastic strategy for searching the ground state (see appendices). The simulated annealing algorithm to minimise the error proceeds as follows. A transition point is chosen randomly. Then it is randomly moved within the distance between its neighbours. And the resulting change in the cost function , ΔC is calculated. If ΔC reduces, the change is accepted. If it increases, the change is accepted with a probability $\exp(-\Delta C/t)$ where t is some fictious temperature. The temperature is reduced with each computational cycle.

The number of transition points.

Determining the starting number of transition points in practice is difficult. However the optimal number of transition points may be determined during a process of hologram design. I developed a simple technique to do this. It is important to have a large enough number of transition points from the beginning (30 - 40 points being enough typically for a 16x16 fan-out). Then we start the algorithm and let it converge to a steady solution. If a final mask contains very narrow stripes (less than 10% of the average width) it means that there is an excess of transition points. These areas contribute to the increase of the DC spot and make it more difficult to fabricate . The algorithm then deletes these stripes and the appropriate transition points. Then the calculation proceeds with temperature 0. After 1-3 such corrections an optimal solution is usually found.

Results.

The obtained results were approximately 5-10 times more accurate than reported in [62] in terms of uniformity ($\eta \approx 0.05\%$). With the simulated annealing technique it

also became possible to significantly increase the number of output dots (we were able to calculate a Dammann grating for 32x32 fan-out).

The pattern chosen for fabrication was a 16x16 fan-out grating. It was fabricated and measured by A.Stevens [56]. The theoretical diffraction efficiency for the one-dimensional grating was 79.5% compared with an ideal maximum of around 81.1%. The theoretical efficiency of the two-dimensional grating is thus 63.2%, which is typical for such elements. The transition points are shown in table 1.

$0 \rightarrow \pi$ transition	$\pi \rightarrow 0$ transition
0.000000	0.039035
0.139320	0.170173
0.224478	0.245961
0.301181	0.361458
0.474307	0.503317
0.538810	0.638775
0.670051	0.720332
0.740412	0.802904
0.858767	0.974260

Table 1. Binary phase transition points for a cell of a 16x16 fan-out element.

The calculated grating transition was used to form a 32x32 replicated pattern with Cadence Edge VLSI tools and an industry standard x 10 chromium-on-glass mask with a geometric accuracy of ~ $0.25\mu m$. The grating was designed to operate in He-Ne illumination, so a silicon nitride film of thickness 3164 $\mathring{A}$ is necessary to produce the required phase shift on transmission.

The optical transmission of the final hologram was measured at 91.6%. The measured spot intensity uniformity is 1.8%, compared with a theoretical uniformity of 0.44% and the diffraction efficiency is 62.5% compared with a theoretical efficiency of 63.5%. The DC spot is about 1.5 times that of the diffracted elements. This result is consistent with an error of 1% in the phase depth. The optical output for this mask is shown on fig. 2.2. The unused light, as it can be seen from the picture, goes into the DC spot and also produces some high frequency spots.

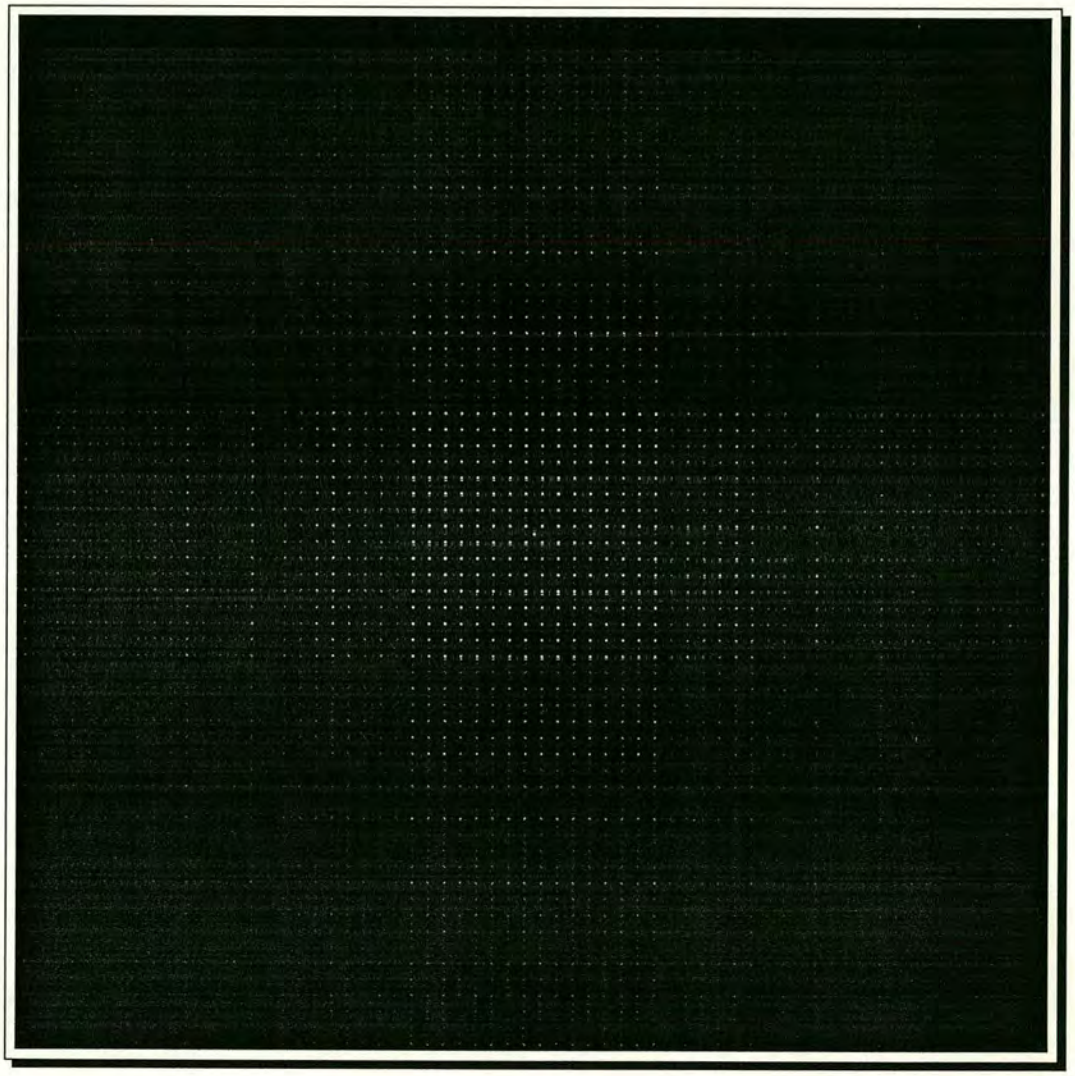

Fig. 2.2 The optical output of a Dammann grating for 16x16 fan-out.

Binary two-dimensional holograms.

Optimal size and the maximum efficiency.

Binary hologram designs with greater diffraction efficiencies than Dammann gratings can be obtained by the use of two-dimensional iterative design algorithms such as simple error reduction and more sophisticated simulated annealing. The hologram is described by *NxN* array of pixels. When designing a hologram it is necessary to select the size of this array. The computational complexity increases linearly with the total number of hologram pixels; it is therefore important that this number is sufficiently small that the algorithm will terminate within a reasonable time. If there are too few pixels however then large errors will be present in the reconstruction. Kirk and Hall [32] found a simple relationship between the reconstruction error and the number of pixels by considering the number of degrees of freedom required for hologram design, these being

$\sigma \geq M^2/4N^2$ - for a binary hologram and

$\sigma \geq \frac{M^2}{(2L-1)N^2}$ - for a multilevel hologram,

where a factor of 2 is removed due to the loss of the inversion symmetry, σ is a standard deviation from the mean intensity, N^2 is the size of the hologram in pixels, M^2 is the number of pixels in the target output. The standard deviation is given by

$$\sigma = \frac{1}{|F_{\max}|^2}\left[\sum_{m,n\in\Omega}\left(\frac{|H_{mn}|^2}{\eta} - |F_{mn}|^2\right)^2\right]^2,$$

where $|F_{max}|^2$ is the maximum intensity in the target function and where the hologram efficiency η is given by

$$\eta = (\sum_{m,n\in\Omega} |H_{mn}|^2)(\sum_{m=0}^{N-1}\sum_{n=0}^{N-1} |H_{mn}|^2)^{-1}$$

These formulae are verified by our experiments. However in practice it is seldom necessary to calculate the optimal size of the designed hologram because the algorithm usually at the beginning starts with the minimal practically possible size for the hologram and when the optimal solution is found, doubles the mask size and repeats all the procedure until the desired deviation value is found . This is discussed in detail later in this chapter.

The diffraction efficiency upper bound.

Consider a phase-only filter. Because of its non-absorbtive nature, it is efficient with regard to the transmission of light energy. Assuming that the filter is a thin diffractive element, its transmission can be described by

$$P(u) = e^{i\varphi(u)}$$

If $P(u)$ is Fourier plane filter, the desired design condition of the response of $P(u)$ is

$$p(x) = \alpha q(x), x \in X,$$

where $q(x)$ is the desired response, $p(x)$ is the response of the filter $P(u)$ (i.e., the inverse Fourier transform), α is a proportionality constant, and X is the region over which the condition is to be satisfied.

According to Wyrowski [70] the upper bound on diffraction efficiency is defined by

$$\eta \le \frac{\left[\int_{-\infty}^{\infty} |Q(u)|du\right]^2}{\int_{-\infty}^{\infty} |Q(u)|^2 du}$$

The function $Q(u)$ is the Fourier transform of $q(x)$. The efficiency bound assumes a zero error within the signal window. Since efficiency is simply a measure of the total

energy within the signal window, which is not the entire image plane, it is possible to achieve efficiencies that are greater than this bound but the results will contain errors.

U. Krackhardt et al [35] devised the expressions for Q(u) for odd and even numbers of target spots and calculated the diffraction efficiency for 1-D binary phase fan-out elements ranging from 2 to 25 output dots. The bound is determined by optimising Wyrowski's expression for the upper bound with respect to the array phase, on efficiency for a phase-only coherent design. For (0, π) - binary-phase elements, it is between 83% and 84%.

Two-dimensional relief holograms.

A multiphase hologram is described by

$$F(k,l) = \frac{1}{N^2} \sum_{m=1}^{N} \sum_{n=1}^{N} f(m,n) \exp(2\pi i \frac{mk+nl}{N})$$

The change in the reconstructed amplitude, $\Delta F(k,l)$, from changing the phase of a single pixel is given by

$$\Delta F(k,l) = \frac{f'(m,n)-f(m,n)}{N^2} \times \exp(-2\pi i \frac{mk+nl}{N}) \quad ,$$

where $f(m,n)$ is the new transmittance of the pixel. In a phase hologram, with p equally spaced phase levels, the $f(m,n)$ takes the value $\exp(2(p-1)i\pi/p)$;
This gives us the following values for different holograms:

- Binary: ± 1.
- Three-phase: $1; -1/2 + i\frac{\sqrt{3}}{2}; -1/2 - i\frac{\sqrt{3}}{2}$,
- Four-phase :± 1 and $\pm i$.

The minimisation is performed with respect to the cost function

$$C_{unif} = \sum_{t.points} (F_{k,l}^2 - T^2)^2 \text{ , for uniform fan-out}$$

$$C_{nonunif} = \sum_{t.points} \frac{(F_{k,l} - T_{k,l})^2}{T_{k,l}^2} \text{ , for non-uniform fan-out.}$$

where $T_{k,l}$ is the amplitude of the target output points and T is the uniform amplitude of the target points.

The minimisation algorithm proceeds as follows. A pixel is chosen at random, its phase is flipped to a new value and the resulting change in the cost function ΔC is calculated. If ΔC reduces, the change is accepted. If not, the change is accepted with a probability $\exp(-\Delta C/t)$, where t is some fictious temperature. The temperature is reduced with each computational cycle. Figure 2.3 shows a typical binary hologram and its Fourier transform.

Since Dames et. al. introduced this technique it became the basic technique for calculation of binary and multi-phase level fan-out holographic elements. The solutions obtained using this method do not usually resemble the distribution of complex output obtained by taking the Fourier transform of the intensity distribution in the object plane. There can exist several different patterns which produce outputs of similar quality and efficiency.

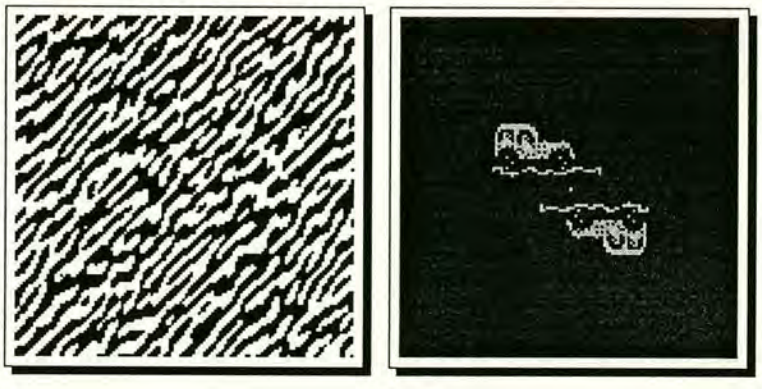

Fig. 2.3 An example of a binary hologram and it's output

General design strategy.

Before we design a hologram it is necessary to analyse the conditions under which it will be used. The quality of the output of the holograph depends on several parameters.

Size of the pixels.

The size of a hologram pixel can vary depending on the material. The best resolution with the pixel size of 0.5-1 μm can be achieved using electron beam lithography or various etching techniques [43, 56]. For photographic methods the pixel size is about 5 μm, and for existing SLMs it is 5-20 μm. The performance of a hologram can be improved by the design methods. It is much easier to fabricate holograms which have hard-clipped appearance, with a clearer divide between different regions, rather than holograms with halftoned (dithered) appearance with many separated single pixels. The proximity effect [61] increases the difficulty of fabrication of halftoned masks particularly by e-beam lithography.

In case of hard-clipped holograms the actual size of continuous areas with the same phase shift is larger than the size of the pixel. For simple masks it can be as large as 15x15 pixels. For complex outputs it is about 2-4 times smaller. So the mask details can be as large as 0.1-0.2 mm. This fact increases the hologram's tolerance to the unwanted diffraction effects and makes the fabrication easier.

Size of the hologram.

The size of holograms we used for experiments varied from 0.2 cm to 2 cm.

Number of periods.

It is always desirable to have at least 4 periods to reduce speckle effects. Experiment shows that eight replications work very well. A combination of high and low frequency terms in the target pattern increases the number of replications for a finally designed hologram. Fig. 2.4(a, b, c) shows three different cases when the

number of replications depends on the initial bandwidth of a defined output.

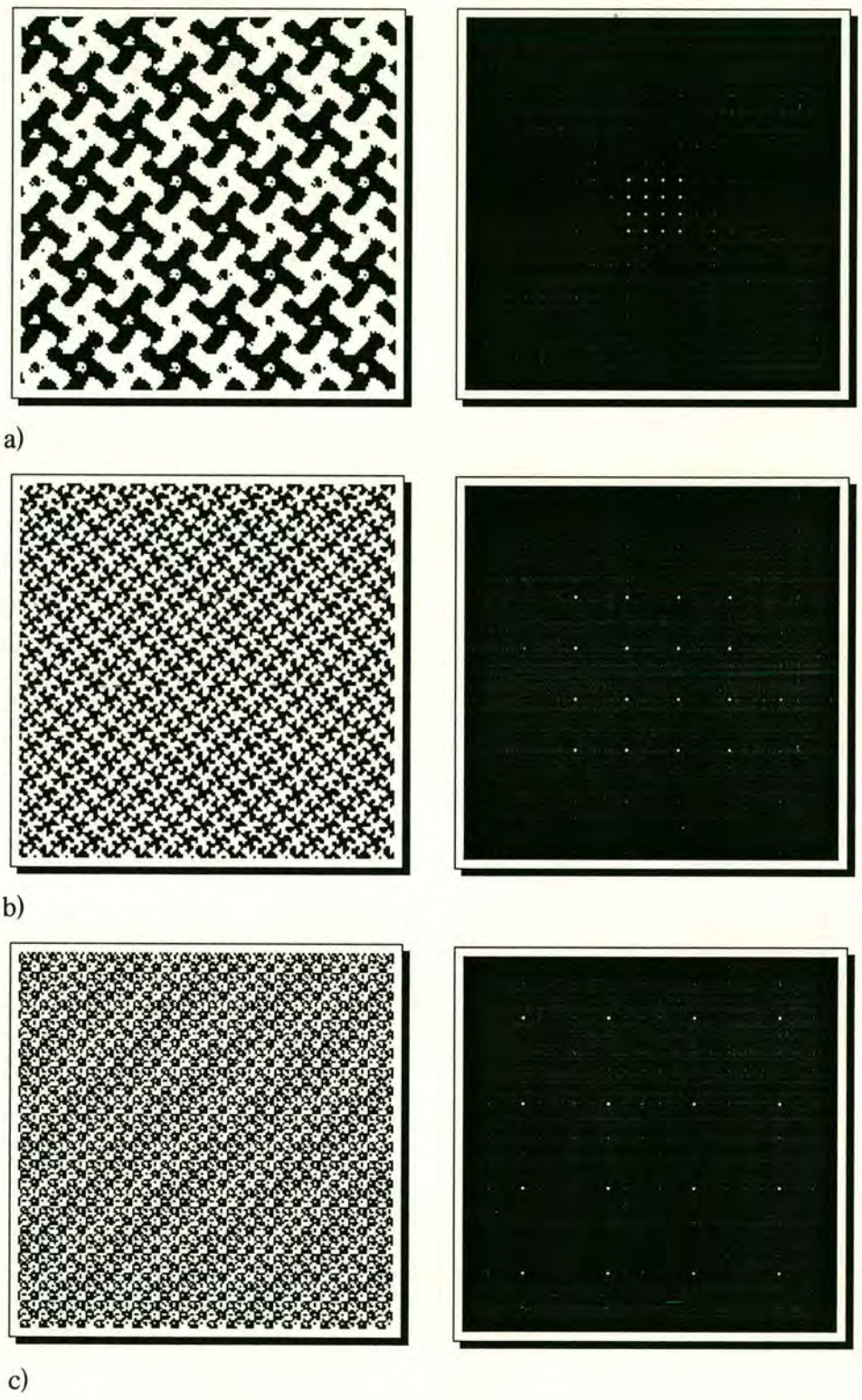

Fig. 2.4. Three examples of masks for a 4x4 fan-outs that are defined differently.

The most effective way to design a hologram is to define a target so that the final holographic pattern consists only of one period. In this case time spent on calculations is minimal and then the obtained structure can be tiled the desired number of times. For holographic media with pixelated structures such as an SLM it is important that the size of a one period of a hologram in pixels is at least 4 times less than the size of the available working area of the device. This ensures at least four replications for the final hologram. The first version of a mask is usually designed to be of a small size. Then the mask is zoomed in, usually doubled. The absolute distances between target spots are not changed. Then the simple error reduction algorithm is applied (with T = 0). The process of increasing the mask size and repeating the error reduction algorithm is repeated until the desired mask size is reached.

Speeding up methods.

The hologram design is a time consuming computational process. The methods to increase the computational speed can be divided into 3 groups:

- **Geometrical.**
- **Algorithmical**
- **Direct.**

The **geometrical methods** take advantage of the symmetrical features of the Fourier transform of binary holograms [44]. The binary holograms are the best to produce a symmetrical fan-out as an NxN array of dots or any other symmetrically shaped outputs. In this case only a half of the target can be defined. The mirror image appears automatically in the replay field of the hologram. This effectively reduces the computational time by half. In order to obtain an asymmetrical fan-out we need to define the whole target. The symmetrical replication of an image starts to play a negative role in this case reducing the efficiency and the size of useful output area to a half. When designing a target have to make sure that two images are not overlapped. We also have to define the target so that the calculated hologram would

consist only of one period. It was found that for a hologram which output is NxM array of dots it is effective to calculate only half of its period. A half of the target is usually defined with 1 pixel space between the output dots (this ensures one period mask) and forces the algorithm to develop only a quarter of the mask, the rest being ignored. After the acceptable solution is found the second and third quadrant of the mask are filled with the inverted images of the first quadrant and the fourth sector is filled with the identical image. This process is illustrated on fig. 2.5.

a) b) c)

Fig. 2.5 (a) - a calculated quarter (half period) of the mask. (b) - mask (a) expanded to the full size (c) its Fourier transform, 4x6 symmetrical fan-out.

This method effectively reduces the calculation time to a quarter. A uniformity of the fan-out can be easily improved by applying, for the short time, an error reduction optimisation to the whole mask.

The **algorithmical methods** involve changes or improvements in the algorithm itself. There are several methods we developed and used in our work:

• ***Using precalculated tables.*** The main formula for update in the Fourier transform with flipping one pixel has the exponential form $\exp\left(-\frac{2\pi i\ (mk+nl)}{N}\right)$ which requires a considerable amount of computer time to calculate. As it repeats with each iteration the time spent on calculation of this part of the formula is very important. In fact it can only take the discrete values which can be found and put in a look- up- table to

avoid expensive calculations and speed up the algorithm. In our experiments we obtained approximately 2-3 times speed increase using this method.

• ***Edge only method.*** The general design strategy as we mentioned above is from small to large. The rough mask is quickly calculated then it is zoomed in to the desired size. Thus the shape of the hologram in general does not change significantly. Under these conditions we can speed up the process significantly at the later stages of the algorithm by considering only the pixels which are located at the edge of the areas of similar phase shift . In case of masks with large areas with similar phase shift this can speed up the process significantly. If a mask has very small details on it, this approach is not that successful because we need some computer time to decide whether the chosen pixel is an edge or an inner pixel.

Let us take a simple approach and approximate an area with the same phase shift as a square with a side of width a.

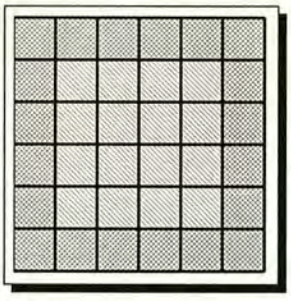

Fig. 2.6. An approximation of an area of the same phase shift by a square of width a.

Then the time T required to scan through the whole square and calculate the cost function for all its pixels is given by:

$$T = t_c * a^2$$

and the time T_{opt} for the optimised process when each pixel is firstly checked if it is inside the area or it is an edge pixel is:

$$T_{opt} = t_s * a^2 + 4t_c(a-1),$$

where t_s is the time required for scanning the pixel and t_c is the time to calculate a cost function of the pixel. We will assume $t_s << t_c$. These two formulas are correct for $a > 1$;

To get an advantage of edge detection technique we must satisfy the condition:

$$t_s < t_c \frac{a^2-4(a-1)}{a^2}$$

and the speed increase can be found from the formula:

$$\frac{T_{opt}}{T} = \frac{t_c a^2}{t_s a^2+4t_c(a-1)}$$

The first chart (see fig. 2.7) shows us how the maximum ratio t_s / t_c depends on the size a. For example for the square area of the size of 7 pixels the time which we spend to decide whether the pixel is an edge or an inner one must be less that two times shorter than the time to calculate the cost function of the same pixel.

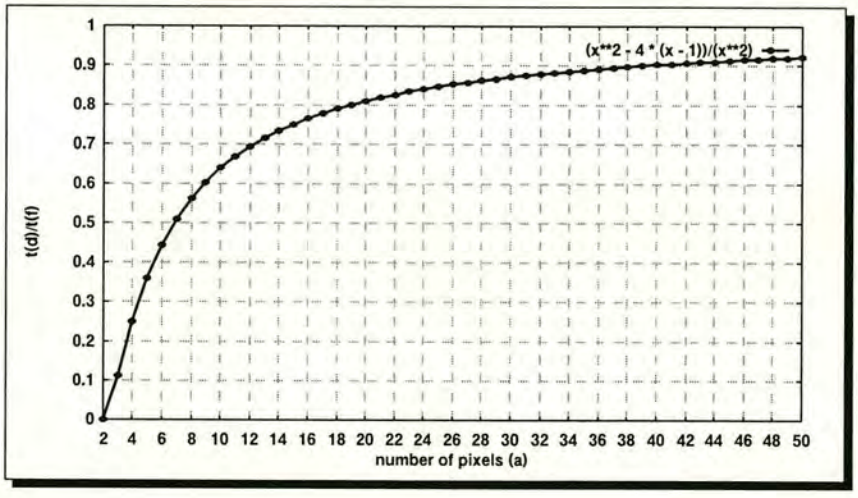

Fig. 2.7 The minimal (t_s / t_c) values versus (a).

The second chart (see fig. 2.8) shows three curves for t_c / t_s values respectively equal 2, 5 and 10. When designing a hologram it is sensible to consider areas of the size of around 4-15 pixels. In case of 10 pixels we can get the calculation speed more than

doubled for the curve number 3. In our practice we were able to achieve a 2-3 times increase in speed using the described method.

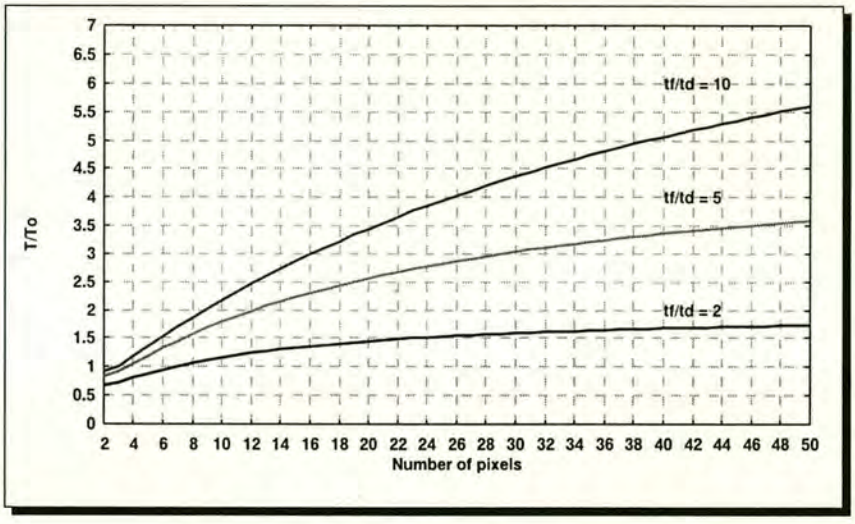

Fig. 2.8 The design speed increase for different values of t_c / t_s (2, 5 and 10) depending on the size a.

The **direct methods** mean using more powerful resources for hologram design. In our case a Sparc Station 2 was used. It is very efficient to use a parallel computer for the design of the holograms for large fan-outs. For all calculations, I used the Connection Machine parallel computer system of Edinburgh University Parallel Computer Centre (EPCC). The following assumptions will be made accordingly to the specifics of this computer. In the data parallel computing model, there are many small processors, each with some associated memory, and all acting under the direction of a serial computer called the front end. Each processor stores the information for one data point in its local memory; all processors can then perform the same operation on all the data points at the same time. This allows us to avoid time consuming loops in the algorithms. In the hologram design such loops exist when calculating $\Delta F_{k,l}$ and the C cost function. With the traditional technique the computational complexity depends on the size of the designed mask N and the number of the target spots M. Fig.2.9 shows schematically the program flow for the hologram design.

Fig. 2.9 the program flow of simulated annealing algorithm for holograms design.

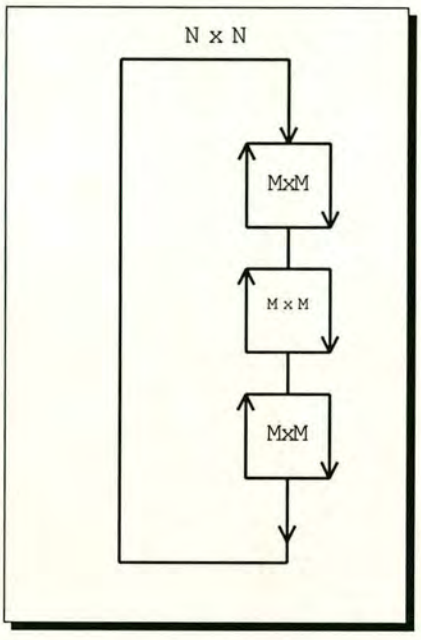

Each cycle of the main loop represents the flipping of one pixel of the designed mask. It is executed the number of times proportional to *NxN* and incorporates three other loops responsible for error calculation, update and copying of the arrays which hold the current and best data. The approximate expression for the total calculation time T is:

$$T = kN^2 t_{ext} M^2 (t_{up} + t_{err} + t_{cp}) / 2 ,$$

where *k* is a coefficient which determines the number of visits of each mask pixel for the algorithm to converge, t_{up} is the time required to the update one point of the current array of target spots, t_{err} is the time needed for calculation of the error in one point of the target, t_{cp} is the time required to copy the updated temporary point into the array which holds best solutions and t_{ext} is the extra time the program spends

outside the inner loops. The division by 2 is explained by the fact that only a half of the mask is used for the calculations. These three loops can be successfully realised on the parallel computer because they operate with arrays which can be calculated in parallel. Unfortunately the main loop must be performed with the traditional methods as we need to flip one pixel at a time. Hence if M<<N the parallel approach does not improve the situation much. On the contrary when M is large, using the parallel computer is very effective. With the restriction for main loop it is impossible to use the whole power of a parallel computer which sometimes can speed up the algorithm significantly.

A source code for a parallel computer differs from a code for a conventional computer. The Connection Machine (CM) of the Edinburgh University can be programmed using special version of Fortran or C* computer languages. C* which I used follows the C syntax but treats arrays differently. There are also many specific keywords and techniques. All this does not make transformation of the C source code into C* easy and intuitive. However once such a transformation is done it is easy to update the existing software. I created a number of programs for the CM to design several types of binary and four-phase level holograms using many of the methods and techniques described in this work. Some of the specific examples of a source code for CM can be found in appendices.

The maximum speed increase for a CM compared to Sparc Station 2 was about 20 times. The actual calculation time for 512x512 mask of 64x64 beam splitter was about 1 hour. This pattern is shown on fig.2.12.

Simulations and optical results.

A large number of binary holograms were designed. Some of them I present below.

Figure 2.10 shows an interesting example of the transformation of a 11x11 fan-out Dammann grating into a binary surface relief hologram by further optimisation of the existing Dammann grating with the temperature equal 0.

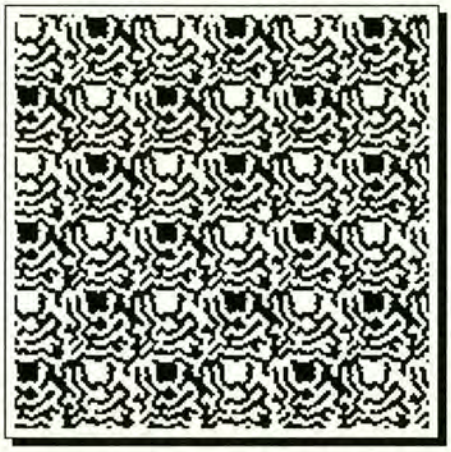

Fig. 2.10 A binary hologram of 11x11 fan-out obtained by using an appropriate Dammann grating as a starting pattern. The iterations were made with temperature 0.

The efficiency of this hologram is about 74% which is better than that of Dammann gratings but worse than the efficiency of properly designed relief holograms. This means that the pattern is stuck at the bottom of a local minimum found during the design of a parent Dammann grating hologram.

The next picture (see fig. 2.11) shows one of the most complex hologram that was designed. This is a hologram for grey-level output of 64x64 pixels. As the output has its symmetrical replication it can be treated as a hologram for 64x128 weighted fan-out. The theoretical efficiency of this hologram was estimated as 82%. The hologram was fabricated by A.Stevens [56]. As it can be seen the optical result is very similar to the computer simulation. The intensity of the DC spot on the fabricated hologram is comparable to the intensities of the output spots.

Fig.2.12 shows a 256x256 pattern for a 64x64 uniform fan-out designed using Connection machine. A total time required to calculate a higher quality version of this mask (512x512) was about 1 hour. The efficiency of the hologram is about 81% and the uniformity about 3.2%.

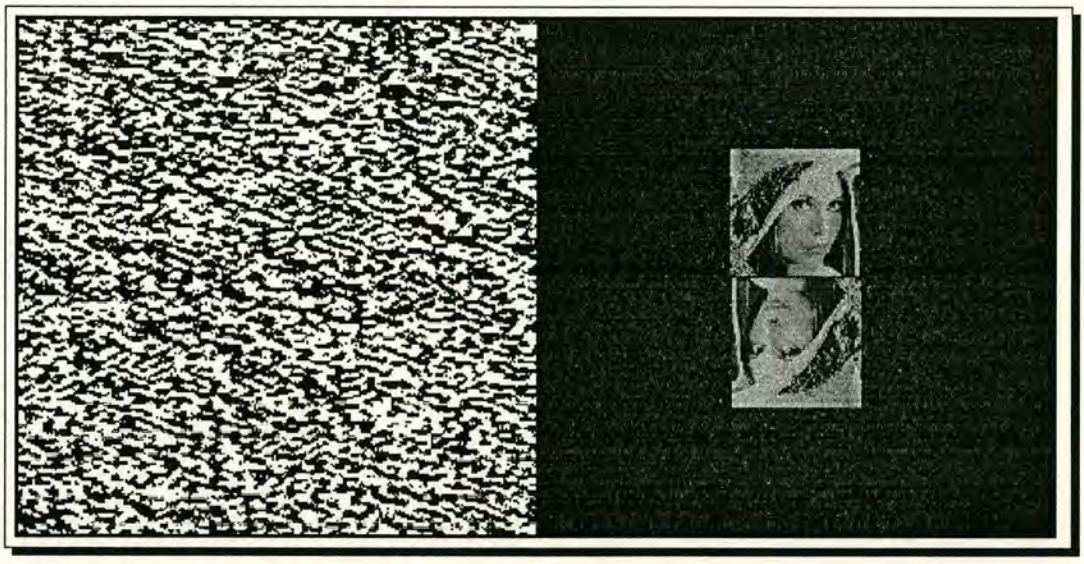

Fig. 2.11. A 256x256 hologram for 64x64 weighted output. The symmetrical replication can be used in case of symmetrical 64x128 weighted fan-out.

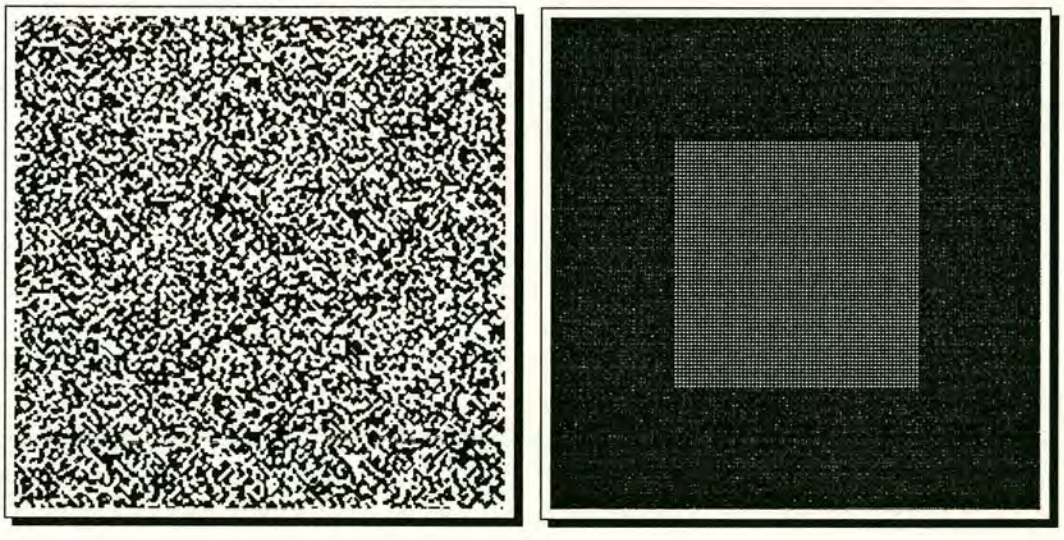

Fig. 2.12 A 256x256 hologram for 64x64 fan-out calculated using parallel computer.

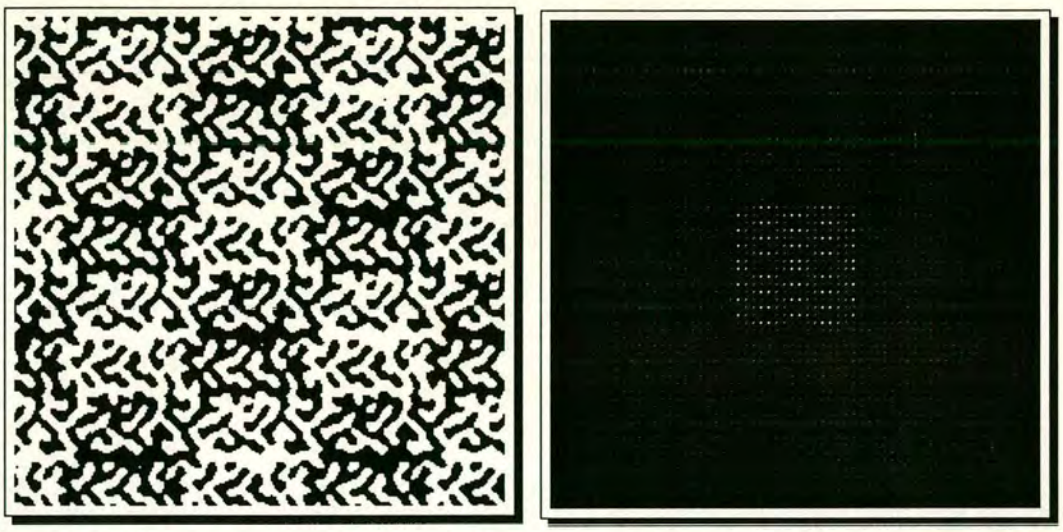

fig. 2.13. A hologram for 16x16 weighted output. The ratio of dots intensities is 1, 2, 4, 8.

fig.2.14. A high quality 512x512 mask for 16x16 fan-out.

Another interesting example is shown on fig.2.13. This is a hologram for a weighted fan-out were the output dots are united in groups of four with intensities values of 1, 2, 4, 8. A configuration of each group or cell is not important and can be easily redefined. By selecting various combinations of 4 pixels in a cell it is possible to obtain 16 different values of intensity. This feature can be used in such applications as neural networks, optical computing or optical interconnects.

Fig. 2.14 shows a high quality mask (size 512x512) for a 16x16 uniform fan-out. This mask is designed to implement statically using high quality fabrication methods such as e-beam lithography, etching or others. The calculated efficiency of this mask is as high as 85% and the uniformity is about 1%.

Connected holograms.

The use of binary holograms may be considerably enhanced if they can be electrically switched. It is possible to make such a device by arranging that the phase modulation is introduced through changing the optical properties of a layer of liquid crystal by applying a spatially modulated electric field. This requires that the phase modulation pattern desired is electrically connected over the spatial extent of the structure. Electrically switchable liquid crystal lenses using patterned electrodes have been reported [41, 68]. The device comprises a liquid crystal cell sandwiched between two glass optical flats. The glass backplane is uniformly coated with a transparent electrode such as indiom tin oxide (ITO). The front plate is patterned, again with ITO, with the required connected structure. On application of a potential between front and back plates the liquid crystal undergoes a spatially variant phase modulation corresponding to the patterned front electrode.

In the switchable lens devices various methods have been used to ensure electrical connectivity in the phase pattern required, from a simple bar connecting the rings in a Fresnel zone plate [68], to using the intrinsic connected structure of a binary Gabor zone plate [41]. Such switchable lenses have applications in imaging, scanner systems, detector protection elements and as optical interconnects.

I will introduce a new approach to the design of CGHs where the electrical connectivity requirement is incorporated as a constraint in the iterative algorithm. Liquid crystal devices fabricated using these holographic electrode patterns have the potential for producing high speed switching and the cell structure allows simple electronic addressing to enable the device. Such predefined fan-out, switchable holograms may have applications in systems where a fixed, predefined, set of optical interconnections are required, such as in optical databases, neural networks, and telecommunications. The speed and easier fabrication may make them more

attractive than fully reconfigurable CGHs, written on spatial light modulators, for some applications.

Requirements and implementation of continuity algorithm.

The design approach is based in the two-dimensional iterative scheme proposed by Dames et al. [7]. As in Dames's scheme the connected structure minimisation is formed by choosing a pixel at random. Then the algorithm tests to see if the pixel should be switched on (set to +1) or off (set to -1) by using the following rules:

1. Switching off the pixel must not break the continuity of the existing pattern. If there are pixels in the neighbourhood of the chosen pixel connected through this pixel it could only be switched off if there exists an alternative connection in a small neighbourhood between them.
2. Switching on the pixel must not lead to appearance of the solitary pixels in the pattern.
3. All the solitary pixels are switched off (this constraint allows non-connected starting patterns).
4. When a pixel suitable for flipping is found the cost function C is calculated. If flipping reduces C the change is accepted. If not, the pixel is flipped back.

The algorithm operates with four-pixel connectivity as shown on fig.2.15, where examples of allowed and forbidden pixel switching is shown. The initial starting pattern can in principle be arbitrary since rule (3) will in general ensure convergence to a connected pattern. In practice, however, good results and rapid convergence have been obtained by starting with a connected pattern, which is then developed by the above iteration. A range of initial structures have been investigated including spirals and frames. All of these initial pattern converge to similar solutions.

The connectivity algorithm is more time-consuming than the algorithm for non-connected masks development due to the process of analysing the neighborhood of the chosen pixel. It is possible to speed up the computational time by defining a look up table (see Appendix A). The neighborhood consists of 8 pixels which can have 2 states. This makes 256 possible combinations. Each of the neighbouring pixels is associated with a position in the 2-byte length binary number. The algorithm analyses the state of the pixel and sets the appropriate bit in the number. The correspondent entrance in the look up table shows whether a central pixel is allowed to be switched off. The process of switching the pixel on is simpler hence we can do the analysis dynamically. For more details see appendix A.

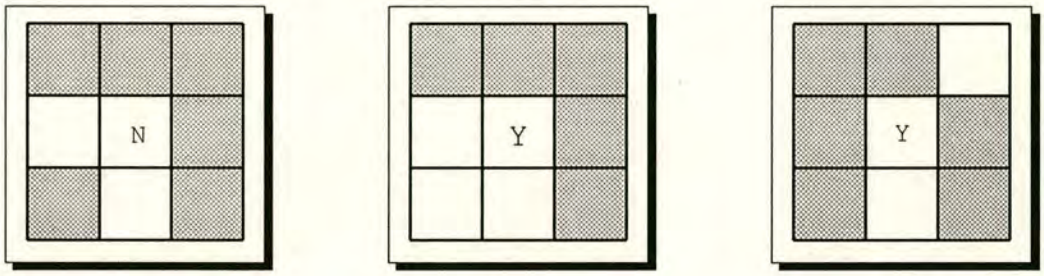

Fig. 2.15. Three examples of pixel transitions. (a) Central pixel is not allowed to be switched off. (b), (c) allowed pixel transitions.

Visual and Other Methods of Design of connected holograms for large fan-outs.

As the connectivity algorithm is restricted by a connectivity constraint the traditional methods of design can guarantee only successful design of structures which produce small number of fan-out spots. We will discuss the methods to optimise the connected holograms design and increase the flexibility of the present algorithm.

The well known simulated annealing method [7] which works well in case of non-connected holograms design, fails for the connected holograms. It creates too many extra connections over the holograms which are impossible to eliminate. In this algorithm an error reduction mechanism is used to find an acceptable local minimum.

The problem of increasing computational time is common for the design of computer generated holograms of large fan-out. In the case of connected holograms this is not the only problem. When a frame is taken as a starting pattern, a connected pattern starts to "grow" from the edges of the mask field towards its centre. In practice it is found that a mask for a relatively large output sometimes might not be developed right to the centre. We might have some black areas which occupy sometimes up to 20% of the hologram (see fig.2.16). One of the explanations of this might be a local minimum which traps the algorithm. Though in such situation we could obtain good uniformity of the output pattern, the efficiency is reduced being diffracted into the zeroth order. It has proved to be rather difficult to automatically control the development of large fan-out holograms . The design process proves to be much more successful if it is visualised and controlled manually. The visual methods of design are successfully used in image processing, ray tracing and other areas. Our approach to visual design of holograms using a specially created software package "Holomaster 1" is explained in chapter 5 and based on examples of development of connected holograms. Firstly we will discuss the methods required to optimise the

design of connected holograms including visual and speeding up methods; secondly we will represent the software tool to realise most of these methods.

Visual methods to optimise the process of developing of connected holograms.

1. Cross copying of quadrants of a symmetrical mask in the early stage of its development to speed up the algorithm and possibly avoid the "black spots" problem. Assuming the mask is symmetrical it is possible to copy its diagonal quadrants into each other with an OR function. This fills the mask and sometimes we get a solution without black areas after 2-3 minutes of the algorithm running. Typically there are still black spots but they are much smaller and more likely to be solved by the algorithm. It is essential to choose the right moment for the cross copying hence to control the process visually. Otherwise many unwanted connections might appear which are impossible to eliminate.

2. Drawing "bridges" across the undeveloped black areas of a mask which is stuck in a local minimum to force the algorithm to continue. This requires a tool similar to a drawing program.

3. Brief changing of the connectivity algorithm to the discontinuous one to plant a group of pixels in the undeveloped area. This needs to be visually controlled in order to minimise the number of disconnected areas. Then we need to apply the connectivity algorithm again. This is a very effective measure but it almost always causes a few breaks in the continuity of the designed pattern. We need to have the facilities to check whether a mask is still connected or not by implementing the floodfill checking function. Then we can manually draw narrow bridges between separated areas using a drawing tool.

4. Minimisation of number of connections on a final mask to increase the efficiency and decrease the intensity of the DC spot. This again requires a drawing tool and a

special floodfill feature to control the continuity of the pattern. Note that usually the holograms are fabricated as multi replicated versions of the originally designed mask. Therefore the floodfill program must work in a slightly different way than those in drawing packages, and assume that the mask is tiled.
These four methods give the best results when used together. It should be noted that in the case of a not fully symmetrical output pattern, method 1 can not be applied. Let us take a look at the figure 2.16 which illustrates how methods 2 and 3 work together.

a)A 64x64 mask after being developed for approx. 2 minutes is stuck in a local minimum. Two black areas in the centre are clearly seen. The uniformity of the simulated output can be calculated as, $unif. = \frac{|\Delta I_{\max}|}{I}$, where I is the required uniform intensity and ΔI is the maximum difference between I and the intensities of the output spots. The efficiency is represented by $eff. = \sum_{i=1}^{n} I_i$ where n is number of output spots. For our mask the uniformity and efficiency values are: unif.=19.7%, eff.= 75%.

b) The same mask with random bridges drawn across the undeveloped areas.

c) This mask is changed by the algorithm which successfully broke through the local minimum (unif.=13.8%, eff.=75%).

d) The size of the mask is increased to 128x128 pixels and the algorithm improves it (2.2%, 80.1%).

e) The same step is applied to a 256x256 size mask (unif.=2.64%, eff.=81.96%). Quite a large number of the connections can be seen. One may guess that there are probably too many connections, but it is extremely difficult for the algorithm to eliminate some of them at this stage. With a facility of the program we can carefully remove extra connections constantly checking the continuity of the pattern with the floodfill feature of the program.

f) Finally we obtained a pattern with a few connections (unif.=2.28%, eff.=83.2%).

g) We applied the non-connectivity algorithm to a final connected pattern in order to compare the results.(unif.=2.6%, eff.=84.7%).

Fig. 2.16 (a, b, c, d, e, f). A process of development of a connected hologram of large fan-out.

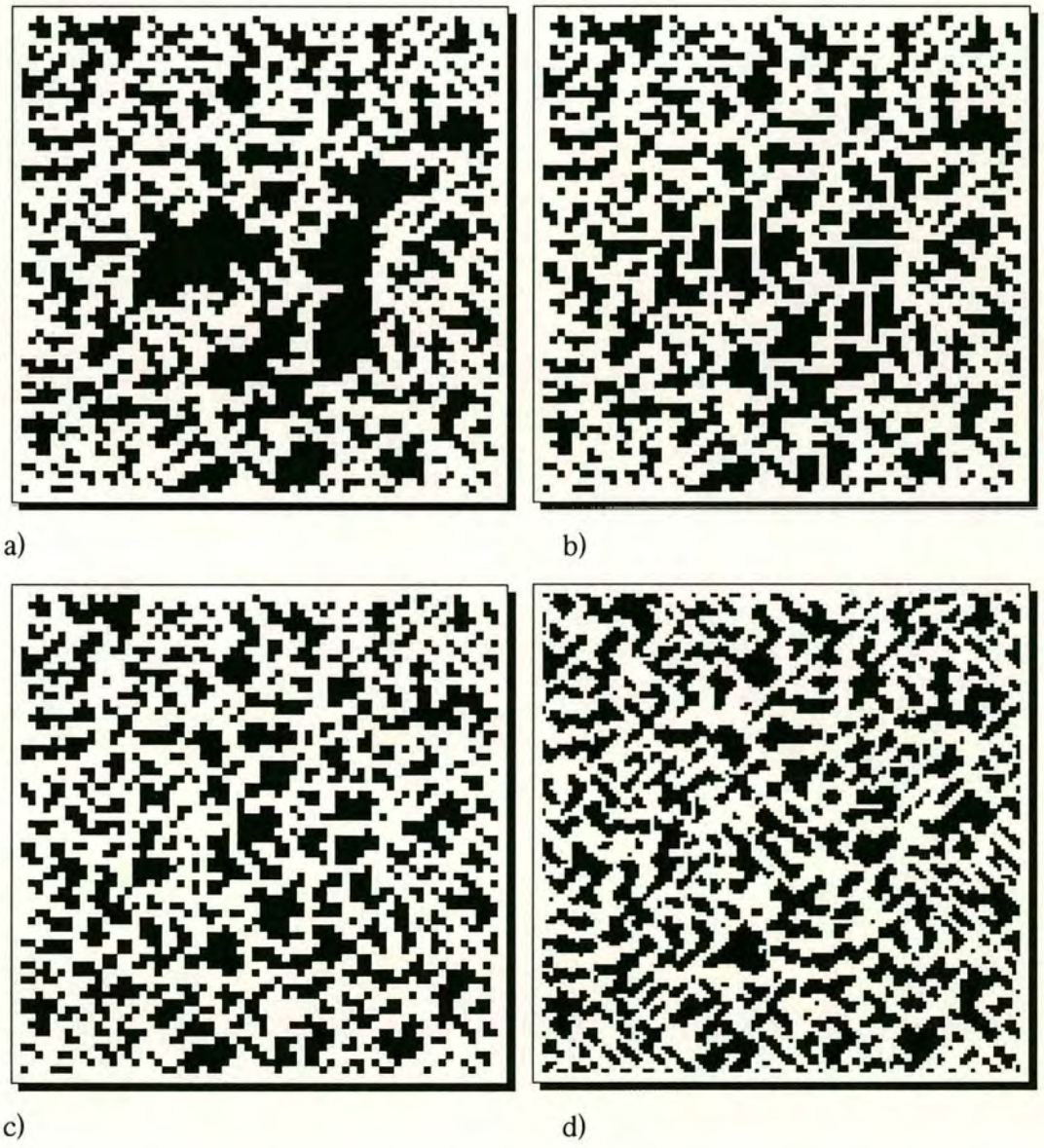

a) b)

c) d)

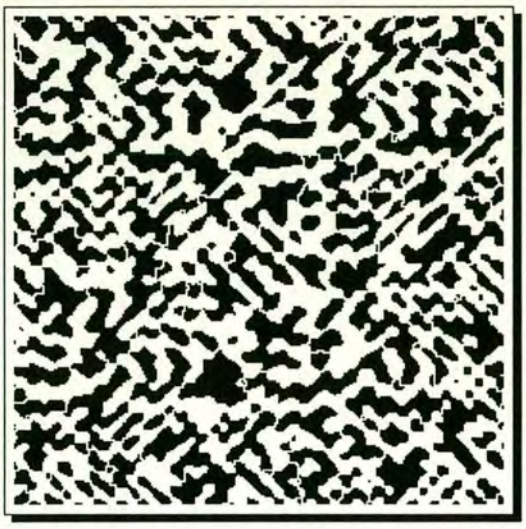

e)

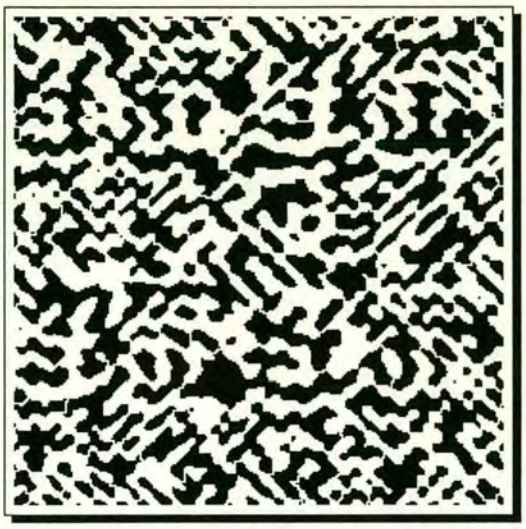

f)

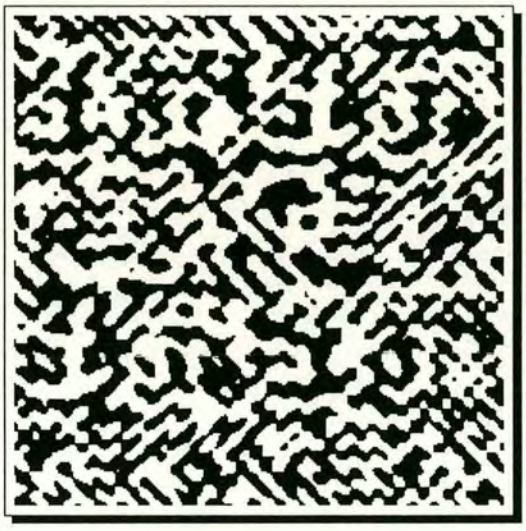

g)

h)

a) A first "draft". 64x64 mask.

b) Bridges across undeveloped areas.

c) Optimised mask b.

d) Zoomed out (128x128) and optimised mask c.

e) Zoomed out (256x256) and optimised mask d.

f) Optimised mask (e) after manual reduction of number of connections.

g) Non-connected mask for comparison with f.

h) An output of mask f.

The actual output is shown on fig. 2.16(h). The pattern consists of 384 uniform dots. Usually it is a good idea to take a start pattern of the hologram which is a frame. The algorithm however allows us to start virtually from any pattern even from an arbitrary disconnected one. When the algorithm runs for a long enough period all the single pixels and disconnected areas eventually disappear. Starting from a random pattern has its advantages and disadvantages. Usually there are no blank areas in the final solution pattern and we do not have to apply the technique described earlier. As a rule the final mask has much more connections than is necessary. These extra connections contribute into the additional error clouds around the DC spot and into DC spot itself. Of course we might as well try to delete a fair number of connections each time checking the pattern for continuity and then apply the algorithm again. This often gives excellent results but can take a considerable time to do.

Decision delay method.

Kiselyov et al [34] proposed to increase the number of rearrangements for one fluctuation in the simulated annealing algorithm. According to their version, a random fluctuation of the cost function $\Delta T_p = \theta \ln 1/p$ is specified where p is a random number in the range (0,1). Then a few random rearrangements are performed. A rearrangement is accepted if a change of the cost function ΔT satisfies the constraint $\Delta T \leq \Delta T_p$. The main difference of this algorithm is that for each fluctuation ΔT_p a few (1,2,...,n) rearrangements rather than one are checked. It was interesting to implement a variation of this idea when designing connected holograms with a simpler error reduction mechanism. We wanted to check whether this could help us to find a better local minimum . In case of connected holograms the technique did not prove to be successful. Even though it took a long time for algorithm to converge to a good solution (3 - 5 times longer) the efficiency and uniformity were on the same level as those in case of the usual error reduction algorithm.

Speeding up methods for holograms design.

There are several ways to speed up the binary hologram design process which we discussed at the beginning of this chapter. All of these methods can be used for the calculation of the connected holograms too.

We can also add one more geometrical method for connected holograms that produce symmetrical output in both dimensions. Consider the calculation of a hologram starting from a frame. As the algorithm proceeds the mask is filled starting from the edges towards its centre. I showed earlier that it is common to design only a quarter of the hologram for 2-d symmetrical outputs. This method does not work for connected structures because of the continuity constraint. However, when one half of the mask is filled, the information about the whole structure becomes available and can be obtained by copying the quadrants of the mask into each other. After this procedure, we can continue the design taking care of a few possible broken connections.

The visual methods are supported by our software package called Holomaster 1 which is described in chapter 6. With Holomaster, the process of simulated annealing can be observed and controlled dynamically as the design process is running. This helps significantly when implementing method 4. We can visually control filling in the blank areas while temporarily switching to the non-connectivity algorithm. With the built in drawing program it is easy to draw and delete bridges. It helps us also to examine a mask for continuity using the floodfill facility. A user can move images between drawing window, mask window and target window via the program's graphics clipboard which also has its own window. It is also possible to load and store images with the file window. It is easy to change simulated annealing parameters with two scale bars as the program is running. We can also switch between normal and "edge" algorithms pressing a toggle button in the process panel.

It is also easy to design required target patterns with a drawing program and preview the actual symmetrical output of the future hologram. The real strength of Holomaster is that all the design techniques and parameters and even holograms and targets can be changed dynamically during the design process.

Four phase holograms

The four phase hologram design technique is similar to the one for binary structures. The main advantage of using multi-phase holograms is the absence of a conjugate image in the output field area. A four-phase hologram can be described by a formula

$$F(k,l) = \frac{1}{N^2} \sum_{m=1}^{N} \sum_{n=1}^{N} f(m,n) e^{2\pi i(mk+nl)/N}$$

The possible four values of a pixel transmittance f(m,n) are: ± 1 and $\pm i$. Since the pixels of the hologram can be flipped into any of 4-phase states compared to 2 for binary holograms the computational time is two times longer.

A possible fabrication method for four-phase holograms is described in [7] involves electron beam lithography and subsequent dry etching of the pattern into four phase levels on silica glass substrates. It is also possible to implement these holograms dynamically on two SLMs, but such an optical system would be very expensive and difficult to align due to diffraction effects. The surfaces of the SLMs should be put as close as possible to each other to achieve acceptable results which is technologically a difficult task. In order to successfully implement a fully dynamic four-phase level hologram and benefit from its high performance and the absence of a secondary image it is possibly needed to create a new type of 2-layered SLM device.

Pseudo four phase (sandwich) holograms.

If the optical system requires asymmetrical fan-out then multi-phase holograms must be utilised. Static multi-phase holograms have been produced by controlled etching, but, at present there are no multi-phase spatial light modulators available for direct dynamic hologram implementation. A technique for pseudo-four level phase

holograms by using a sandwich structure of a random binary fixed hologram overlaying a binary spatial light modulator has been proposed by Wilkinson [67]. The principle of a sandwich hologram is shown on fig.2.17.

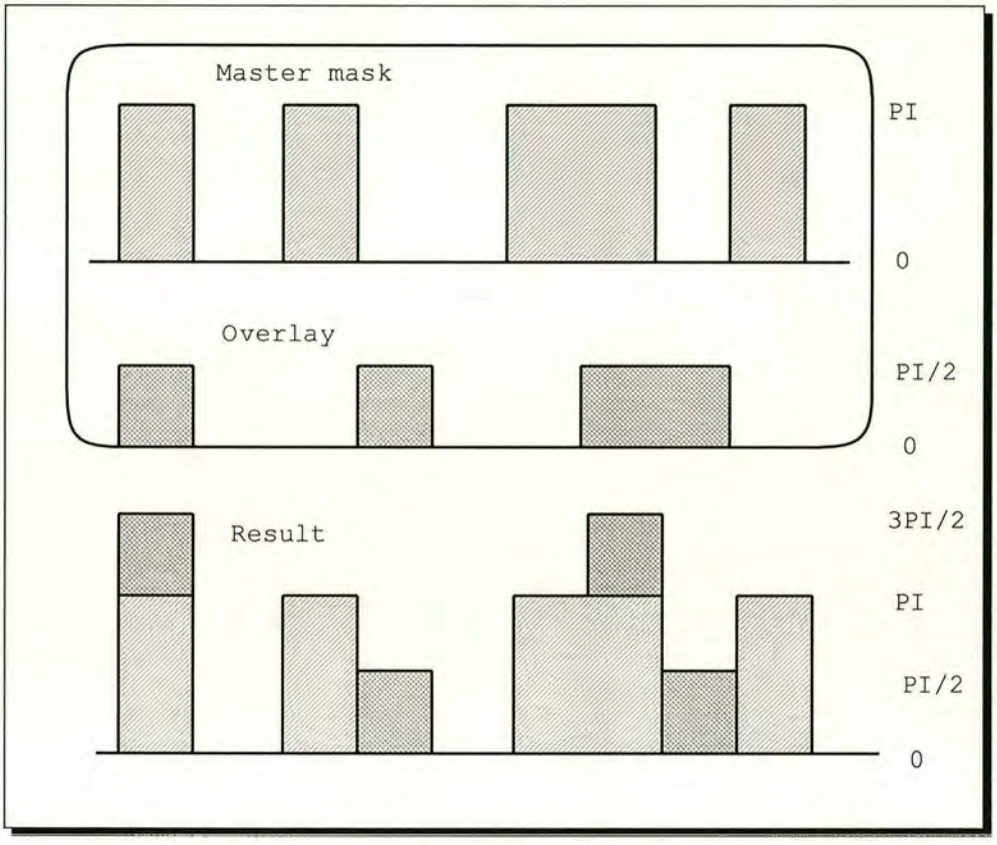

Fig. 2.17 A sandwich concept.

A binary master mask usually has 0 and π phase levels and an overlay has 0 and $\pi/2$. The combination of these two masks produces pseudo four phase structure with phase levels of $0, \pi, \pi/2, 3\pi/2$.

The overlay is usually a static hologram but may also be dynamic, being implemented by a second SLM tuned to 0 and π phase shifts. There can be two different approaches to the design technique of a sandwich hologram. The first one is to design a four-phase level single hologram [67] and then split it into two. This method works well in the fully dynamic system. The theoretical efficiency in the ideally implemented system is as high as with the original four-phase hologram. In case of a dynamic-static pair this method is not preferred because it restricts its

usage. The dynamic features of the SLM can not be used efficiently because it is not possible to use different base masks with one overlay.

The other method is to design the base mask in a similar way as for binary holograms but in respect to a predefined overlay pattern. In this case the efficiency of a sandwich hologram is generally reduced to the level of its binary analogue. Putting the permanent overlay on top of an SLM restricts its universality. The SLM cannot be used for any other purposes in this case.

A detachable device is much more flexible, allowing an SLM to be used with different overlays or without them for other tasks. The main obstacle to the realisation of such system is the difficulty of alignment. Obviously the smaller the overlay's details are, the more difficult the alignment is. The minimum size of the continuous area with uniform phase transmission of a sandwich hologram is defined by the smallest size of the area of either base mask or an overlay. In the case of reference [67] the smallest details will be comparable with the pixel size of the overlay i.e. 5-20 μm. The distance between a base and an overlay also becomes quite important in this case due to diffraction effects.

The diffracted amplitude for a sandwich hologram is given by

$$F(k,l) = \frac{1}{N^2} \sum_{m=1}^{N} \sum_{n=1}^{N} (b(m,n) + o(m,n)) \exp(2\pi i \frac{mk+nl}{N}) \ ,$$

where b(m,n) is the transmittance of the pixel (m,n) of the base mask which takes values ±1 and o(m,n) is the transmittance of the pixel (m,n) of the overlay mask which can take values 1, i.

The change in the reconstructed image, $\Delta F(k,l)$, from changing the phase of a single pixel of the base mask is given by

$$\Delta F(k,l) = \frac{b'(m,n)+o(m,n)-b(m,n)}{N^2} \times \exp(-2\pi i \frac{mk+nl}{N}),$$

where b'(m,n) is the new transmittance of the pixel of the base mask. The minimisation is performed with respect to the cost function for uniform output:

$$C = \sum_{\text{target points}} (F_{k,l}^2 - T^2)^2,$$

where T is the amplitude of the target points. The algorithms proceeds as follows:
A single pixel of the base mask is flipped. The cost function C is calculated. If flipping reduces C the change is accepted. If not, the pixel is flipped back.

Large area random overlays.

Fig.2.18(a) and fig.2.19(a) demonstrate a four-phase and a binary holograms of the same object. The symmetrical and asymmetrical outputs of the holograms are shown on Fig.2.18(b) and fig.2.19(b).

Fig. 2.20(b) shows a totally random overlay. Fig. 2.20(a) shows a base mask calculated in respect of this overlay. Their sandwich and the Fourier transform are shown on Fig.2.20(d) and 2.20(e) respectively. Fig.2.21 shows an alternative solution. A high frequency random overlay is replaced by a random overlay that consist of much larger areas of uniform phase shifts. This is equivalent to having the smallest detail of the overlay mask large comparing to the pixel spacing on the SLM. The random overlay was designed on 16x16 rectangle and then was zoomed in to the required size (64x64).

The outputs 2.20(e) and 2.21(e) are of comparable quality. The contrast on pictures is reduced in order to demonstrate the development of error clouds around the image. The quality of the output in the case of the totally random overlay is slightly better, however, what is really important is that this sandwich 2.21(d) is very resistant to the movement of any of its component.

The misalignment of the base mask and overlay is simulated by shifting both overlays by one (two) pixel down and one (two) pixel right. As soon as the shift happens the sandwich 2.22(a) with pixelated random overlay loses the asymmetrical feature of its replay. However, the sandwich 6a with large areas random overlay is quite stable even with a 2-pixel shift, as we can see on fig.2.23 and fig.2.24. Larger shifts give a considerable error.

The large area overlays approach also gives us another possibility. Instead of designing the random overlay first and then fabricating it, it is also possible to fabricate an overlay with arbitrary size of the pixels (areas) and then design the mask in respect to it. The pixel size of the overlay does not have to be the same as the pixel size of the base mask.

Fig. 2.18. Four phase hologram for letter P.

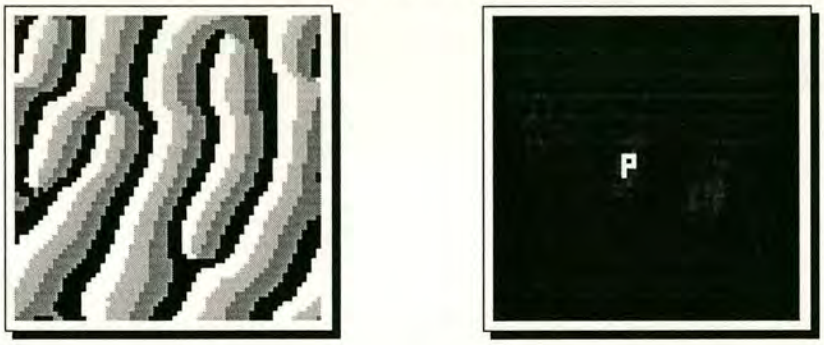

a) Four phase mask and *b) its Fourier transform.*

Fig. 2.19. A binary hologram of for the same output.

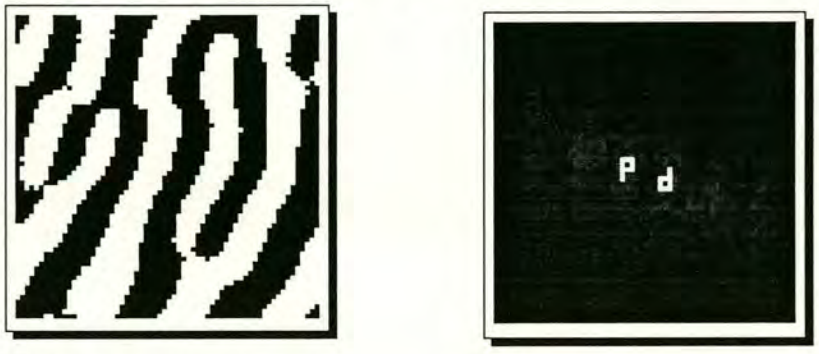

a) Binary mask and *b) its Fourier transform*

Fig 2.20. Pseudo four-phase sandwich.

a) base mask *b) random overlay and* *c) its Fourier transform*

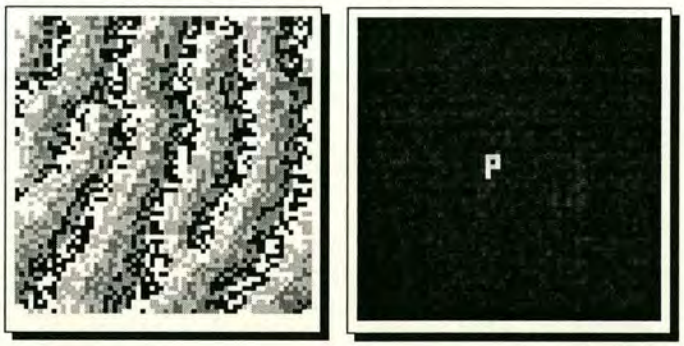

d) The "sandwich" and *e) its Fourier transform*

Fig. 2.21 Pseudo four-phase "sandwich" with large areas overlay.

a) base mask *b) overlay and* *c) its Fourier transform*

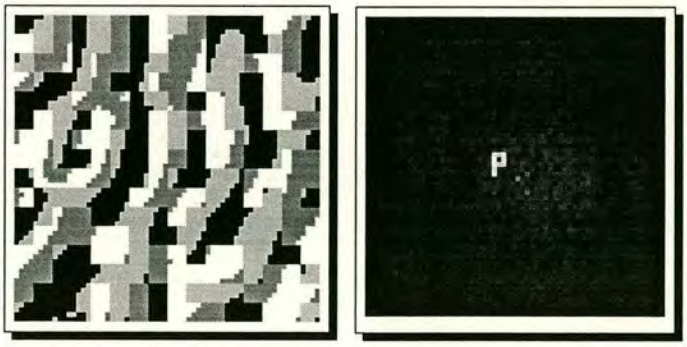

d) the "sandwich" and *e) its Fourier transform*

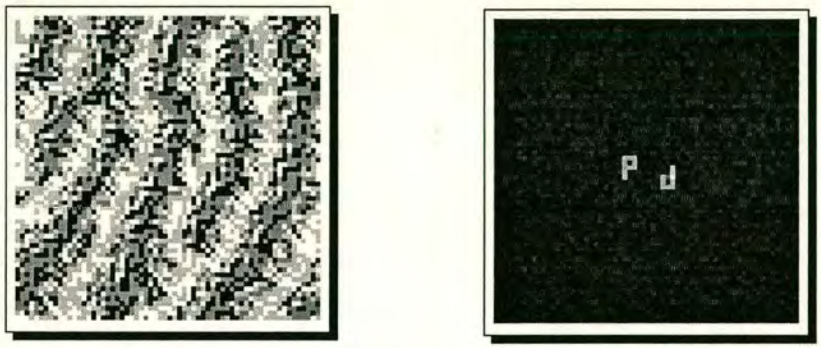

Fig 2.22 One pixel shifted normal "sandwich" and its FT. The symmetry effectively comes back.

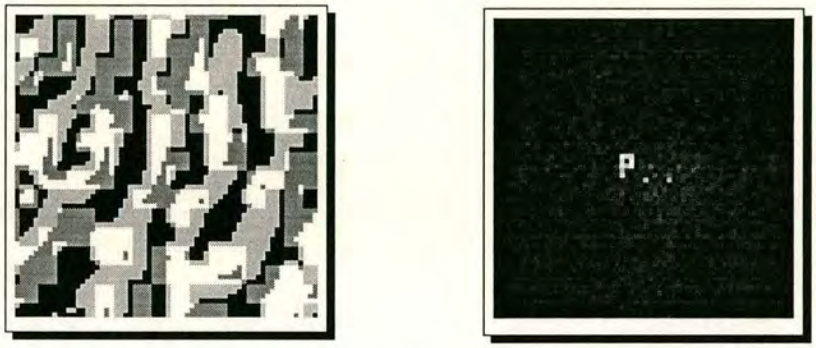

Fig 2.23 One pixel shifted modified "sandwich" and its FT. It is almost as good as for a totally random overlay.

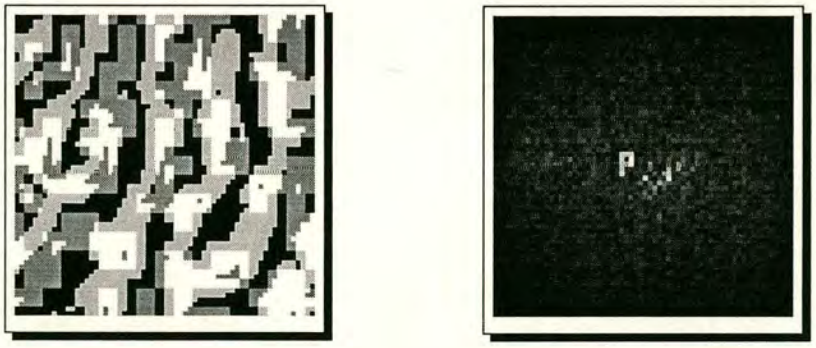

Fig. 2.24 Two pixels shifted modified "sandwich" and its FT. Even in this case there is still no symmetrical image though the noise has increased.

Structured overlays.

Another direction in the sandwich techniques is using an overlay which is not random, but produces a structured output. Even highly structured overlay patterns combined with the masks designed in respect of them can produce an output of acceptable quality. In fact it is possible to predict the distribution of the error clouds in the output pattern field. This could be of advantage because we can always choose the overlay mask which gives almost no noise in a particular area. For example, it is very effective to use the overlay mask that itself produces the frame. This solution is shown on fig.3.25. The Fourier transform of the overlay is a frame. The error clouds are moved towards the edges of the replay field of the sandwich that gives higher contrast ratio. However this scheme is sensitive to misalignment because of small details of the overlay pattern.

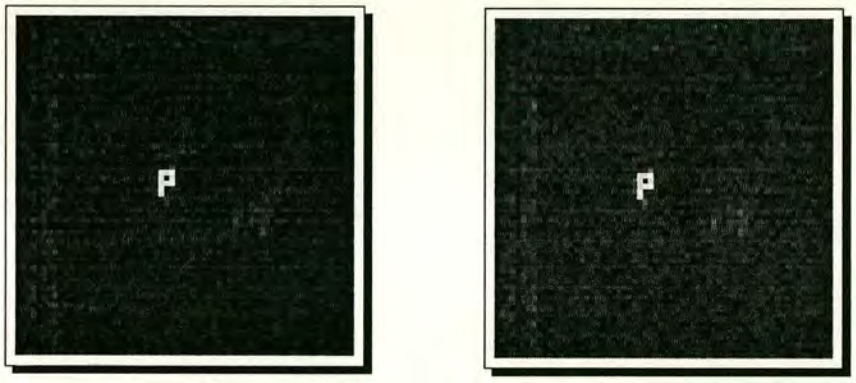

a) b)

Fig.3.25 (a) - output of the sandwich with frame-producing overlay.
(b) - the same output with reduced contrast. Error clouds pushed to the edges can be seen.

I found some other interesting solutions of the sandwich overlay. Fig.2.26. shows an overlay with a Fourier transform which is a rectangle in the centre of the output field.

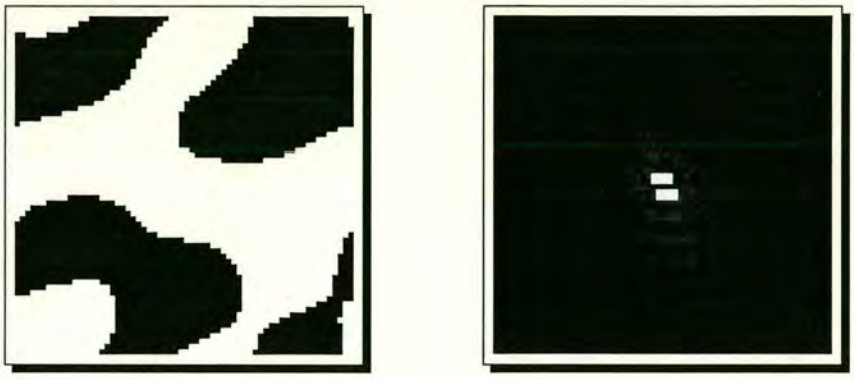

a) b)

Fig.2.26 An overlay (a) that produces a small rectangle in the low-frequency zone (b).

This pattern has very large details that is even more tolerant to mask misalignment than a large areas random pattern. The table below shows how the intensity of the symmetric output depends on NxN pixel shifts of the overlay.

Shift NxN	Intensity of the symmetrical spot	Intensity of the required spot
2	72	255
3	82	255
4	100	255
5	136	255
6	171	255

As we can see, 5x5 pixel shift still results in a symmetrical spot of only a half of the intensity of the original. This overlay works well when an output of a sandwich is limited to a small number of spots. Usually for the ideal binary grating there are always minor replications of the output spot which have values around 25% of the output. Therefore 3-pixel shift is perfectly acceptable.

Another implementation for a structure of an overlay is a checkerboard-like mask that produces a single spot in the corner of the square output field (see fig.2.27).

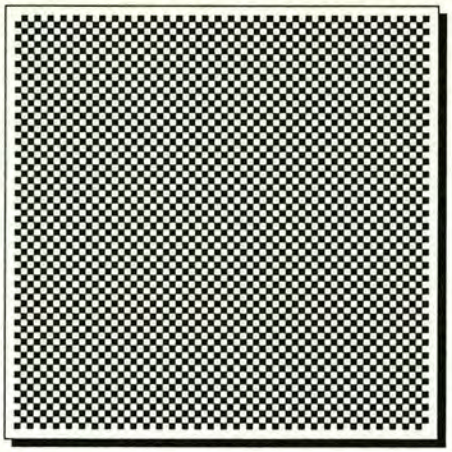

Fig. 2.27 A checkerboard-like overlay, that produces a single spot in the corner.

This pattern does not remove the symmetrical image it merely shifts it towards the corners so that the square area in the centre of the replay field, shown on fig.2.28, can be used for scanning instead of the rectangular area of the binary hologram.

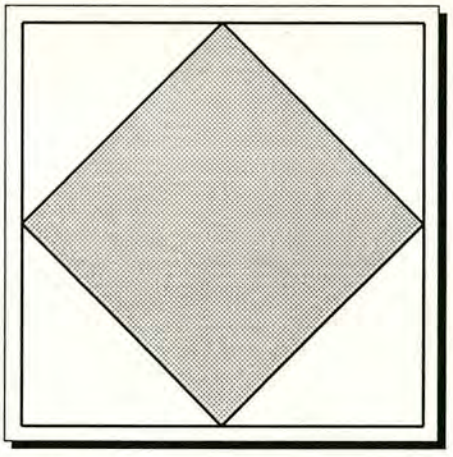

Fig. 2.28. The square area free from replications when using checker-board overlay.

Although the sizes of these two areas are the same this solution has two advantages: Firstly it is a square and secondly the beam scanning can be implemented on-axis. The overlay itself has a unique feature to be absolutely tolerant to misalignment. Any shift will only result in a rotation of the output image and this can be easily corrected by rotation of a sandwich. There are two examples of sandwich holograms with checker overlays shown on Fig. 2.29 and 2.30. The secondary images appear

outside the square area marked on fig.2.28. The side lines of this square become symmetry axes for a pair of output images.

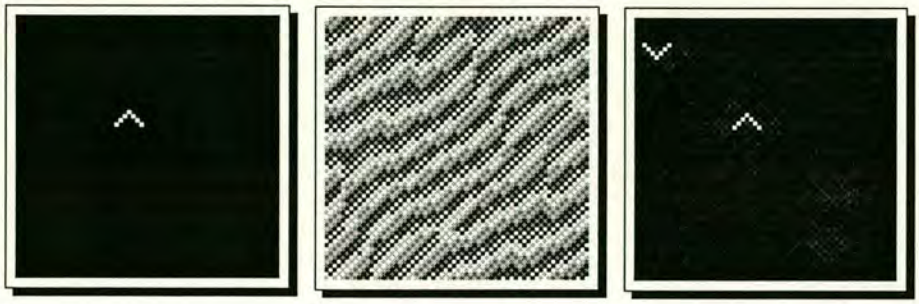

a) The target b) The sandwich c) The output

Fig.2.29 A sandwich with checker overlay on top.

a) The master mask b) The sandwich c) The output.

Fig. 2.30. Another sandwich of letter P with checker overlay.

Conclusion.

The technique of using large area overlays for sandwich holograms permits high tolerance of sandwich holograms to misalignment. Using the predefined sandwiches allows the spreading of the error clouds into the desired regions of the output field. Using the large areas overlays with the different pixel size than that of the master mask makes it possible to design and fabricate the mask after the overlay is designed and fabricated.

The comparison analysis of different types of fan-out holograms.

We have discussed five different types of holograms each of which has its advantages and disadvantages. The four-phase holograms produce outputs of better quality and without a secondary conjugate image. However they are very difficult to fabricate compared to binary holograms and are extremely difficult to implement in dynamic systems. It also takes twice as much time to design a four-phase hologram as for its binary equivalent. Four phase hologram cannot be made switchable like connected ones. The easiest holograms to design and to implement are simple binary non-connected structures. They can be implemented on an SLM and hence can be used in dynamic optical systems. The secondary image feature can be used in case of symmetrical fan-outs. If the switching time is important the connected holograms are the best to use. The sandwich holograms can be used for any purpose in the dynamic systems; quite successfully doing all tasks. The table 2.31 classifies the features of each of the five holograms types.

	On SLM	Dynamic	Switch-able	Non-symm.	Easy to fabricate
Binary n/cont.	√√√	√√√	√		√√√
Binary cont.			√√√		√
Sandwich n/cont.	√√	√√	√	√	√√
Sandwich cont.			√√√	√	√
Four-phase				√√	√

Fig. 2.31. A comparison table for five different types of holograms.

Chapter 3. Using holograms. Implementation on SLMs.

Introduction.

The implementation of binary holograms on SLM opens wide areas for their applications [4, 16, 46]. At present SLMs are the only way to create dynamic holograms. Dynamic holograms may be used in such areas as beam scanning, optical interconnects, neural networks, holographic animations, three-dimensional displays, optical computing and others.

However, the surface of the SLM is not the media which provides holograms of the best quality. There are some disadvantages of SLM devices in comparison with traditional static media:

1. Less than 100% fill factor. The early SLMs had only ~30% of their entire surface covered by the controllable pixels. The 176x176 samples we worked with were significantly improved by a planarisation technique developed by A.O'Hara [47] and their fill factor was ~80%. It is possible to achieve a fill factor to > 95% by improving the planarisation methods.

2. Large size of the pixels. The best samples of the static holograms fabricated with one of the following technologies: photolithography, direct e-beam, etching, have the size of pixels of 0.1-2 μm. In the contrary the size of the SLM pixels is 20-40 μm. This contributes additional errors and loss of efficiency.
3. Small space bandwidth product (SBWP): This is the number of pixels across the hologram. The SBWP of the SLMs we used were 176^2 and 256^2. This is much smaller than that achieved using static CGH recording techniques. This is one of the main limiting factors which restricts realisation of complex holograms on SLM devices.
4. Binary only structure creates a mirrored image in the output field of the hologram. In the case of asymmetrical fan-out, one half of the efficiency is lost and only half of the replay field can be used. Sandwich holograms techniques eliminates the symmetrical output but it does not improve the efficiency.

Despite the disadvantages described above, the SLM is still a very attractive device for implementing binary holograms because of its dynamic features.

Fabrication methods (static holograms).

A number of different techniques have been used to fabricate binary holographic structures, including controlled exposure and bleaching of photographic materials [23], lithographic or electron beam exposure of photoresist [64], controlled deposition of SiO_2 [25] , and controlled etching into solid material. The most successful technique to date appears to be the controlled plasma etching of fused silica [24, 43]. This etching technique requires careful calibration of the etch rate, and uniformity across large substrates is difficult. In addition the etched regions tend to be rough, which contributes to light scattering. An alternative fabrication technique developed by A.Stevens [56] was used for the fabrication of our binary static

holograms. The technique is based on accurately controlled deposition of silicon nitride on a sapphire substrate that is subsequently patterned and etched with the sapphire acting as an etch stop. This process results in optically smooth transmissive phase gratings with a phase thickness with a maximum variation of 1.5% across a wafer 75 mm in diameter. All processing operations in this fabrication technique are standard in very-large-scale integrated (VLSI) fabrication, and all patterning and etching were performed with modified fabrication facilities normally used for standard 3-μm CMOS (complementary metal-oxide semiconductor) processing.

Implementation on SLMs (dynamic holograms).

The dynamically implemented phase holograms can be realised using an SLM. Phase modulation has been demonstrated previously with magneto-optics [38], twisted-nemtatic liquid-crystal [3], and transmissive matrix addressed ferroelectric liquid-crystal (FLC) SLMs [4]. We used FLC upon very-large-scale-integration (VLSI) silicon backplane SLMs [63] The SLM devices used in our experiments have a 176x176 and 256x256 pixel backplanes. The device is electronically addressed and operates in a reflection mode: with the use of reflective SLMs to fold the optical paths, highly compact optical subsystems may be formed. The CMOS circuitary forms a two-dimensional array of dynamically and randomly addressed memory cells in which metal pads act as both mirrors and the electrodes of the FLC-filled strorage capacitors. The aluminium mirrors have size 24 μm x 28 μm and are positioned on a 30 μm pitch, giving a pixel fill-factor of ~80% and overall active area of about 5 x 5 mm. The pixels are addressed a row at a time by on-chip shift registers and interfaced to a microcomputer by a custom-designed high-speed frame store. With this interface, frames can be written to the SLM at an image update of 1 kHz, including the complementary voltage balancing frame to avoid electrochemical degradation of the FLC.

Binary phase modulation with the FLC SLM is shown in Fig.3.1 [14, 16] The stable orientations of the optic axis of the FLC indicate that the optic axis switches through an angle θ under the control of the applied voltage signals. The direction of the polarisation vector of the incident light as aligned symmetrically between the two directions (separated by θ) of the FLC's switchable optic axis. In the general case, propagation of light through the two liquid-crystal states produces elliptically polarised light (dependent on θ, the cell depth, and the birefringence) from the incident linear polarisation. The sense of the polarisation depends on which side of the optical axis ($\pm\theta/2$) the polarisation vector of incident light falls, i.e. either clockwise or anticlockwise. Light in these two elliptically polarised states then passes through an analyser, orthogonal to the first polarizer, which reduces the elliptical polarisation to a linear polarisation exhibiting a relative 0 or π phase difference, independent of switching angle or path length. The FLC material used in the device switches through an angle of $\theta = 45^\circ$, so therefore only 50% of light is transmitted by the analyser. For 100% transmittance (and hence no analyser required) an FLC material switching through an angle of $\theta = 90^\circ$ is required.

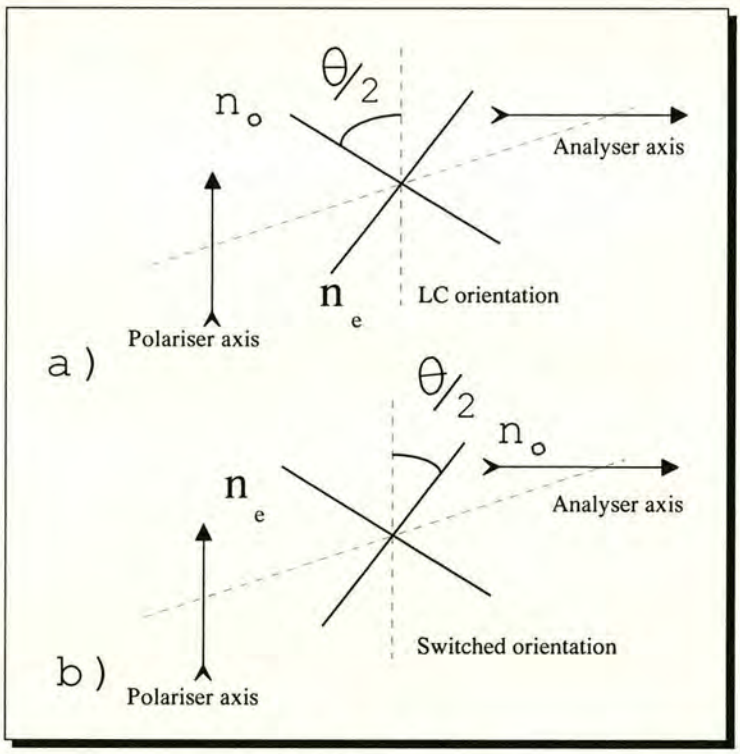

Fig.3.1. Phase modulation in SLM: (a) - zero phase difference
(b) - π phase difference.

The optical system used to implement binary dynamic reflection phase holograms is shown in Fig.3.2. A collimated He-Ne beam is first transmitted through a polarizer to determine the input polarisation orientation. A nonpolarising beam splitter is used to reflect the beam from the SLM. The beam is modulated by the phase pattern written on the SLM. The beam passes through an analyser. The modulated beam is then Fourier transformed by a lens to form an intensity distribution on a CCD array camera at the back focal plane of the lens. The camera is adjusted to give a linear response to light intensity. The focal length of the lens we used for this setup was 250 mm.

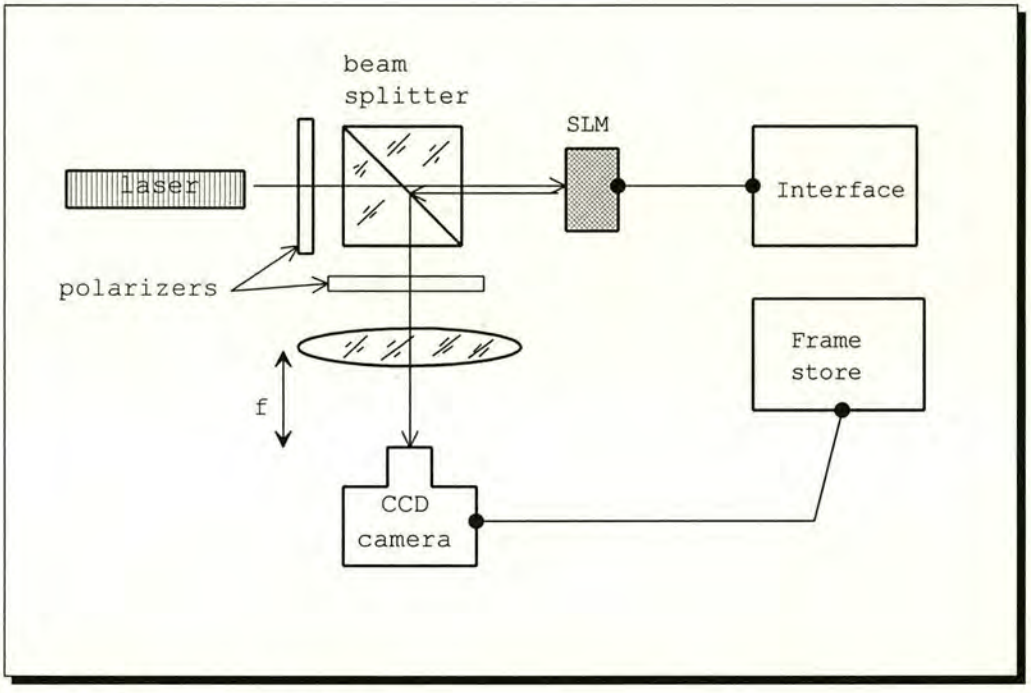

Fig. 3.2. SLM optical system.

Spreading the error into a frame in an SLM with a 25% fill factor.

Non-planarised SLMs are usually characterised by a very poor fill factor. Not only the efficiency of such hologram is low, the signal/error contrast ratio in the output plane in this case is very low too. The implementation of a mask for an 8x8 fan-out

on a non-planarized SLM is described in [14] by J.Gourlay et al. The theoretical diffraction efficiency for the 8x8 fan-out hologram which I designed to experiment with using non-planarized SLM was calculated at 81% assuming a 100% fill factor, and reduced to only 5.5% when simulated with a 25% fill factor at the 176x176 elements. The central DC term is very large, as in the case of the grating experiment and in the simulation with a 25% fill factor. The efficiency was measured by J.Gourlay at ~2.5% and the peaks were found to vary in intensity by ~ 10%. The optical results show that the evaluated experimental diffraction efficiency is lower by a factor of ~2 than that expected from the simulations with a 25% fill factor. Also, the large spread of diffracted light around the on-axis DC spot may restrict the use of this SLM device for reflective phase holograms. The low values of diffraction efficiency are caused mainly by the low fill factor of the device, but the FLC defect structures, poor mirror reflectivity, and any optical nonuniformity also contribute. The planarisation techniques must be used to overcome the problems associated with the VLSI fabricated circuitry and mirrors by burying them beneath a polished dielectric film, depositing high quality metal mirrors on the surface, and providing small interconnection vias through the dielectric layer between the original and the new metal layers. This processing is expected to increase the reflection efficiency of the devices by a factor of ~2 and increase the fill factor to nearly 100%.

For plain 25% devices I developed a simple technique of spreading the error into a frame which increases the signal/error contrast ratio significantly. Consider a mask which produces a simple square-in-a-circle fan-out (see fig.3.3 a). An SLM with 25% fill factor can be simulated using a square area of 2n x 2n size, where n is the size of one side of the hologram. (see fig.3.3 b)

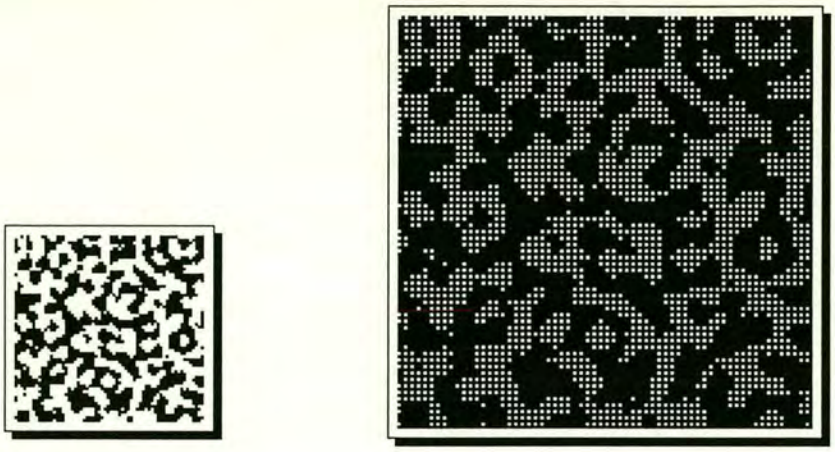

a) b)

Fig. 3.3 a hologram for a simple fan-out (a) and its 25% fill factor simulation (b).

A huge DC appears for the 25% fill factor mask and makes it impossible to implement such holograms on-axis. In order to eliminate disadvantages connected with the presence of DC spot I proposed the following method.

The hypothetical SLM of 128x128 pixel size was taken. Its surface consists of two parts: the actual working pixels which cover 25% of the whole area and the static pattern which covers the rest of the SLM's surface. The filling pattern itself is a binary hologram which produces the frame target, which is shown in fig. 3.4

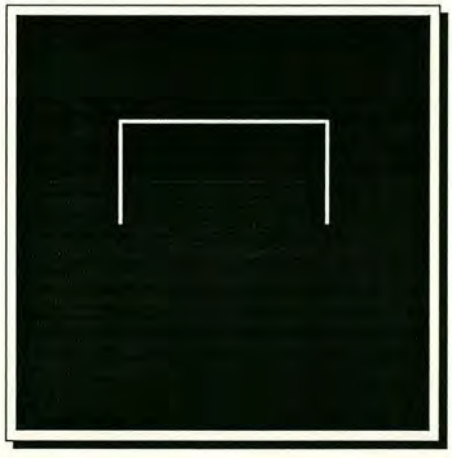

Fig. 3.4 A target for a error-spreading hologram. 3.5

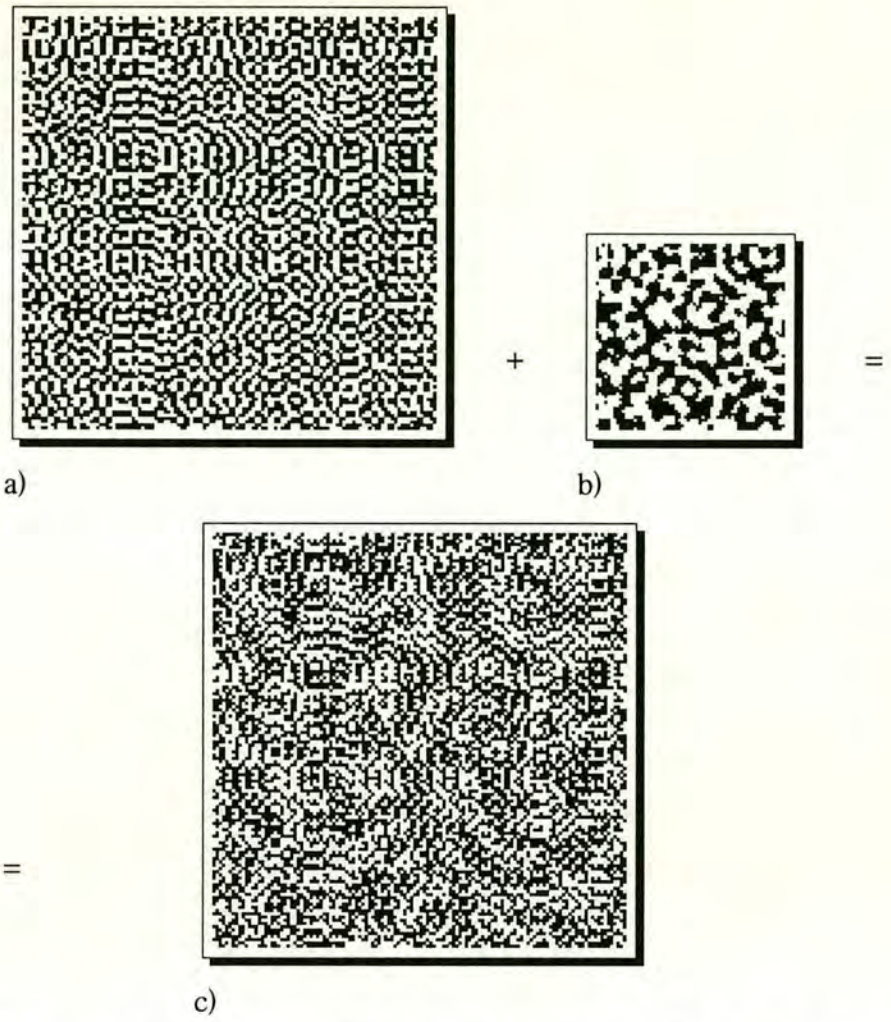

Fig. 3.5 Combination of a frame hologram (a) and a working hologram (b) makes hologram (c).

The 256^2 mask shown on Fig.3.5 incorporates both the working pixels array and a filling pattern. Each four pixels of the mask represent one cell of the SLM with the working pixel in the left top corner. Thus the SBWP of the hypothetical SLM is 128x128 pixels. Actually at first we designed the filling pattern over 256x256 mask and then copied in the 128x128 working pixels mask which was calculated to produce a different output. The additional annealing with t = 0 of the summed mask improves the quality of the required output. It is done by flipping the pixels in the mask which correspond with the appropriate pixels of the working pixels mask. The other areas of the mask are not changed. This method became a prototype for the precalculated areas method described in Chapter 2.

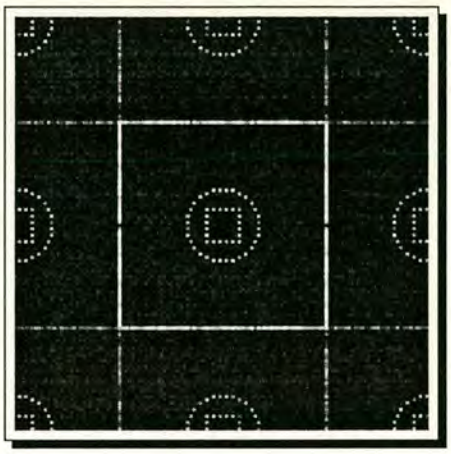

Fig. 3.6 The final output.

The size of a correcting frame is important. It should be placed in the centre of the mask area and equal to the size of a smaller target mask (see fig. 3.5). Otherwise the unwanted replications overlap the central working area. The final output is shown on fig.3.6. The intensities of the frame and side replications of the output are comparable to the intensities of the dots of the fan-out. The DC spot is very small, which makes it possible to implement such holograms on axis. The implementation of such structures can be done using the technique similar to the fabrication of sandwich holograms which we discussed in chapter 3.

Beam steering.

The dynamic computer generated holograms are perhaps one of the most promising elements for the realisation of beam steering. The laser beam scanning holographic elements based on SLMs have some very attractive features:

- Allow two-dimensional beam steering. Usually the output field is a rectangular area with sides lengths of a and a/2 for binary holograms with the number of possible discrete positions of the scanned beam determined by the SBWP of the SLM device. For sandwich devices the output field is a square.

- Very high precision. Since an SLM is not a mechanical device and its pixels positions are fixed it is possible to achieve very high accuracy and sability of beam scanning.
- The time required for a single shift is always the same and does not depend on the scanning angle. The scanning frequency is determined by the switching time of the SLM (up to 1000 Hz) and the time required to load the required holographic pattern (this can vary significantly depending on whether predefined or dynamically calculated holograms are used).

There are also some disadvantages:

- Scanning can be realised effectively only within a restricted angle.
- The scanning speed is relatively low. This can be very low when gratings are calculated dynamically for each position of the beam (0.1-1 sec). If predefined gratings are used the scanning frequency is determined by the switching time of the SLM (up to 1 kHz).
- Low efficiency (less than 45%) for binary holograms due to the secondary conjugate image. Generally speaking, pseudo-four phase sandwich holograms do not improve the efficiency because they simply spread the secondary image over the output area without contributing into the main image.

The laser beam steering can be described as one of the applications of optical interconnects. In the next section I will introduce an scheme for optical interconnects using SLMs and discuss some problems of its implementation which are also relevant to beam scanning.

Optical interconnects.

Optical information channels have extremely high bandwidths, can transfer information across free space, and do not suffer cross talk when they encounter another beam of light. One simple example of optical interconnects is the optical

crossbar developed by Goodman et al [13]. The scheme is shown in fig.3.7. This is a vector-matrix multiplier crossbar. The device transfers each input channel into a column of an interconnect shutter and the transmitted light from a row is focused onto an output channel.

Another device is shown on fig.3.8. This is a matrix-matrix crossbar switch that works in two dimensions [31, 32] . It improves the scalability of the previous device by avoiding the use of cylindrical lenses. The two NxN matrices are interconnected via an N^2xN^2 shutter matrix which is implemented on SLM. The input matrix is replicated using a holographic beam splitter. Each copy is multiplied by an SLM matrix and then focused onto an output matrix.

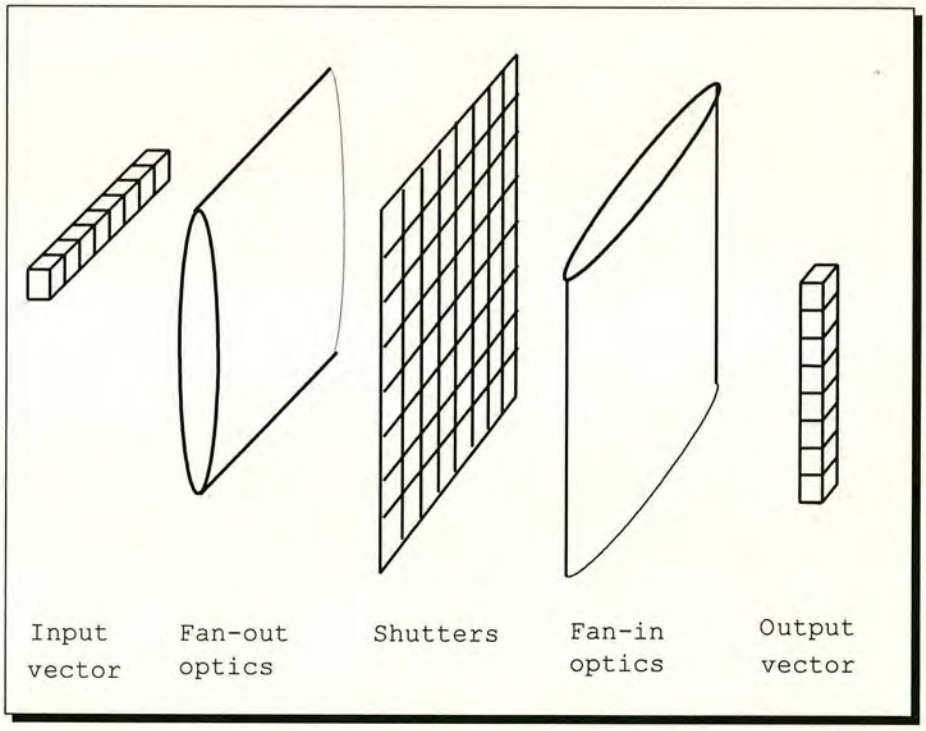

Fig. 3.7. The vector-matrix multiplier optical crossbar.

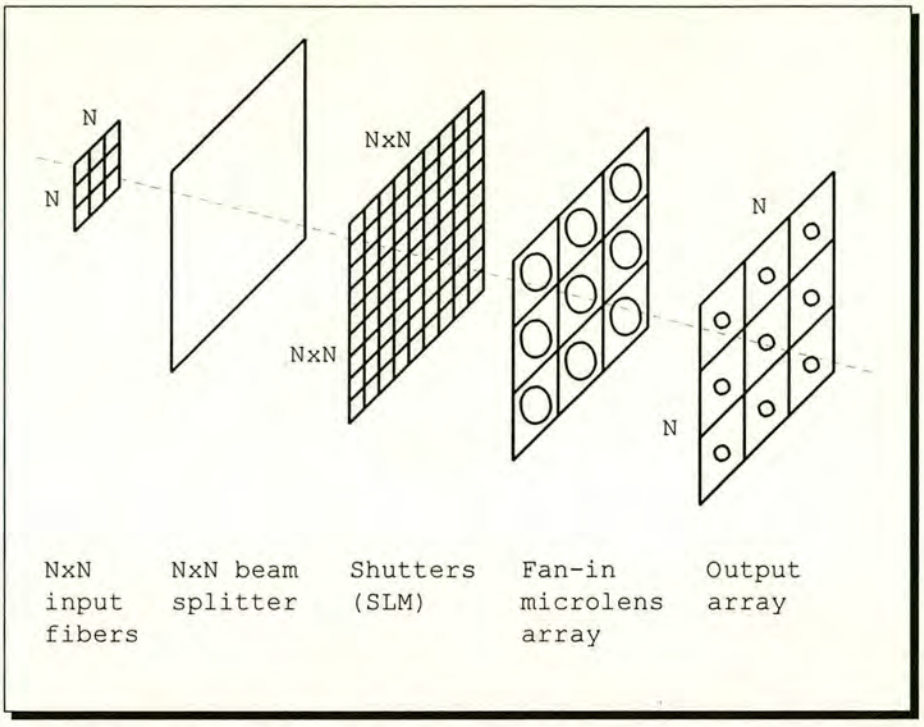

Fig.3.8. The matrix-matrix crossbar.

The efficiency for both schemes decreases dramatically as the number of channels increases. Another problem for these two devices is that they rely on the good quality of the SLM. If there are "dead" pixels on the SLM the interconnects can not be realised properly. Several other schemes of interconnects using SLMs were reported recently [15, 57, 58].

Fig.3.9 shows a multi-purpose high efficiency set up for optical interconnects that can be used for multiple applications such as beam scanning, optical crossbars, optical neural nets and others. This device is also tolerant to small defects on the SLM surface. I developed and simulated this scheme independently in 1993 and the similar set up was introduced by O'Brien et al in 1994 [45]. The scheme is capable of providing one-to-one, many-to-one and one-to-many interconnects. An array of 4x4 inputs illuminates 4x4 sub-holograms formed on a 256x256 SLM. Thus the size of each sub-hologram is 64x64 pixels. This setup is possible using sandwich holograms which eliminate the symmetrical output. Otherwise only one half of the replay field can be used. This scheme can be very advantageous for one-to-one routing. The holograms for each of the sectors of the SLM are simple gratings for beam steering.

We only need 16 of them to be able to send any input to any of 16 sectors of the output plane. The storage space for it is the same as if we needed to store one 256x256 binary picture. The elegant function which does the job could look like this: *one_to_one(input_source, output_sector)*. The computer's job is to actually choose the sector of the SLM which corresponds to the number of input fibre (source) and send a hologram which is stored under the same number as the number of the desired output sector. A hologram can operate within limited number of orders which is restricted by its size in pixels. Therefore the size of the output plane is also 64x64 pixels, not 256x256. And it must be divided into 16 sectors which makes the size of each output sector 16x16. It is not possible to completely fill the area of the sub-hologram with the input beam without overlapping the neighbour sectors. Actually an area much less than 64x64 is illuminated.

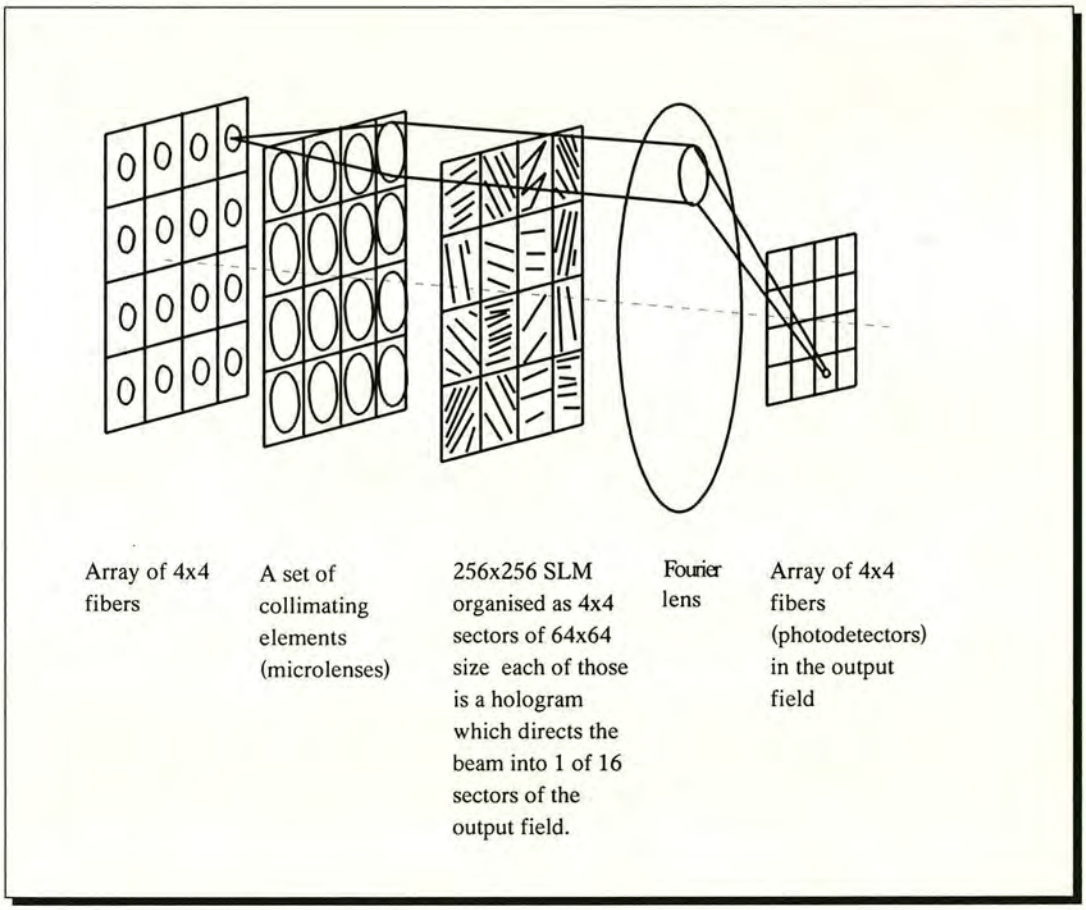

Fig. 3.9. A scheme for multiple optical interconnects.

These two factors put considerable restrictions on using complicated many-to-many interconnects. An overlap can produce some strong influence from the neighbouring sector. As a single output dot is typically defined by as little as an 8x8 square the output can be noticeably corrupted with images produced by overlapped subholograms. The possible alternative to one-dot output can be a circle which represents only one spot. In this case a small overlap does not do as much damage as in the previous case. Fig.3.11 and fig.3.12 show the sequence of holograms of two dots for sector 1 and 6 and two circles for the same sectors, their simulated Fourier transforms and optical results for 176x176 SLM.

I simulated a very simple model of a one-to-one optical crossbar using a 256x256 SLM. The upper half of the SLM was divided into 4x2 squares of 64x64 size each (see fig. 3.10)

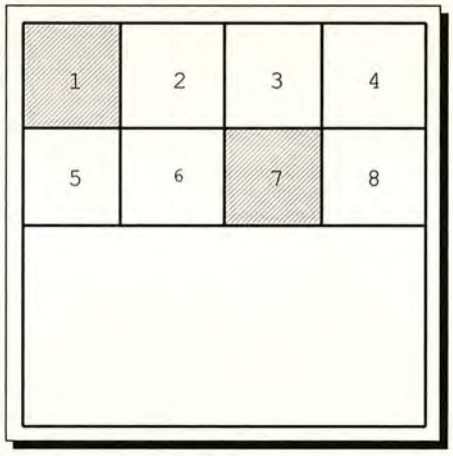

Fig. 3.10 output sectors for optical crossbar implementation.

The aim was to inspect the behaviour and quality of the redirected image by a sector of an SLM of less than 64x64 pixel in size. Two sets of holograms were designed. The holograms for one dot steering and the holograms for steering an image of the size comparable to the size of one sector (64x64). The holograms were designed to redirect the image into a high frequency sector number 1 and a low frequency sector number 7. The holographic patterns were initially designed in a 32x32 pixel area and

then replicated to ensure a full period was covered by the laser beam. The holograms and their Fourier transforms are shown on fig.3.11 and fig.3.12.

The holograms of the dots are virtually noise free except for one replication with intensity of about 85 compared to the 255 value for a true spot. The replication of the dot in sector 1 gets into the sector 6 and the replication for a dot in sector 7 lies in the sector 4. These secondary dots are not likely to be mistaken for a true signal because of a good signal/noise ratio. The optical output is very good with a small DC spot in the middle. In spite of the fact that the area covered by the laser beam was less than 64x64 pixels the quality of the output did not deteriorate much. We found that it is enough to have the beam diameter as small as 10 pixels in order to get a good quality output. The nearly uniform intensity of the laser beam was achieved by using only about 10% of the light in the centre off the beam and cutting off the rest of light with an aperture.

This is in good agreement with a theoretical value because one period of the mask is 8x8 pixels as we can see from the picture. This means that the particular SLM can provide acceptable results for an optical crossbar divided into as much as 32x16 sectors and good results for 16x8 sectors.

The outputs of the holograms for a circle are much noisier but there is no distinctive secondary circle image. The error clouds are smoothly spread over the whole area of the output field. This increase is an advantage over the dot model since there is no secondary image which could be mistaken for the correct signal. However compared with 8 periods for dot holograms the circle one has only 2 periods. This makes it impossible to obtain a suitable output when the diameter of the laser beam is less than 16 pixels in size. The experiment showed the same. So the lower limit for such a crossbar is 8x4 sectors.

Another interesting question is how the output image is corrupted when the laser beam overlaps neighbouring sectors. We simulated such a situation by combining 1/4 and 3/4 of different masks in one 32x32 square pattern. This is shown in fig. 3.13
The dot hologram is much more tolerant to such distortions as we can see from the pictures.

As it was mentioned before, the analysed set up is very effective for the realisation of one-to-one and many-to-one interconnects. It is also easy to implement a one-to-many model but there is one drawback. The holograms required for this task are not simple gratings any longer and cannot be calculated analytically, hence we have to predesign N^2 fan-out holograms, where N is the number of defined sectors. It is still easy for our simple 16 sectors model but, in the real systems, 16x8 and more sectors can be used . There is another restriction. With the increasing of the number of sectors the complexity of the fan-out holograms will increase too. Therefore the minimal sector size must be large enough to represent the most complex fan-out. Our experiments showed that 4x4 dots of a hologram represent well 1 output dot. Therefore the minimal size of the sector for a 4x8 sectors model must be at least 32x32 pixels.

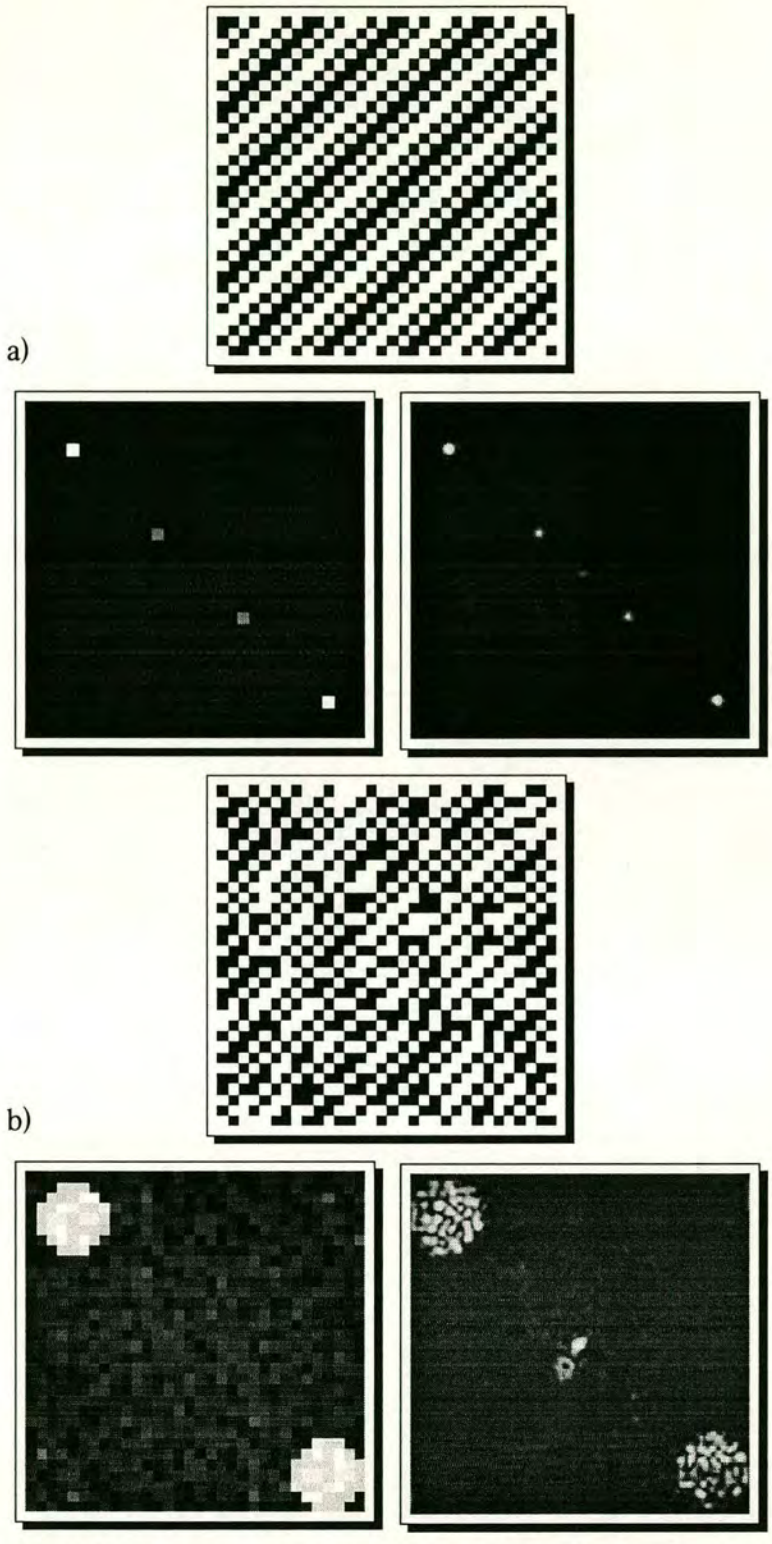

Fig. 3.11 The masks for sector 1 and their simulated and optical outputs.

a) single dot

b) a circle

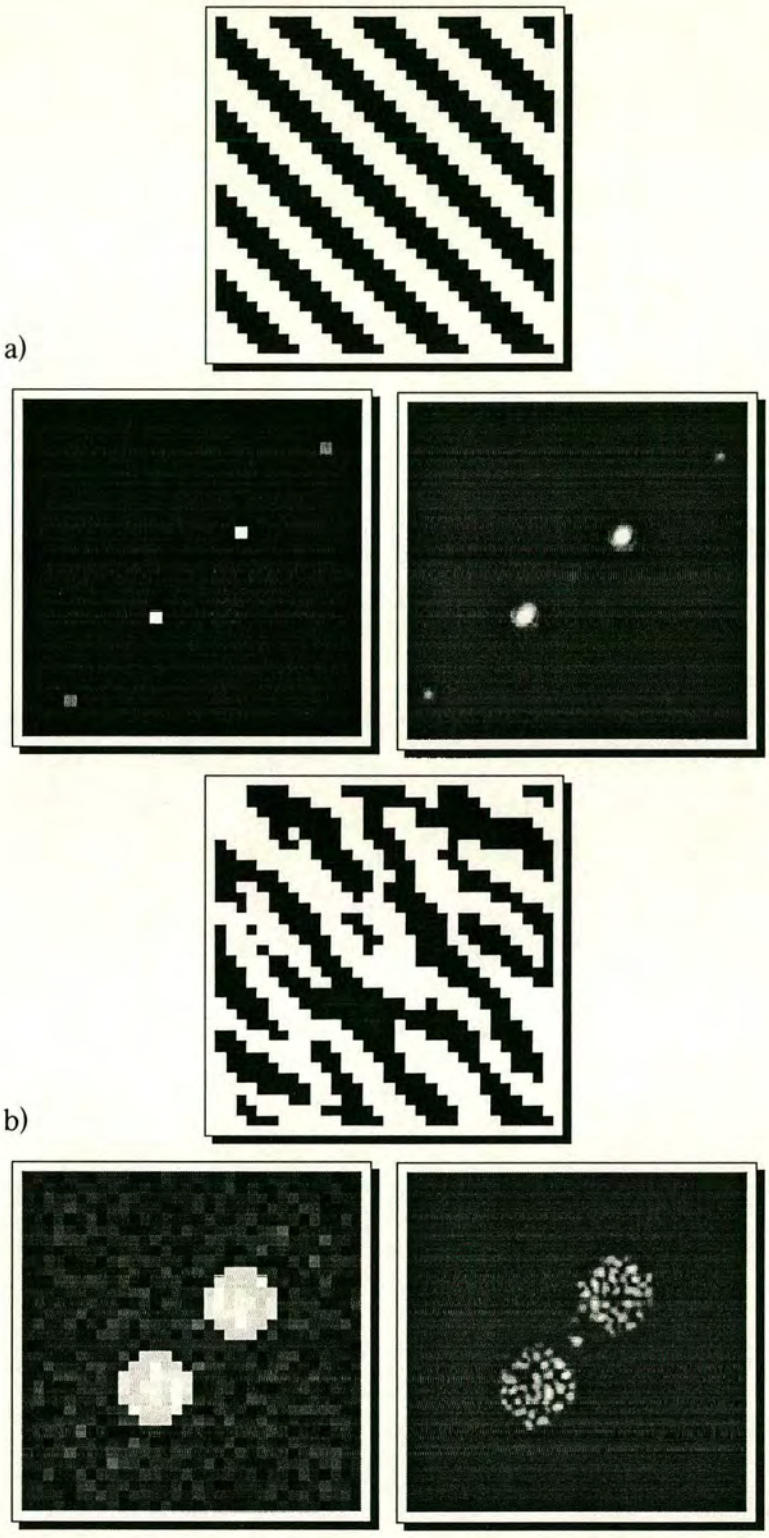

Fig. 3.12 The masks for sector 2 and their simulated and optical results.

a) single dot.

b) circle.

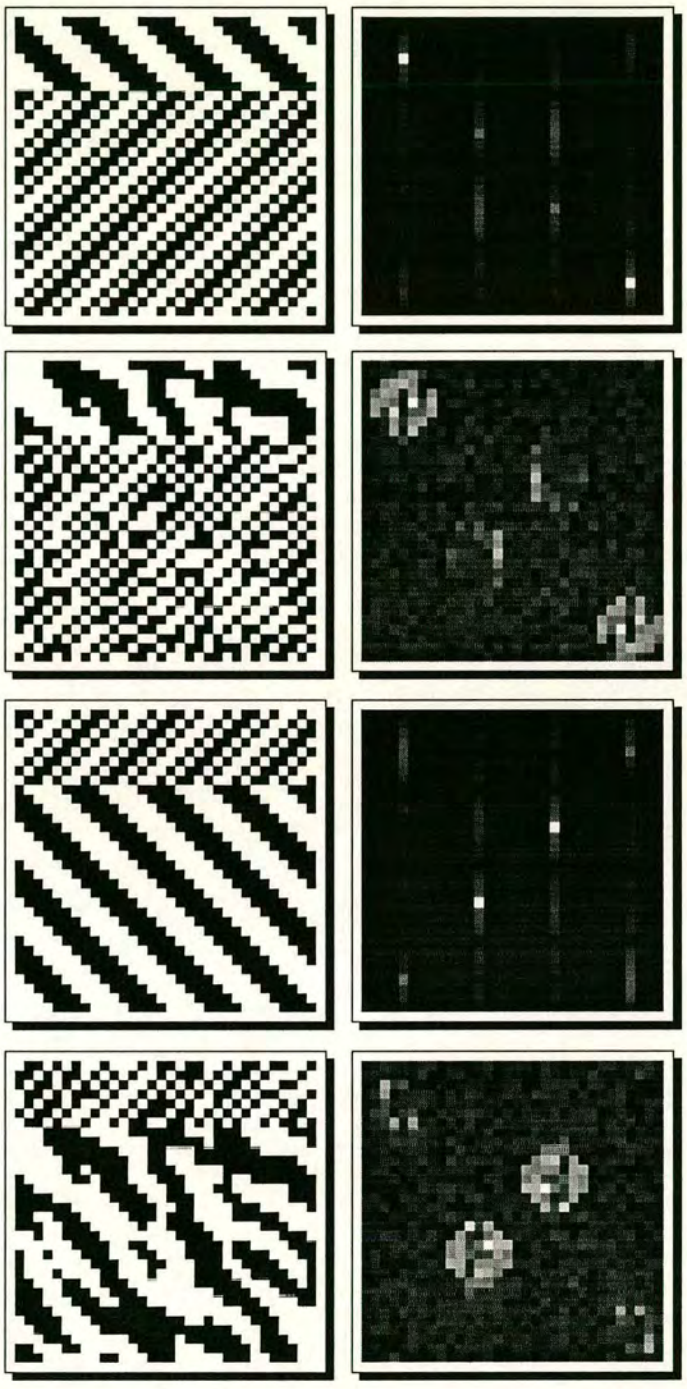

Fig. 3.13 Simulation of sectors overlaps.

Animations.

In order to demonstrate dynamic facilities of holograms implemented on SLMs, we designed several series of animations using a planarised 176x176 SLM [14]. Fig. 3.14 shows a sequence of holograms and their Fourier transforms which were loaded to the SLM at a cyclic rate 2 frames / sec.

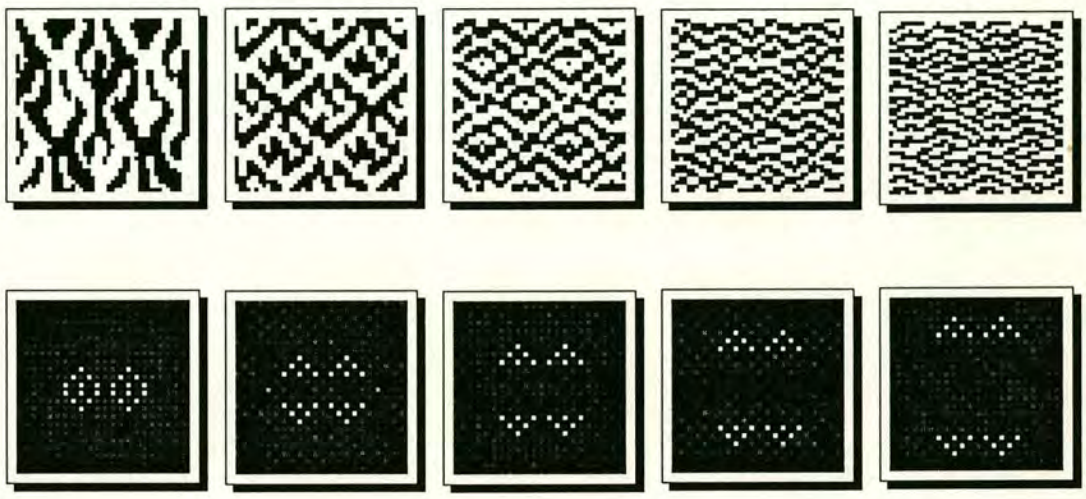

Fig. 3.14 A sequence of 5 holograms and their simulated outputs for animations display on SLM. All holograms were designed on 44x44 pixel area and then 4 times tiled to the size of SLM (176x176).

Conclusion.

The dynamic features of SLM devices greatly expand the usage of CGHs. The holograms now can be effectively implemented in such modern areas as optical interconnects, neural networks, beam steering and others. However SLMs cannot provide good quality output for large fan-out holograms. For complex systems a large number of predesigned holograms must be used which also creates difficulties for implementation of such systems.

Chapter 4. Methods of fast design of weighted and uniform holograms of small fan-out.

Introduction.

It is difficult to overstate the importance of computer generated fan-out holograms is such areas as optical interconnects, neural networks and some others. Especially when implemented on SLMs these holograms become extremely powerful and elegant solutions to some long lasting problems such as efficient dynamic optical interconnects or 2-D beam steering. Earlier I presented a multipurpose optical interconnects setup implemented with one SLM and 16 predesigned sandwich holograms to realise one-to-one or many-to-one optical routing. However if we were to use this device for one-to-many approach we would have to predesign many more holograms. If we also wanted to vary the intensities of the outputs, the number of holograms we would need to precalculate would be enormous. In large systems the

number of predesigned holograms may be hundreds or even millions. The time to design a single hologram using methods described before can vary from 0.5 minute to 2 days mainly depending on the size of the hologram, number of output spots and computer resources. Even the design of the simplest structures takes considerable time. In other words some systems which require many holograms are difficult to implement. The main obstacles are the computational time required to predesign all the possible patterns and the large amount of data needed to be stored.

It is possible to speed up the process of holograms design using optical optimisation by implementing feedback between an SLM and an array of photodetectors. K.Weible et al [65] used simple liquid crystal television instead of the SLM for this purpose. This approach still does not solve all problems. The system is expensive and cumbersome. The speed advantage is also not that great because the same principles of optimisation using simulated annealing are used and the relatively slow response of LCTV or SLM limits the speed of modifications. Still as it was reported in [65] after rough mask design a familiar error reduction algorithm using a computer must be applied to improve uniformity and to remove any noise introduced during the optical optimisation and this process effectively slows the design down.

In this chapter I will present a new approach which allows fast update of hologram structures in order to change an output pattern configuration and/or intensity distribution.

Missing pixel holograms.

Consider a hologram that splits a beam into n spots. If we wish to vary the intensity of the spots over L output values then, in general we would need L^n individual holographic patterns each designed separately. If n or L are large, this rapidly becomes a computationally impossible task. For example, the simple task where we

need to change any of four output spots intensity within 8 levels requires 4096 holograms. For an eight spot problem, this number increases up to the enormous figure of 16 777 216. Obviously this task is impossible to achieve using conventional methods.

The visual methods of holograms design, which we will discuss in chapter 6, opens the possibility to observe the process of hologram creation as it is running. If the solution for n-dot fan-out is found it is also possible to find a solution for n-1 dot fan-out using the n-dot mask as a starting pattern with the simple error reduction algorithm (T = 0). Although the algorithm allows any configuration of the mask, the intermediate states of half-developed patterns are developed only in certain areas. We also noticed that as the algorithm progresses the intensity of the spot missed in the second target falls. The intensities of other spots do not change significantly.

Two dots model.

Consider the 2 by 2 binary fan-out hologram shown in figure 4.1. If the hologram is binary phase, then the output pattern will always be symmetric. This hologram has been designed on a 64 by 64 pixel grid, denoted by mask 1. Figure 4.2 shows a 2 point hologram of the same spacing formed by additional annealing at temperature zero of the mask 1 but with a new target. This is denoted by mask 2. Further we will consider only upper halves of the outputs due to their symmetrical nature. The difference between two outputs is that there is no right spot in the second case. We will call mask 2 a "missing pixel hologram" and mask 1 a "master mask". Figures 4.3a and 4.3b show the holograms which are designed to produce two - pixels outputs with different intensities of the right spot. The intensities are respectively 0.4 and 0.8.

Fig.4.4 shows masks 1, 2 and 3a added together in a way we would put 3 transparencies on top of each other. We can clearly see that there is a definite link between all these holograms. The holograms for weighted outputs are changed only in the grey and dark grey areas.

Fig. 4.1(a,b) 2x2 hologram and its FT.

Fig. 4.2(a,b) missing pixel hologram and its FT.

Fig. 4.3(a,b) pure holograms for 1&0.8 and 1&0.4 outputs

Fig. 4.4(a,b) added holograms: 1 + 2 + 1 + 3a and 1 + 2 + 1 + 3b.

Fig. 4.5 added holograms 1 + 2 + 1

Fig. 4.6 synthetic hologram which replaces Fig. 4.3a

Fig. 4.5 shows the master mask (1) and the missing pixel mask (2) added together in a sequence 1+2+1. The pattern consists of 4 values:

0 - areas where two masks overlap (black)

1- areas of master mask only (dark grey)

2 - areas which belong only to the missing pixel mask. (light grey)

3 - clear areas (white)

We shall call 0, 3 'and' areas and 1, 2 'or' areas. The 'or' which is created by the master mask is darker because it is overlapped twice. We will call the 'or' areas 'or 1' for master mask and 'or 2' for missing pixel mask. Considering fig.4.4a and 4.4b. We

can see that the original holograms for weighted intensities pixels change only in `or' areas. Two extreme cases are our master mask and missing pixel mask. If we need the solution with the intensity of the right pixel closer to 1 the 'or 1' area will be filled more and the 'or 2' area associated with missing pixel mask - less. And the other way round it will be for the intensity of the right pixel closer to 0. The 'and' areas are not changed at all. Simulation suggests that the fraction of area filling is proportional to the intensity of the right pixel. This can be approximated by randomly filling the region 'or 1' proportionally to k and 'or 2' proportionally to 1-k where. The method works even if the `or' areas consist of single pixels or small number of them. Fig.4.6(a,b) shows the final solutions for the synthetic masks which produce 2 pixel output with the intensity distributions (1, 0.8) and (1, 0.4). The above said can be expressed in the following algorithm.

The algorithm for changing the intensity of a single output pixel.

The above observations can be generalised, for any pair of masks of n and n-1 fan-outs resulting in the following algorithm for changing the intensity of a single output pixel:

1. Design a master hologram which produces the required output with intensity of the changeable pixel equal to 1.
2. Design a missing pixel hologram which produces the same output with intensity of the changeable pixel equal to 0. The rules for the missing pixel hologram design are:
    a) The starting pattern for the hologram must be its master mask.
    b) The missing pixel mask design must be done using simple error reduction algorithm (the simulated annealing with T = 0).
3. Calculate the synthetic hologram using the latter two patterns, following the rules:
    a) The pixels with the same phase shift for both masks are not changed.
    b) The pixels with π phase shift for master mask and 0 phase shift for the missing pixel mask are changed to 1 with the probability k, where k is the desired intensity coefficient.

c) The pixels with 0 phase shift for master mask and phase shift for the missing pixel mask are changed to 0 with the probability 1 - k.

The success of the algorithm depends on the accuracy of the two holograms. We found that the structures which produce asymmetrical outputs are more stable. The replication orders of the image are usually lying symmetrically which causes sometimes the contribution of the replication into the missing pixel's intensity.

The multiple dots model.

A fan-out of n-dots with 0 and 1 intensities of output spots can be represented by 2^n binary numbers. We also found that the set of $2^n - 1$ pure holograms with outputs corresponding to binary numbers in the range $(1 , 2^n - 1)$ can determine any combination of intensities distribution of n output dots. All these holograms must be derived from the mask with all pixels 'on', which corresponds to binary number $2^n - 1$. The technique for the design of the synthetic mask for m weighted outputs (where $0 < m < n$) involves the recursive creation of missing pixel pairs of synthetic masks starting from a set of 2^m predesigned pure holograms. This set of holograms becomes the bottom layer of a binary tree of m + 1 layers, each of which is responsible for the intensity value of one of the output dots. The number of holograms in each layer is determined by 2^{m-L} where L is the layer number starting from 0. The lower layers of the tree serve as parent missing pixel pairs for the calculation of the synthetic holograms for the next layer using the method described earlier. The scheme involves calculation of $2^{m-1} - 1$ synthetic holograms. The tree ends with one synthetic hologram which is a solution to a weighted m-dot distribution for n-dot fan-out. These observations can be generalised, resulting in the following algorithm for changing the intensity of multiple pixels:

The algorithm for changing the intensities of m dots in n-dot fan-out.

1. Design the starting pattern for all the holograms which produces n-dot fan-out with all pixels on. Represent the output of this pattern as a binary number 2^n - 1 and associate all the output spots with the positions of the digits of this number.
2. Design 2^n - 1 pure holograms starting from the above hologram and using the error reduction method so that their outputs correspond to the binary numbers within the range (1, 2^n - 1).
3. Design the binary tree from top to bottom following the rules:
   a) represent the final synthetic mask as an indexed binary number $X_{a(1), a(2), ..., a(m-1), a(m)}$, where a(1), a(2),...,a(m-1), a(m) are the positions of the digits of the changeable dots in the binary number 2^n - 1. These indexes can be put in any order. All the changeable intensities represent as 1 in the correspondent bits of X. The permanent 'on' pixels also represent as 1 and the 'off' pixels represent as 0.
   b) Find the missing pixel parent pair for layer m - 1 with which the final mask can be obtained using the following rule:
   - The left parent is represented by an indexed binary number $X_{a(1), a(2), ..., a(m-1)}$.
   - The right parent is represented by an indexed binary number $(X \hat{} 2^{a(m)})_{a(1),a(2), ..., a(m-1)}$, where ' ^ ' is an exclusive OR binary operation.
   c) repeat recursively this procedure for each of the parent hologram descending to the bottom layers until the holograms are represented with binary numbers without indexes. These will be pure holograms predesigned before (see 1, 2).
4. Start from the bottom of the found tree and calculate synthetic holograms for upper layers using the step 3 of the algorithm 1. Choose the intensity coefficient k which corresponds to the rightmost index of the formula for a child hologram.

The Fig. 4.7. shows an example of a binary tree design for 4-dot fan-out with number of changeable dots m equal 3. The intensity of the dot 3 is not changed and equal to 1.

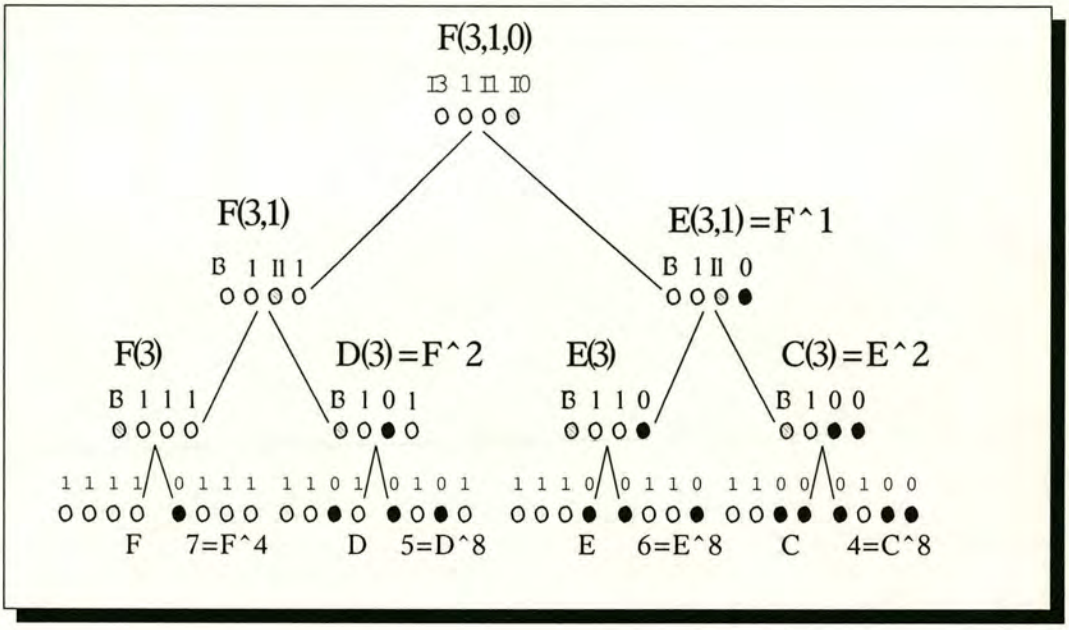

Fig. 4.7 A calculation tree for 4-dots fan-out.

We accomplished the simulation for 4-dot fan-out using the algorithms. The results for combination (0.8, 1, 0.4, I_0) are shown on fig. 3. The intensities of dots 1, 2, 3 were fixed at the values 0.4, 1, 0.8 using synthetic holograms and the intensity of the dot 4 changed gradually from 0.01 to .99. The results proved to be very stable and linear as it can be seen from the graph shown on fig. 4.8 .

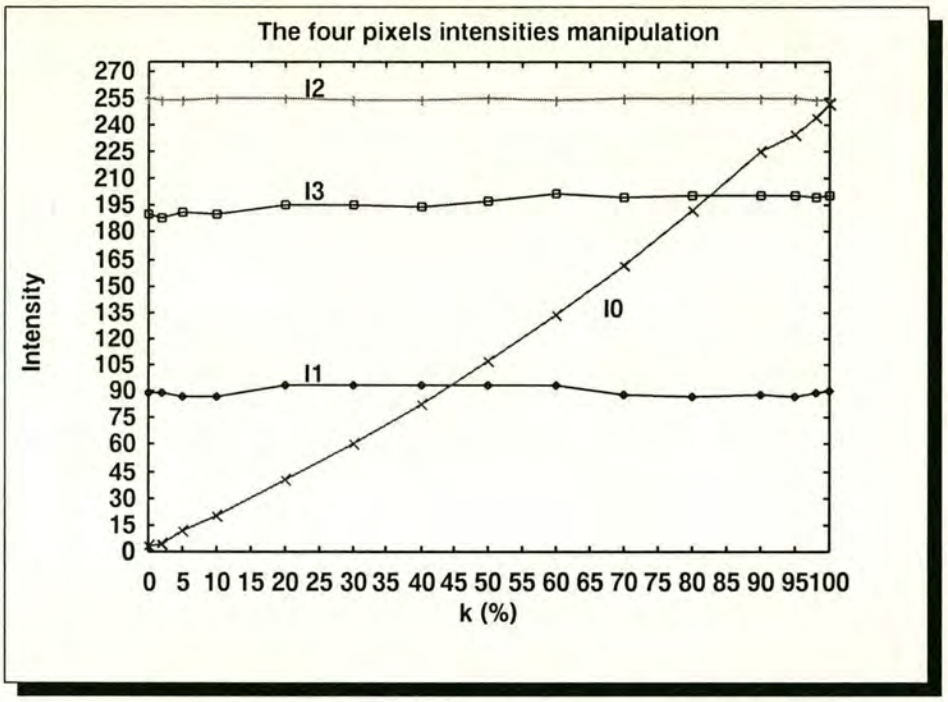

Fig. 4.8 A graph of changing the intensity of the 4th dot.

The target pattern is shown on fig.4.9 The asymmetrical shape of target pattern proved to be more stable. It ensures than the replications do not overlap with images of desired dots hence do not increase the overall error. The optical results were obtained using a 256x256 SLM. The calculated 64x64 pixels hologram was tiled to the 256x256 size. A sequence of pictures (see fig.4.10) shows the results of changing the intensity of the right pixel from 20% to 90%. The actual values of intensities of the output pixels were estimated with the aid of a video camera, however this camera was not calibrated to measure absolute intensity. The relative distributions of intensities can be estimated by visual comparison of the brightness and the size of all four dots.

Fig. 4.9 A target pattern for an experiment .

Fig. 4.10 The experiment result. Missing pixel method implemented on an SLM.

a) (0.4, 1, 0.8, 0.2)

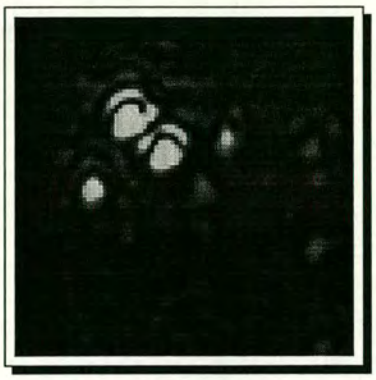

b) (0.4, 1, 0.8, 0.3)

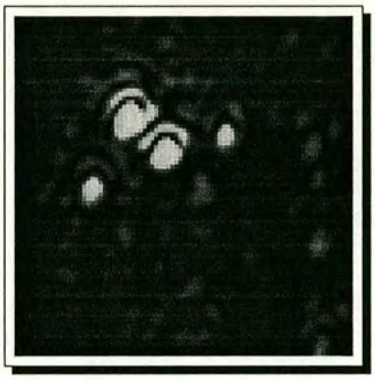

c) (0.4, 1, 0.8, 0.4)

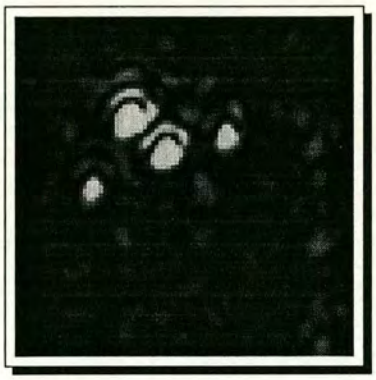

d) (0.4, 1, 0.8, 0.5)

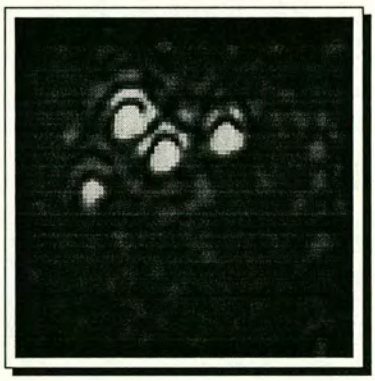

e) (0.4, 1, 0.8, 0.7)

f) (0.4, 1, 0.8, 0.9)

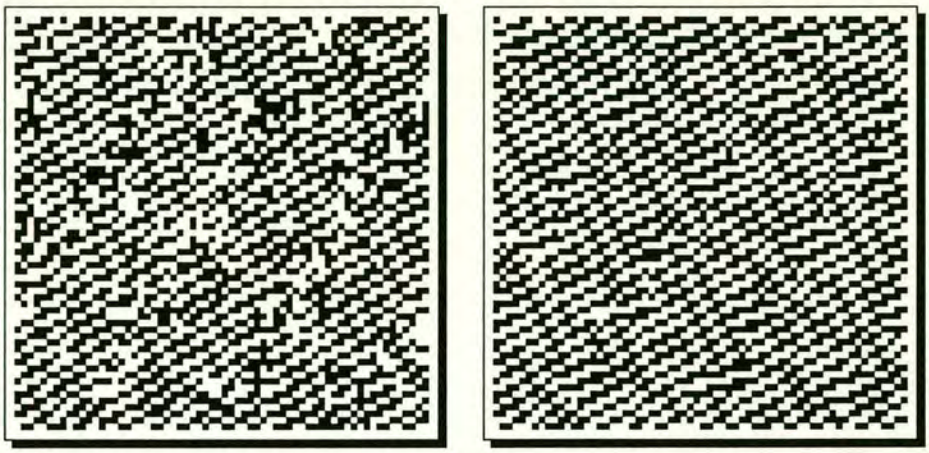

a) b)

Fig. 4.11 Two masks synthetic (a) and ideal (b) for (0.4, 0.8, 1.0, 0.5) fan-out.

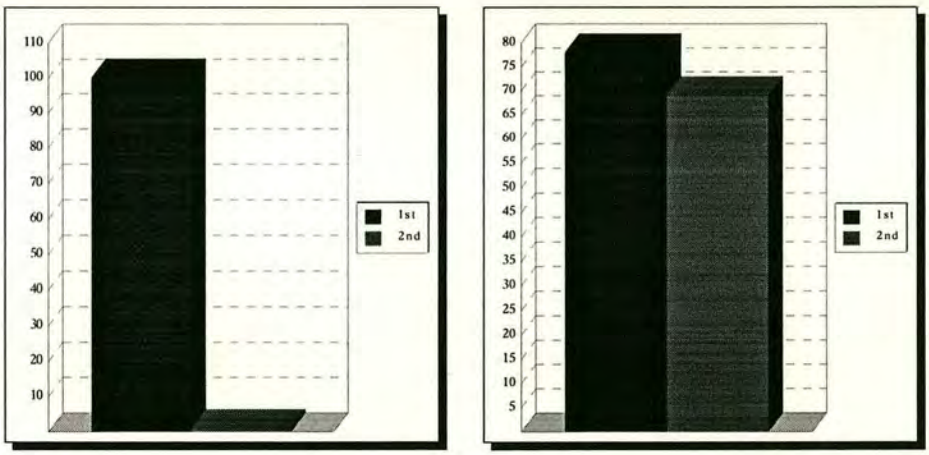

a) b)

Fig. 4.12 Comparison of a design speed (a) and efficiency (b) of ideal (1st) and synthetic (2nd) holograms.

A synthetic and an ideal masks (designed using simulated annealing) are shown on fig. 4.11. As we can see these two patterns are similar with a difference that a synthetic mask looks a bit rougher and this affects the efficiency which drops from

around 80% to about 70%. These two patterns are much more similar to each other than those for 2-dots fan-out. As all pure masks are mutually coherent all the synthetic changes take place only in the same areas and the efficiency increases with the increase of the number of participating holograms.

The comparison of design speed and efficiency for 4-dots ideal and synthetic holograms is given on fig.4.12. The time required for design process can be reduced to a factor of 100-1000 while the efficiency only drops from 75-80% to 60-70%.

Combined holograms. Fast calculation of holograms of small fan-out using combinations of simple gratings.

Experiments with simple holograms show that a configuration of a hologram of n-dot fan-out can be obtained by combining a hologram of n-1 fan-out and a grating which defines a single missing spot. Fig.4.13(a,b) shows two gratings which outputs are single pixels in different positions. If the two masks are added together, as we did it before for missing pixel holograms, the resulting picture is shown on fig.4.13(c). Applying the autocorrelation operation to this pattern; the result is shown on fig.4.13(d) being a halftone picture that resembles a binary hologram for two dots output. The simple binarisation procedure results in an almost ideal binary hologram for two pixels output (see fig. 4.13e)! The binarisation is performed as follows:

- The number of grey levels of a picture is calculated.
- The areas that correspond to the brighter half of grey levels are set to π .
- The areas that correspond to the darker half of grey levels are set to 0.
- If there is an odd number of the grey levels the areas that correspond to the central level are randomly set to 0 or π with probability 0.5.

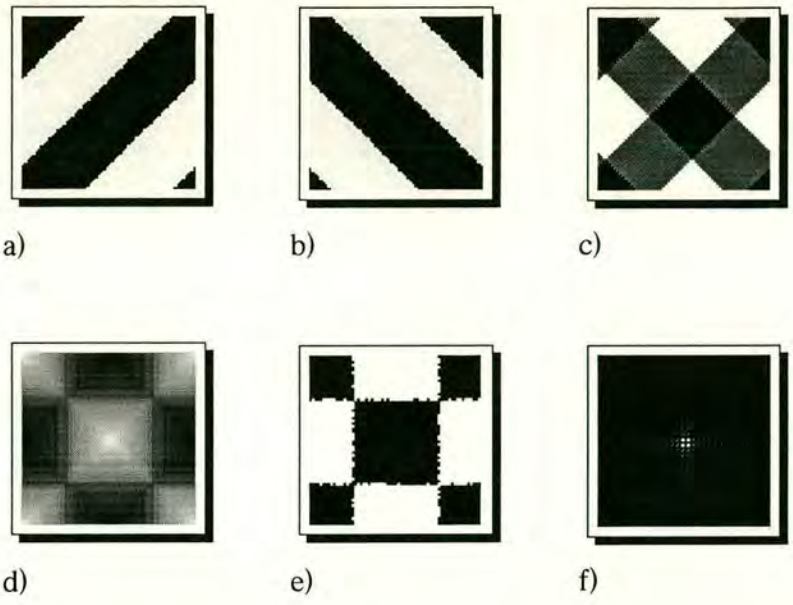

Fig. 4.13. (a,b) Two 1-dot gratings
(c) Summary mask (a+b)
(d) The autocorrelation of mask (c)
(e) The final solution (binarised mask d)
(f) The output of mask (e).

The output of this final mask is shown of fig.4.13(f), and it is the same as for the master mask in missing pixel section of this chapter (see fig. 4.1).

Now we will replace the addition operation (mask 1 + mask 2) by an operation similar to what we did with missing pixel masks (mask 1 + mask 2 + mask 1). This allows us to distinguish between two different 'or' areas. The random filling of the 'or' areas proportionally to the coefficient 0.5 gives us the same binary mask after autocorrelation and binarisation procedures. Filling the 'or' areas differently results in a sequence of patterns whose shape is a linear approximation to the weighted 2 pixel masks. The Fourier transforms of these patterns are also solutions for weighted intensity distribution of two pixels. A similar result can be obtained if instead of random filling of the 'or' areas we simply change the intensity of their grey levels. For our models the 0 phase shift corresponds to 0 and π is 255. Thus 127 will

correspond to the 0.5 coefficient of the fill-factor. Experiments show that it is possible to apply missing pixel concept to this model and vary the intensity of one of the dots by changing the intensity of the grey levels of 'or' areas and then using the method of autocorrelation and binarisation described above. This approach works well. Fig.4.14 and fig.4.15 show two solutions for coefficients .1 and .05. The patterns are ideal holograms which we can get using conventional hologram design techniques.

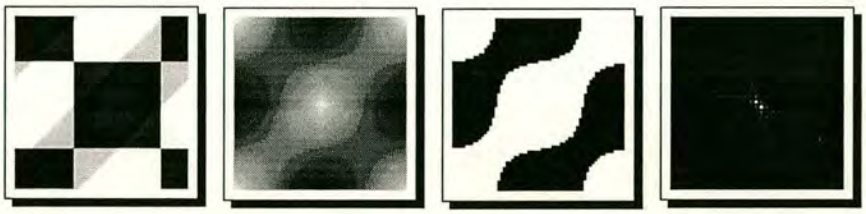

a) b) c) d)

Fig. 4.14 Combined holograms for missing pixel pair (coeff. = 0.1)

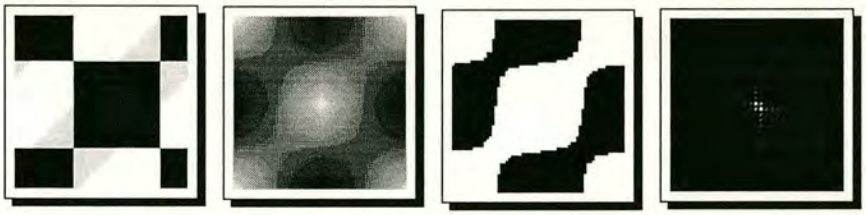

a) b) c) d)

Fig. 4.15 Combined holograms for missing pixel pair (coeff. = 0.05)

a) A master and missing pixel holograms added together with a required coefficient of the grey levels intensity.

b) An autocorrelation of mask (a)

c) A final hologram (binarised mask b)

d) A Fourier transform of (c).

The graph in fig.4.16 summarises the results of this experiment. The experimental curve can be relatively well approximated by the expression 12.5/(x + 0.4). The total calculation time for any of such masks is much less than a second compared to 1-2 minutes of a proper design. Having obtained such good results it is tempting to look if this method works for more than two pixels. Due to the binary nature of the holograms, no theoretical study was undertaken. The features of combined holograms were investigated experimentally using digital simulation and optical results.

Experiments showed that it is possible to calculate holograms for outputs numbered up to 8 pixels using the combinations of simple gratings. The efficiency of such holograms is only 2-4 percent less than of an optimised one and the calculation time is hundreds times less. However there is a tendency for the uniformity of the output pattern to decrease. As the number of output pixels grows the coefficient of filling 'or' areas becomes smaller. The following sequence of coefficients is found experimentally to work quite well for calculation of holograms of up to 6 dots output:

Number of dots	Coefficient
2	0.5
3	0.375
4	0.325
5	0.300
6	0.280

The uniformity for 2-3 dots holograms does not exceed 2-5%. However the uniformity value for 6 dots may vary as much as 10-25%. In many optical systems it would not be a significant difference and the speed of calculation of such hologram is much more important. The time needed to design 6 dot output hologram on a Sparc station 2 is about 2-4 minutes. And the time the algorithm spends to calculate a quick hologram using our method is less than 1 second.

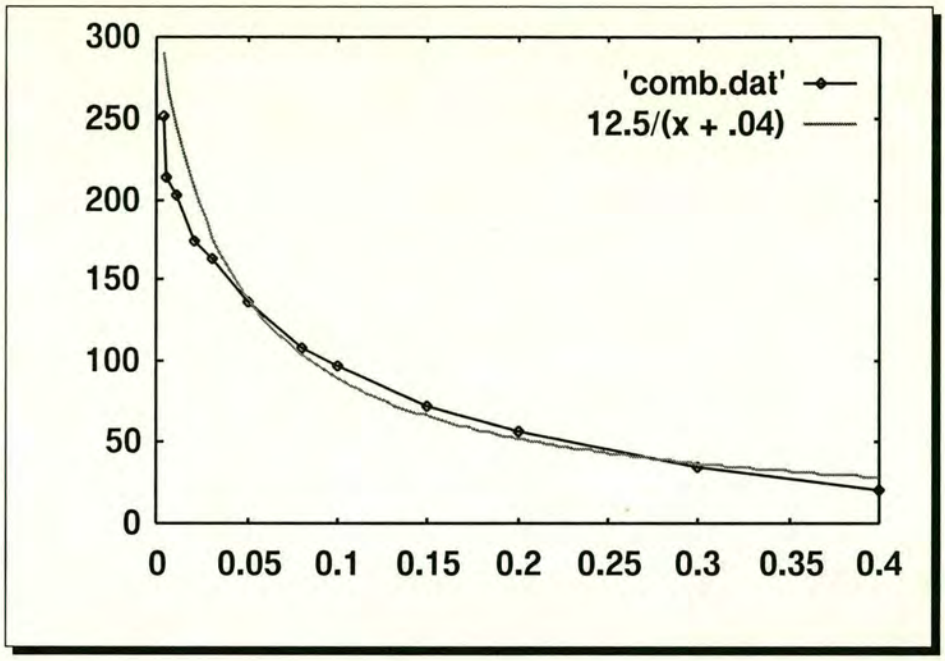

Fig. 4.16 Dependency of the intensity of output spot on the grey level value of the 'or' areas for missing pixel pairs.

In order to demonstrate this technique we designed 8 gratings those outputs are single dots in different positions. The set of all 8 dots is shown in fig.4.17.

Fig. 4.17. A set of 8 dots, for each of those a simple grating structure was designed.

A computer program to manipulate any four of eight gratings was written. Given as arguments the names of a combination of any four files it creates three files which

are holograms of 2, 3, and 4 pixel outputs. The optical results for two combinations of four pixels are showed on fig. 4.18 and fig 4.19. The first one is a solution for a combination 0, 2, 4, 7.

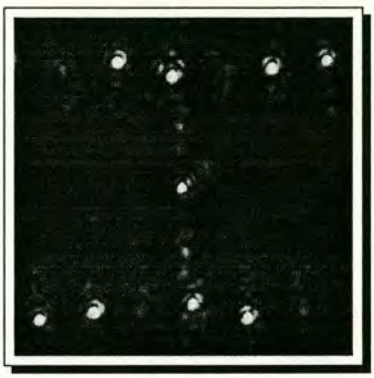

Fig. 4.18 An output of quickly designed hologram for combination 0, 2, 4, 7.

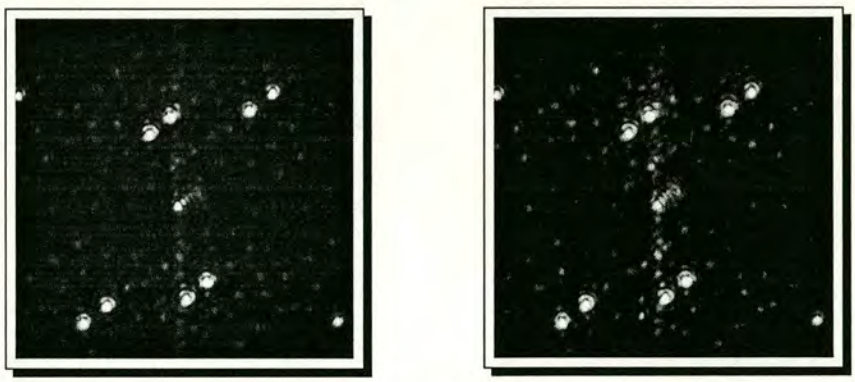

Fig. 4.19 (a, b)

(a) - output of properly designed hologram for 1, 2, 4, 6 combination

(b) - output of quickly designed hologram for the same combination

As it can be seen from the figures the optical quality of the two outputs is acceptable for many applications. It is interesting to compare the outputs of a properly designed hologram and its quick analogue. The calculated efficiency is nearly the same (about 82 %). The distribution of noise clouds is almost identical in both cases which suggests that the solutions found are in the same global minimum.

With the increase of number of output dots this technique produces holograms of the nearly maximum efficiency, but the uniformity becomes poorer. A hologram of 6 dots output may have the uniformity of the output varying from 5% to 15%. Being quite acceptable for some optical systems (optical interconnects), such uniformity is not satisfactory enough for other applications (neural networks). It seems that a great deal of the degree of accuracy of the uniformity depends on the distribution of background noise of the initial masks outputs. The most important criteria is that the symmetrical replications must not overlap with any of the target output spots. The positions and intensities of any of the replications can be analytically calculated for such simple holograms as one dot fan-out gratings. The replications are always symmetrical to their main images. For this reason our set of 8 holograms produced 8 dots which are not symmetrical.

Conclusion.

In this chapter I introduced two approaches to fast design of binary holograms. The missing pixel method can be used when non-uniform dynamically changeable fan-outs are required. The method of combined holograms is mainly useful when it is necessary to dynamically change the configuration of uniform fan-out. The experiments showed that these two methods can be applied very effectively for small fan-outs (up to 8 dots). The method of missing pixel is implemented using simple binary logic which contributes to the design speed increase, however it requires N^2 predesigned holograms. During the design the holograms can be scanned up to N^2 times and thus the design speed is inversely proportional to N^2.

The method of combined holograms can be used without predesign of initial holograms. The expensive autocorrelation operation is used but the number of mask scans is proportional to N thus the speed is inversely proportional to N. The

efficiency of the designed holograms is similar to the efficiency of the optimised structures and in fact similar optimal minima are found using both combined and conventional methods.

Both methods for fast design offer great speed advantage (100-1000 times) over the conventional methods that enhances significantly the range of applications for dynamic binary holograms. These two methods also provide nearly the optimal efficiency performance for the holograms of small fan-out.

Chapter 5. Visual methods of design. Holomaster 1.

Introduction

The design of holograms is a complex process which involves much preparation. Firstly, we have to design a target or half of a target if it is symmetrical. The only reasonable way to do this is to use one of the available drawing programs to create a target file. If non-uniform fan-out is required, this gives some additional difficulties. Suppose we have a target with all the dots of equal intensities. In this case we have to think of some way to associate the array of intensity values to the array of target dots. The other possibility is to design a grey level target. It is easier but we must be able to know the numeric values for grey levels in order to do exact calculations for a hologram.

After the target is designed the next step is to choose the type of hologram we need and calculate an appropriate pattern. Different types of holograms require different methods of design. Therefore we have to either provide several programs to implement these different methods or to incorporate all of them in one package.

The large numbers of holograms sometimes required for the design of dynamic optical systems requires sophisticated file handling methods.

Simulated annealing is a process that requires a number of parameters to be tuned over time. It is relatively difficult to estimate the right values of the starting temperature and the speed of its decrease. Tuning of the annealing may be improved by a visual representation of the process of creating the mask. Most of the methods of connected holograms design require a visual feedback between a computer and a user.

In other words we need a sophisticated software tool which provides interactive visual control, drawing and storage facilities and the ability to use different hologram design techniques in the same package. For this purpose I created the hologram design package called "Holomaster 1" [50, 51.] It supports the design of 5 basic types of holograms:

1. Binary holograms. Introduced by Dames et al [7] in 1991. This basic technique is based on the simulated annealing scheme.
2. Four-phase holograms [7]. Calculated using the same principles as binary holograms.
3. Connected holograms [49]. The electrically switchable holograms designed with a constrained growing technique that ensures electrical conductivity.
4. Pseudo four-phase (sandwich) holograms [67]. These are asymmetric binary phase holograms. The symmetry is broken by using a sandwich structure of a random binary fixed hologram overlaying a binary hologram which is calculated in respect of its overlay.
5. Connected pseudo four-phase holograms [49, 67] incorporate features of connected and sandwich structures.

All of these types of holographic beam splitters have been discussed earlier in this study in chapters 1-3. Holograms can be designed either to produce uniform or

weighted fan-out. The basis of the program is its four main windows: the process window, the mask window, the target window and the drawing window. The process of simulated annealing can be observed and controlled dynamically as the designing process is running. This helps a great deal when implementing the method 4 of connected holograms design (see chapter 2). We can visually control filling in the blank areas while temporarily switching to the non-continuous algorithm. With a built in drawing program it is easy to draw and delete bridges. It helps us also to examine a mask for continuity using a floodfill facility. The floodfill function considers not the ordinary but tiled mask and acts accordingly. A user can move images between the drawing window, the mask window and the target window via the program's graphics clipboard which also has its own window. It is also possible to load and store images with the file window. It is easy to change the simulated annealing parameters with two scale bars as the program is running. We can also switch between the normal and the "edge" algorithm pressing a toggle button in the process panel. It is also easy to design required target patterns with a drawing program and preview the actual symmetrical output of the future hologram. The real strength of Holomaster is that all the design techniques and parameters and even holograms and targets can be changed dynamically during the design process.

As the program runs we can observe updates of the current mask and compare it to the best found solution. At the same time we control the uniformity and efficiency values and see the actual output Fourier transform (FT) of any of the masks. It is also possible to see the FT of sandwich hologram as a whole or a FT of either a master mask or its overlay separately. Holomaster is easy to use. It does not require an expert to create high efficiency holograms. It also helps the user learn many features of designed holograms and this is very important because holograms created using stochastic methods of optimisation can not always be described analytically.

Holomaster was written for X-Windows using Motif and X-Designer. I also used an image library written by W.Hossack. In the next section I will briefly describe the main windows of Holomaster and then explain how to use it.

Using Holomaster 1.

Main panel.

The master window which holds all the icons of other windows (see fig. 5.1)

Fig. 5.1. Main window includes menus and a toolbar.

All main windows can be invoked or closed by clicking appropriate buttons of the main panel. The process icon (a boiling pan) is also animated when a process of hologram design is running. The pull down menus provide some additional facilities such as installing a process to the background or picking up a running process, opening the environment configuration which was saved in a file and others.

Main process window.

This window is the main hologram design window (fig. 5.2). It is divided into four areas:

1. Parameters. With two options menus installs the type of calculated mask and the type of the target, uniform or non-uniform.
2. Controls. A set of push buttons to control the process of hologram design.
3. Display and annealing. Several labels show the current state of the design process. There are also two sliders to control the annealing temperature value and its dropping speed.
4. Initial conditions. Installs initial parameters for an annealing process and some others.

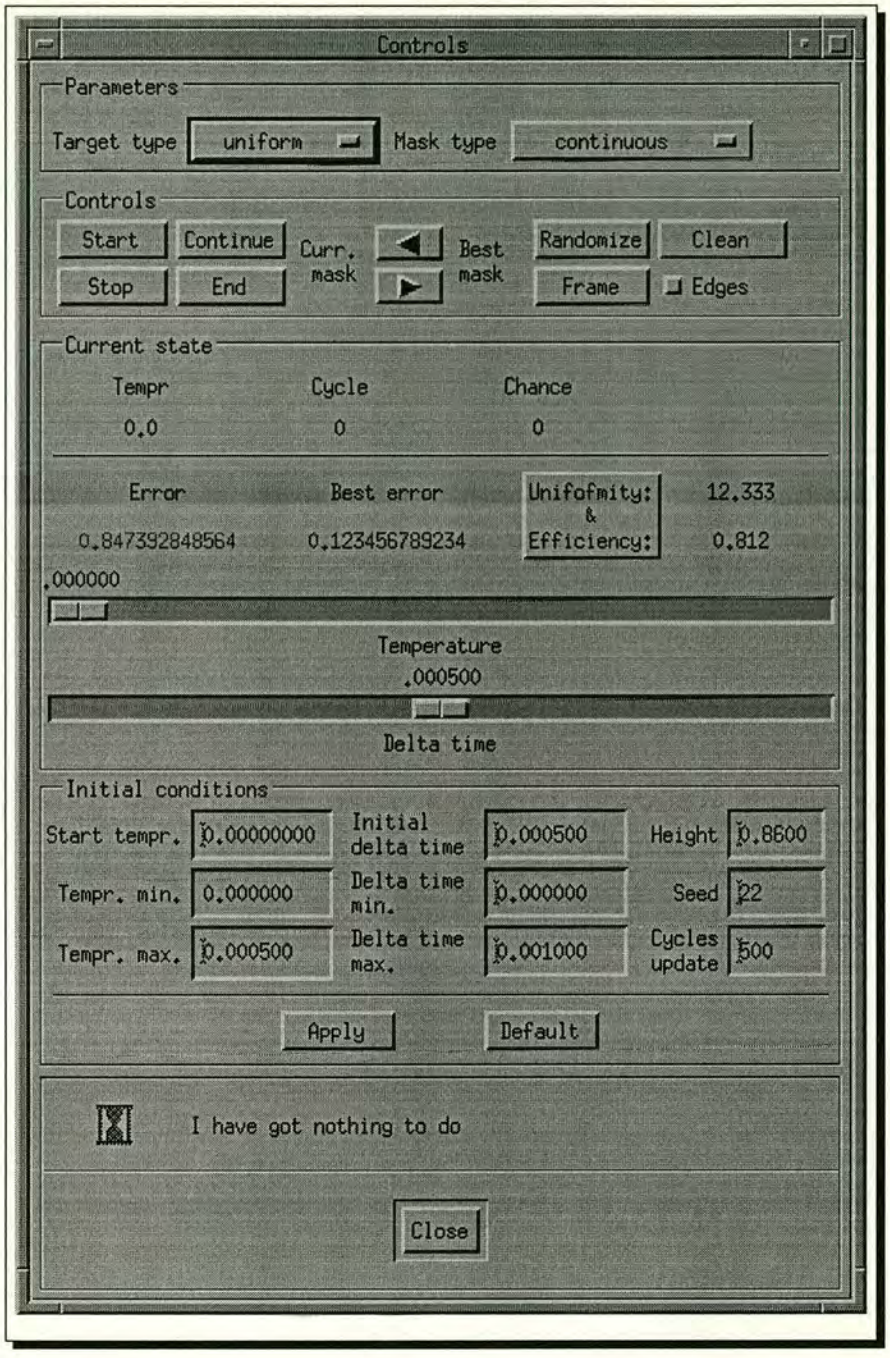

Fig.5.2. The 'process' window. A main control window of the program.

Mask viewer.

Consists of two drawing areas and some control buttons and option menus (see fig. 5.3). It shows current and best holograms, overlay and a sandwich of current or best hologram with an overlay. Masks can be copied into each other using arrows.

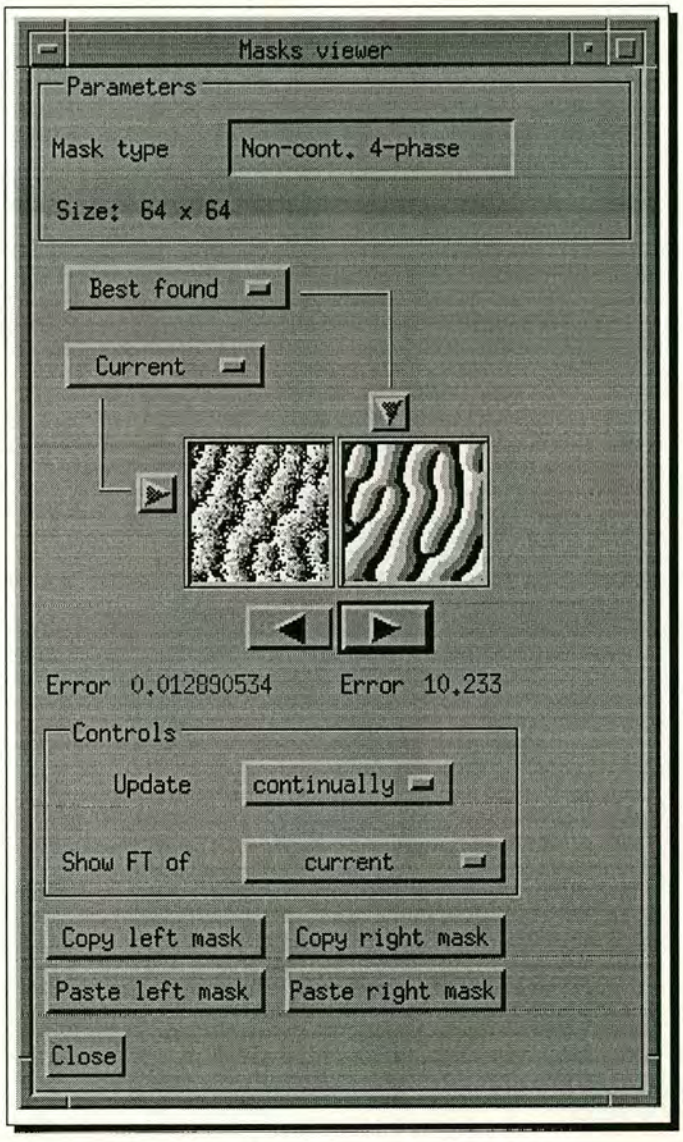

Fig. 5.3. Mask window.

The 'Controls' section of the mask window regulates the frequency of right mask update and defines which picture's Fourier transform will be shown in the target window. .

Target viewer.

Consists of two drawing areas and some control buttons and option menus (see fig. 5.4). It shows the target pattern and the Fourier transform of one of the masks defined in the mask window.

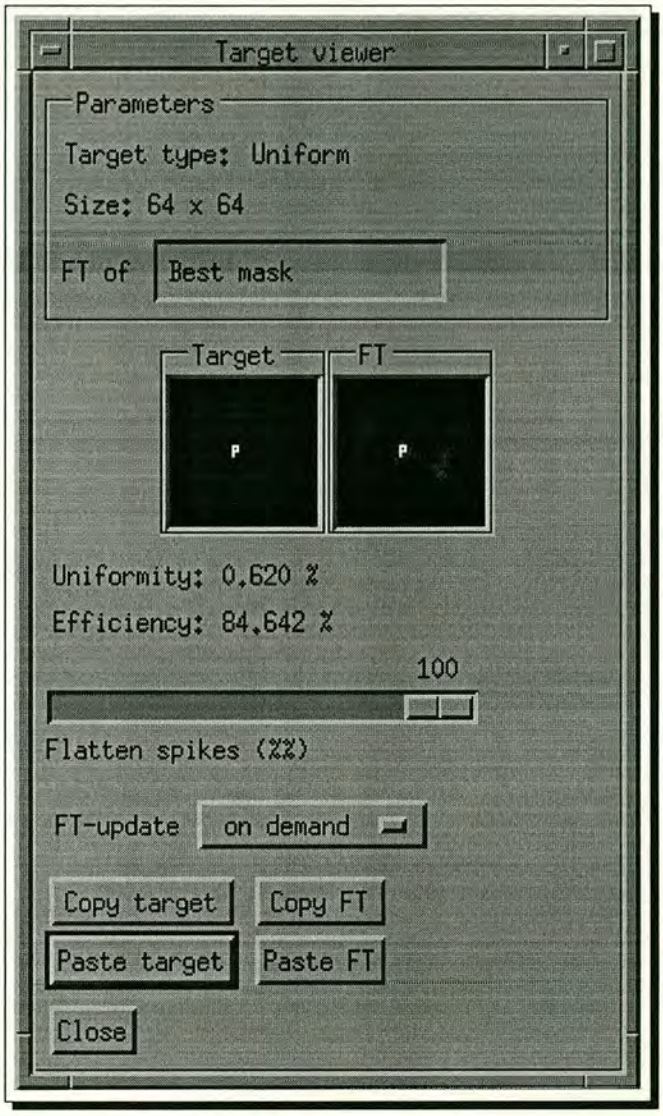

Fig. 5.4. Target window.

The Fourier transform of five masks (combinations of masks) can be taken: current mask, best mask, overlay, current+overlay and best+overlay. With a slider it is possible to regulate a signal-noise ratio by lowering the intensity of the highest spikes and to see the distribution of error clouds.

Edit window.

This is a drawing program with unique features to support the design of the targets and masks (fig. 5.5).

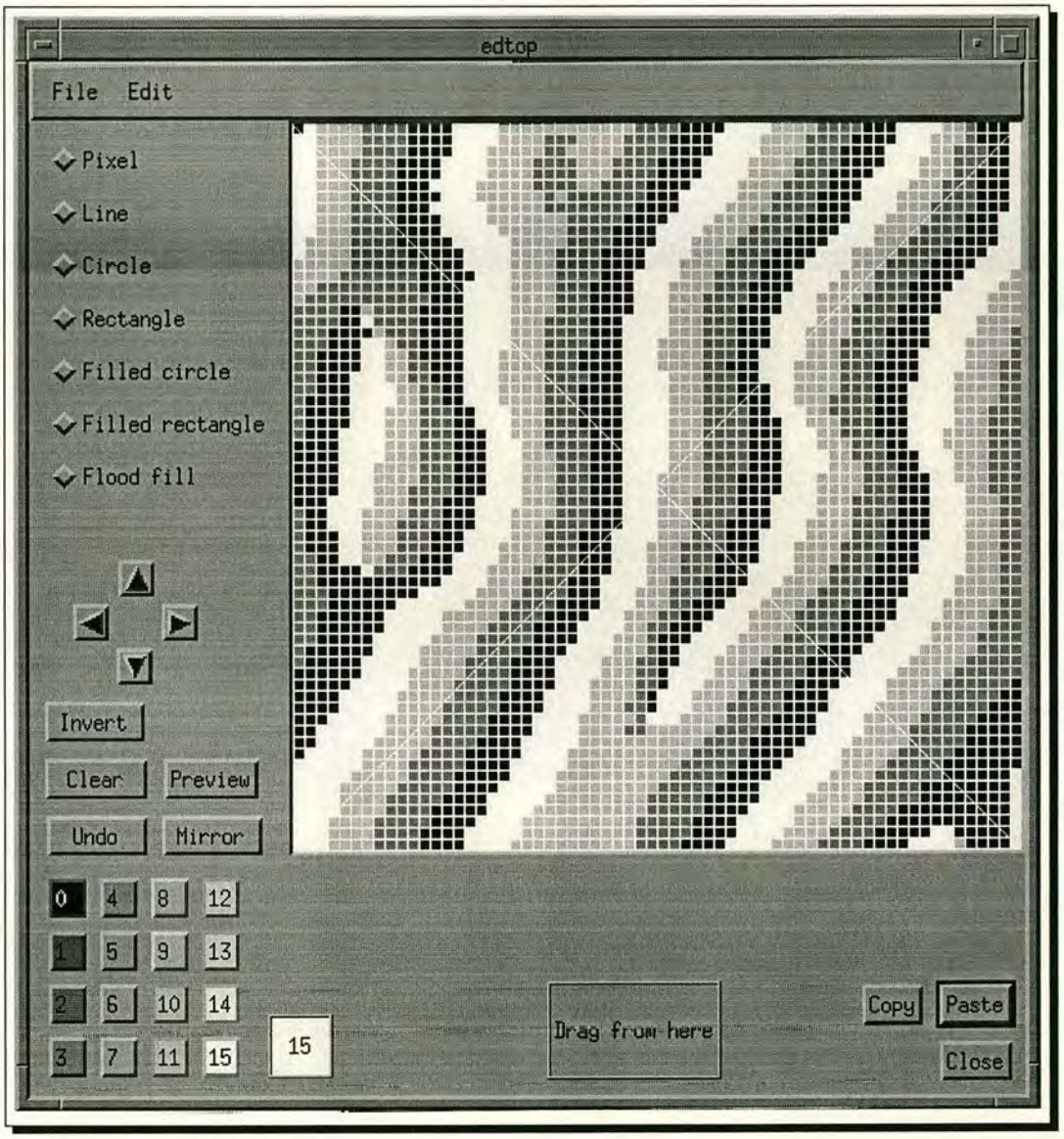

Fig. 5.5. Edit window.

The edit window supports basic features for drawing programs: line, rectangle, circle, filled rectangle and filled circle. It also provides some unique features specially created for designing holograms:

- Shift. The image can be shifted in any of four directions using arrows. As the program considers an infinite number of periods in the edited hologram the shift operation does not really change the image structure. This feature is very helpful when we want to design a target with a symmetrical image which will be a continuation of the desired pattern. It helps to analyse the stability of sandwich hologram prior to the misalignment of an overlay.

- Floodfill. This is a feature that is standard for many drawing packages. However our floodfill considers that pattern has an infinite number of periods therefore it works differently. Floodfill is used when checking a pattern for connectedness. It ensures that a tiled version of edited pattern is electrically connected.

- Mirror. This feature helps creating images symmetrical to the y-axis.

- Preview. This is a very useful feature when creating a target. Usually for binary holograms we must create a half of a target and consider a symmetrical conjugate image as well. So the preview shows where this image will be in the system. It makes it much easier to design symmetrical targets.

There are some additional windows as well:

Graphics clipboard window.

The graphics clipboard is a medium for transferring images between mask viewer, target viewer and edit window. By pressing the 'XV' button we can invoke powerful image processing package called 'xv' (John Bradley, © 1989, 1994) and analyse in detail the structure of the Fourier transform of a designed hologram.

Memo window.

A simple text editor to help the user memorise the process of hologram design and save it. Some of the visual methods described earlier require complex tactics and in each particular case it can be unique.

File window.

File manipulation window. Loads files into the graphics clipboard and saves them from it onto the hard disk.

Tutorial.

The process of hologram design usually involves dealing with many files. It is recommended to create a separate directory for each design procedure.

Basic binary holograms design.

Type *hm&* to load the Holomaster as a background process. The main panel will appear with the icons of most of the program's windows. Invoke editor and graphic clipboard windows by clicking their buttons. The editor's drawing field is of 64x64 pixels size. Draw a simple curve in the upper half of the drawing field. Click 'preview' button. The symmetrical image appears. This feature is very important if we want to create a binary phase hologram which always produces a symmetrical output. That is if the symmetrical output needs to be made we can calculate the mask for only the half of the target and save computer time for the calculations.

Now press 'undo'. The symmetrical image disappears. Try pressing arrows. Each time the image shifts in one of four directions. It is easy to put the image in the position when its symmetrical replication will touch it so that two images appear to be one continuous curve. Press 'undo' and 'copy'. The image now is copied into the graphics clipboard. Now invoke the process, mask, and target windows. Press 'paste target' button in the target window. The target picture will then be drawn in the left window. Take a look at the mask window. Two drawing areas are filled in with the

same random pattern. This is the pattern we are going to start our design from. Press 'randomise' button in the process window. The pixels distribution of the left drawing area in the mask window will change to another random pattern. Pressing right arrow either in the process window or in the mask window will copy the left mask into the right one. The left arrows do the copying the other way round. Now choose from the 'mask type' option menu 'non-cont binary'. Press 'start'. The hologram starts to form in the left drawing area of the mask window. From time to time the right area is updated when the best solution is found and the program has run the defined number of cycles. As the algorithm progresses try pressing 'Uniformity & Efficiency' button in the process window. You will see the increasing of efficiency value which grows towards the 'height' coefficient defined in the 'Initial conditions' section of the process window. Simultaneously the right drawing area of the target window is updated and you can see the result of the Fourier Transform of the current mask there. Gradually it resembles more and more the target which we defined earlier. The main difference is that it has the symmetrical replication situated in exactly the same place as we have designed before. It is easy to see when the algorithm has found a good solution. The Fourier transform image should look similar to the defined target. Also the calculated mask must be a contrast picture and should not contain many single pixels on it. If the calculated target is uniform the uniformity value showed both in the process window and the target window should be within 0.5-4%.

The efficiency should take the value close to the height defined in the initial conditions section of the process window. If there are still single pixels in the final solution it means that the initial height is too low. Try to redefine it up to 90 % (0.9) and for 1-2 pixels output up to 100% . All the time the algorithm is working the process window's icon in the main panel is animated. This is useful when calculating big masks with all windows hidden. Now press 'copy right mask' button. The mask is copied into the clipboard. Press file icon in the main panel. Now type the file name of the mask in the file window and press 'save from clipboard' button. If your system has 'xv' - image processing program you can benefit from it by using it from within the Holomaster and doing closer inspection of the image which is currently in the

clipboard. This is done by pressing 'xv' button in the graphics clipboard window. This feature is especially useful when looking at Fourier transforms. The mask solution you have found is not the unique one. It is likely that there exist some more successful patterns t. If you are satisfied with the output then it is fine. Otherwise you could try again with the simulated annealing facilities of the program. Press the 'randomise' button in the process window a few times. Each time you will get a different random starting pattern. Press 'start'. Try moving the two sliders which represent the current temperature value and its rate of cooling speed. It takes much longer for the algorithm to converge with the temperature not equal 0 but there is a chance that you can find better local minimum using this feature of the program.

You can also design a hologram which produces non-uniform output (half tones). Change 'target type' option in the process window to 'non-uniform'. Open the editor. Try to create a simple figure as you did before choosing different colors. Now repeat the whole procedure again.

Connected holograms design.

The steps for the design of a connected mask are similar to the ones described before. There are some differences though. First of all it is quite important to choose a starting pattern. It often happens that you will need something different from a random one. Press 'frame' button. The single lined default frame is drawn in the left drawing area at its edges. This is a good pattern to start with. Choose 'continuous' from the option menu. Press 'start'. You will see the mask 'growing' towards the centre. Starting from such a frame ensures that there will not be too many extra connections in the final solution. If you are lucky the mask will be developed all over the drawing area. However it happens quite often that the algorithm is stuck and there is a black blob of undeveloped area somewhere in the centre of the mask or sometimes you can see even two or three such spots. Of course you can start again but you are not guaranteed that next time the result will be better. It is time to use the drawing facilities of the Holomaster. Press 'stop' then 'copy left (right) mask'. Invoke

the drawing window and press its 'paste' button. Now use your imagination and try to draw a few 'bridges' across black areas of the mask. Copy the drawing back into the mask window. Press 'start'. Usually the algorithm succeeds and the black areas are filled with the rest of the hologram pattern using these narrow 'bridges' like crystals use a thread for growing. Copy the mask to the drawing window. Choose one of the grey colors and press floodfill. Then click on the one of the white areas of the mask. All the white space of the mask will be filled with a chosen color. This shows that the all these areas are connected. The floodfill algorithm fills the mask as if it was tiled and there were the same patterns surrounding the original one. Now press 'undo'. Choose black color and try to fill with it some extra connections between the same areas. This will improve the mask efficiency. From time to time check the continuity of the mask with the floodfill feature. When there are few connections left and the mask is still continuous copy it to the mask window and press the 'start' button in the process window for the last time. This technique lets you get a continuous solution of the quality which is close to the non-continuous binary analogue.

The faster alternative is to start with the random pattern mask. It is not continuous but if the algorithm runs for a long time it connects all disconnected areas. There will not be a non-developed blob in the centre but the final pattern can have far too many extra connections which contribute into the DC spot error of the final Fourier transform. If you are patient enough you can of course erase most of them with the facilities of the drawing window and then apply the algorithm to the changed mask again. By repeating this technique a few times you can achieve a good result.

Four-phase hologram design.

The design of the four phase holograms is similar to the design of binary non-continuous holograms. The only thing you have to do is to change the mask type to 'four-phase' with the option menu of the process window. A four-phase hologram does not produce a mirrored output. This gives the designer more flexibility in using the whole area of the output field.

However the binary holograms are much easier to fabricate. Therefore when the absence of a symmetrical output is not essential the binary solutions are almost always preferred.

Pseudo four-phase (sandwich) holograms design.

This type of holograms is a synthesis of binary masks which produce pseudo-four phase hologram. Usually there is a master pattern with phase shifts 0 and π and the overlay mask with phase shifts 0 and $\frac{\pi}{2}$. The overlay is not changeable. It is defined only once when the program starts. Quite often it is a random pattern. However there could be different distributions. The master mask is designed in a similar way to a binary one with the difference that it is calculated assuming the contribution from the overlay. The overlay can be seen in the mask window's left drawing area which can show the master mask, the overlay and the 4-phase solution of master+overlay. In the right drawing area you can see either the best found mask (master mask) or master+overlay. You can also choose the pattern whose Fourier transform you wish to see in the target windows right drawing area by choosing the appropriate option in the 'Show FT of' option menu. The default pattern for the overlay is an arbitrary one. Choose non-continuous pseuso-four-phase type of the hologram with the 'mask type' option menu and repeat the previous steps for binary mask design.

You can also design a *connected pseudo-four-phase hologram* using the same technique.

All the holograms may be designed to produce either uniform or non-uniform output.

Chapter 6. Discussion and conclusions.

In this chapter I discuss the performance of the methods of holograms design developed in this study and possible improvements. I also highlight the perspective directions for future work.

Dammann gratings.

The incorporation of simulated annealing in the design of Dammann gratings proved to be very successful for finding the optimal one-dimensional solutions. The simulations and the optical results nearly reached the theoretical limits. However the increase of computer power for the last 3-5 years created new possibilities for using a more advanced 2-dimensional relief technique proposed by Dames et al. and some other methods [29]. The severe limitation of Dammann gratings is that they can only produce rectangular arrays of spots and therefore can be used in a very limited number of applications. Even though the design speed of Dammann gratings is much faster than that of Dames's holograms they cannot compete with the latter in other performance measures.

Two dimensional surface relief holograms.

These holographic structures have been successfully substituting Dammann gratings during the last 3 years. Most of my study was devoted to the design of varieties of these holograms. The outstanding performance (the efficiency nearly to the theoretical limit) and flexibility makes them ideal for many applications especially in such dynamic fields as optical communications and artificial neural networks. Various methods of increasing the speed of design have been developed by us and others. The most effective appear to be the geometrical methods based on the symmetry features of the holograms and using the power of parallel computers. For the peculiar types of these holograms such as continuous and sandwich solutions all these methods can be applied too.

The **connected holograms** are the promising fast switching devices. There are several difficulties in their design due to the extra constraint of connectness. However with the help of visual methods it is possible to create connected holograms of large fan-out. The future research of connected holograms should involve their fabrication and finding suitable applications.

The **sandwich holograms** are powerful devices for dynamic optical systems. The difficulties of fabrication of sandwich holograms basically depend on the difficulties of fabrication of an overlay which is placed on top of an SLM. With various overlays developed by the author which are partially or completely tolerant to misalignment the fabrication process of these holograms becomes much easier and the overlays can be made removable, that secures the universality of the SLM device. I have only investigated the behaivior of sandwich holograms using computer simulations. Future work would involve fabrication of a real device and

further experiments and calculations to determine how the quality of the output depends on the distance between the master mask and its overlay.

However no matter how good the discussed holograms are, they all suffer one major shortcoming which is the long time required for their design. This leads to the necessity to predesign and store a large number of holograms (could be hundreds and even thousands) if we want to update them rapidly on an SLM in a truly dynamic optical system. Generally speaking using of any of the developed speed increase methods does not fundamentally change the situation.

Fast holograms.

I can see a great importance of the thorough investigation of the **missing pixel** and **combined holograms** methods that I developed and presented in chapter 5. As far as author is aware these ultra fast methods have not been reported anywhere else. The ability to increase the design speed up to 100-1000 times creates absolutely new areas of the applications for such holograms. Using these methods we can dynamically create holograms for given output without predesigning process. Even if the fan-out of such holograms is limited to 8 spots this technique can be indispensable in hundreds of applications in such areas as neural networks or optical interconnects. The further research can be carried on towards the creation of a solid theoretical background of found effects (especially for combined holograms technique) and increasing of the number of output spots. It is very important to devise the mechanism of compensation of noise pixels in the output plane for combined holograms. If this is done I believe the number of output spots can be increased dramatically. The final aim of research in this area should involve the development of real and powerful dynamic devices.

Software.

Such successful yield of results and ideas in this study could only be achieved with the help of computer power and the visualisation of the hologram design process. The **software package** for holograms design called **"Holomaster 1"** is my response to today's requirements in computer generated holography. The discussed methods and new types of holograms should be all added to the "Holomaster" package in the future. I believe that there is scope for improvements in the implementations of missing pixel and combined holograms algorithms to achieve even greater performance. These techniques are quite complex from a point of view of a computer programmer. A good library of classes must be created so that it is possible to get all the advantages of instant dynamic holograms design.

Other directions.

There is a countless number of ways for developing the field of CGH. As the fabrication technology becomes more and more advanced it becomes possible to create very complex surface architectures. This gives the possibility of making complex holographic elements which combine several optical units in one or create white light CGH. It is also interesting to look at the theory and the potential of the holographic elements with size of the minimal elements close to the wavelength of light. The 3-D holograms is another area for implementation of the above described iterative principles of holograms design.

Appendices.

A. Fast simulated annealing method.

Simulated annealing is a stochastic strategy for searching the ground state [55, 45]. A fast simulated annealing (FSA) is a semi-local search and consists of occasional long jumps [1]. The cooling schedule of FSA algorithm is inversely linear in time which is fast compared with the classical simulated annealing (CSA) which is strictly a local search and requires the cooling schedule to be inversely proportional to the logarithmic function of time.

When a cost function has C has a single minimum, the unique ground state can be found by using method of gradient descent. However, when C has multiple extreme, the optimization technique that allows hill climbing for escaping from local minima is needed. For illustration of the process consider a boll rolling over a hilly terrain inside a box. It is necessary to shake the box gently enough that the ball cannot climb up the global minimum valley and vigorously enough to escape from local minimum valleys.

A sufficient condition for the convergence to the global minimum has been proven in 1984 by Geman and Geman [12] for the classical simulated annealing (CSA) based on a strictly local sampling. It is required that the time schedule of changing the fluctuation variance, described in terms of the artificial cooling temperature $T_a(t)$, which could be different from the true thermodynamic temperature T, is inversely proportional to a logarithmic function of time given a sufficient high initial temperature T_0.

$$T_a(t) / T_0 = 1/\log(1 + t)$$

Such an artificial temperature cooling schedule is too slow to be practical. Instead, for arbitrary $T_0 \neq 0$ the FSA has

$$T_c(t) / T_0 = 1 / (1 + t)$$

The Simulated Annealing algorithm requires a number of time tuning of parameters. It is rather difficult to estimate the right values of the starting temperature T_0 and the speed of its decreasing because these values vary significantly for different tasks.

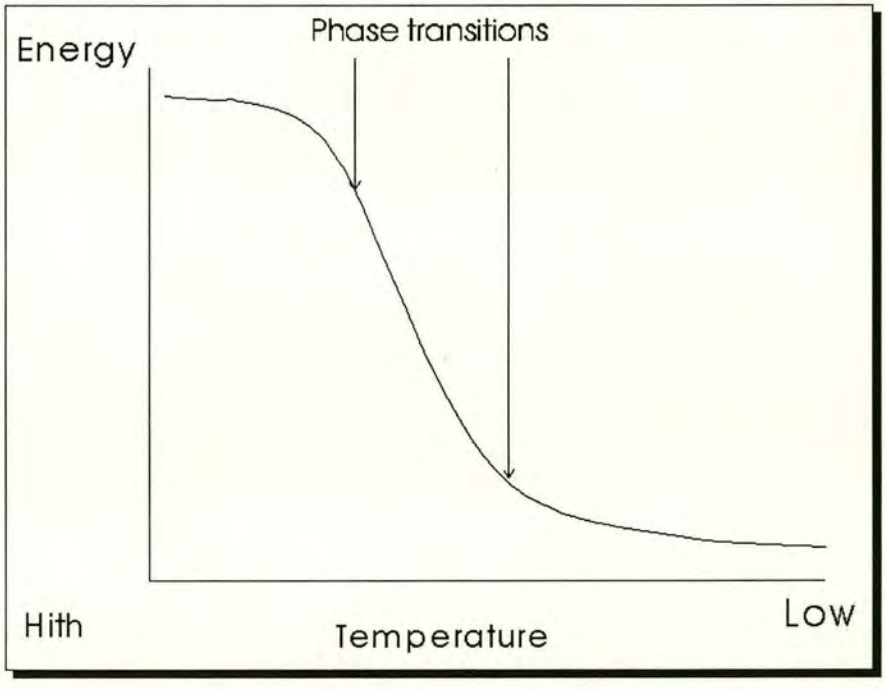

Fig.A.1 simulated annealing behaviour.

The behaviour of simulated annealing algorithm is sketched on fig. A.1. Fastest convergence to a good global minimum will occur if the temperature is decreased in such a way as to spend most of the time in the linear part of the graph. However, actually determining the transition point in practice is difficult and for each particular holographic pattern the values of starting temperature and the optimal speed of it's decreasing will vary significantly. Tuning of the annealing may be improved by a visual representation of the process of the mask creation which is described in details in chapters 2 and 5.

.

B. Continuous holograms.

Predefined table.

The predefined table is calculated to save the computer time to analise if the pixel which is taken randomly on the hologram plane can be flipped

```
char table[] = {
        1,1,1,1, 1,0,1,1, 1,1,1,1, 1,0,1,1,
        1,0,1,0,  0,0,0,0, 1,0,1,0, 1,0,1,1,
        1,1,1,1, 1,0,1,1, 1,1,1,1, 1,0,1,1,
        1,0,1,0, 0,0,0,0, 1,0,1,0, 1,0,1,1,

        1,0,1,0, 0,0,0,0, 1,0,1,0, 0,0,0,0,
        0,0,0,0, 0,0,0,0, 0,0,0,0, 0,0,0,0,
        1,0,1,0, 0,0,0,0, 1,0,1,0, 0,0,0,0,
        1,0,1,0, 0,0,0,0, 1,0,1,0, 1,0,1,1,
```

```
1,1,1,1, 1,0,1,1, 1,1,1,1, 1,0,1,1,
1,0,1,0, 0,0,0,0, 1,0,1,0, 1,0,1,1,
1,1,1,1, 1,0,1,1, 1,1,1,1, 1,0,1,1,
1,0,1,0, 0,0,0,0, 1,0,1,0, 1,0,1,1,

1,1,1,1, 0,0,0,1, 1,1,1,1, 0,0,0,1,
0,0,0,0, 0,0,0,0, 0,0,0,0, 0,0,0,1,
1,1,1,1, 0,0,0,1, 1,1,1,1, 0,0,0,1,
1,1,1,1, 0,0,0,1, 1,1,1,1, 1,1,1,1 };
```

A set of functions to implement continuous algorithm.

Before the error reduction mechanism is used it is necessary deside whether the chosen pixel can be flipped or not. The set of following functions can be used for this purpose.

SQSIZE is a number of pixels in a hologram. Must be calculated before using the functions.

```
// bow() - a function to determine a current pixel's state

int bow(int which, float* image,)
{
  if(image[which])
    return 1;
  return 0;
}

// east(), west(), north(), south() - returns a number of a neighbor pixel
//   of given pixel
```

```
int east(int which)
{
  if((which + 1) % SQSIZE == 0)
    return(which - SQSIZE + 1);
  return(which + 1);
}

int south(int which)
{
  if(which / SQSIZE >= SQSIZE - 1)
    return(which % SQSIZE);
  return(which + SQSIZE);
}

int west(int which)
{
  if(which % SQSIZE == 0)
    return(which + SQSIZE - 1);
  return(which - 1);
}

int north(int which)
{
  if(which / SQSIZE == 0)
    return(n_sq - SQSIZE + which);
  return(which - SQSIZE);
}
```

```
// round_word() - a  fuction that calculates a 8-bit number by the inspecting the
// neighborhood of a given pixel. This number is  an entrance of precalculated table
// shown above.

int round_word(int which)
{
 int res = bow(east(which));
 res += (bow(east(south(which)))     << 1);
 res += (bow(south(which))           << 2);
 res += (bow(west(south(which)))     << 3);
 res += (bow(west(which))            << 4);
 res += (bow(west(north(which)))     << 5);
 res += (bow(north(which))           << 6);
 res += (bow(east(north(which)))     << 7);
 return(res);
}

// CanFlipToBlack() and CanFlipToWhite() functions which take the desision if the
//given pixel can be flipped withut breaking the conneciton of the pattern

int CanFlipToBlack(int which)
{
  return(table[round_word(which)]);
}

int CanFlipToWhite(int which)
{
  if((0xaa | round_word(which)) == 0xaa)
    return(0);
  return(1);
}
```

C. Amplitude-phase image transform.

```
/* ****************************************************************
  A fragment of C-code which detects the number of gray levels of the
  picture, then transforms the amplitude picture into the phase one with
  n equally spaced levels.  This code is essential for many functions
  of hologram design.
****************************************************************/

#include <stdio.h>
#include <stdlib.h>
#include <complex.h>
#include <math.h>


void rewrite_image(float *dpoint, complex *cpoint, int  size)
{
  int i, count;
  unsigned char  levels[256], sorted[256];
  float phlev;
  memset(levels, 0, 256);
  memset(sorted, 0, 256);

// determine the number of gray levels and set  levels[i] to 1 if the intensity
// of current gray level is equial i
  for(count = 0, i = 0; i < size * size; i++)
    if(levels[(int)dpoint[i]] == 0)
```

```
    {
        levels[(int)dpoint[i]] = 1;
        ++count;
    }
  phlev = (float)count;
// form count array setting level values from 1 to count
  for(count = 1, i = 0; i < 256; i++)
    if(levels[i])
        sorted[i] = count++;

// form a complex array and set appropriate values of real
// and imaginary part
  for(i = 0; i < size * size; i++)
  {
    phi = (float)sorted[(int)(dpoint[i])];
    (cpoint[i]).r =  cos(2 * (phi - 1) * pi / phlev);
    (cpoint[i]).i = -sin(2 * (phi - 1) * pi / phlev);
  }
```

D. Fragments of source code for the Connection Machine.

```
// Instead of defining arrays we define shapes which can be processed parallelly thus
// avoiding expencive loops.

float newerr, error, olderr;
// shapes declaration
shape [65536]sh;    // this shape can be used  to replace 2-dim arrays of the size up to
                    // 512x512

// 4096, 8192, 16384, 32768, 65536, 131072, 262144
```

```
// -----        ------        ------        ------
//  64          128           256           512  */

long:sh    shPaddr;
fcomplex:sh    shPict, shTemp, shSketch;
float:sh                shSolution, shK, shL, shErr, shHeight, shVeto;
// ******************************************************
float error()
{
  newerr = 0;
    shErr = fabs(shHeight - shVeto *
          sqrt(fabs(shTemp.r * shTemp.r + shTemp.i * shTemp.i)));
    newerr +=  shErr;
  return(newerr);
}

void anneal(tempr, delta_t)
            float tempr, delta_t;
{
  float chance,  ir = tempr, eold, dev_delt, re;
  int wh, count = 0, m, n;
  long cycles_num;

// always start shape loop using with(sh)
with(sh)
{
  error(picture);
  eold = newerr;
  bestdev = newerr;
  printf("\n first... error: %f%%", bestdev);
```

```
for(cycles_num = 0; ;cycles_num++)
{
        wh = (int)(ran() * n_sq);
        re = -2.0 / (float)n_sq;
        if(flip_pixel(wh) == 1)
          re = -re;
        m = wh / SQSIZE;
        n = wh % SQSIZE;

// the main calculations are done using shapes without using loops.

        shK = shPaddr / SQSIZE;
        shL = shPaddr % SQSIZE;
        shA = 2 * pi * (m * shK + n * shL) / SQSIZE;
        shTemp.r = nabrosoks.r + cos(shA) * re * shVeto;
        shTemp.i = nabrosoks.i + sin(shA) * re * shVeto;

// the end of shapes calculations
        error(temp);
        if(ir == 0.0)
          chance = 0.0;
        else
        {
          ir = ir/(1.0 + delta_t);
          dev_delt = fabs(eold - newerr);
          chance = exp(-dev_delt/ir);
        }

        if(eold > newerr || ran() < chance)
        {
          eold = newerr;
```

```
            //    parallel
                  shSketch.r = shTemp.r;
                  shSketch.i = shTemp.i;
            }
            else
            {
                  shTemp.r = shSketch.r;
                  shTemp.i = shSketch.i;

             //    end of parallel

               flip_pixel(wh);
            }
     if(newerr < bestdev)
     {
          bestdev = newerr;
          im_copy(picture, solution);

     }
   if((cycles_num % 100) == 0)
    printf("\n cycle: %d error: %f, bestdev: %f, tempr: %f \nnabr4r: %f, nabr4i: %f,
                  temp4r %f, temp4i %f\n",
            cycles_num, newerr, bestdev, ir, [4]nabrosoks.r, [4]nabrosoks.i,
            [4]temps.r, [4]temps.i );
  }
 }
}
```

E. Author's publications.

1. S.Samus, P.McOwan and W.Hossack, "An iterative algorithm for connected structure computer generated holograms", Optic Communications 104 (1994) 266-270.

2. J.Gourlay, S.Samus, P.McOwan, D.G.Vass, I.Underwood, and Worboys Appl. Optics, "Real-time binary phase holograms on a reflective ferroelectric liquid-crystal spatial light modulator", Vol.33, No 5, (1994)

3. J.Gourlay, S.Heddle, A.O'Hara, S.Samus and D.Vass, "Optical interconnect using pixellated spatial light modulators," Opt. Comput. Int. Conf., Edinburgh, 1994.

4. A.Stevens, W.Hossack and S.Samus, "Very-large-scale-integration fabrication technique for binary-phase gratings on sapphire", Appl.Optics, Vol. 34, No.1 (1995).

5. A.Stevens, J.Gourlay, S.Samus, W.Hossack, D.Vass, and D.Burns, "Experimental investigation of free space optical interconnects," conf. Salt Lake City, March, 1995.

6. S.Samus, and W.Hossack, "Simplified design of binary phase holograms for analogue weighted fan-outs," Photorefractive effects, materials and devices conf., Colorado (1995).

7. S.Samus, "Visual aspects of phase holograms design: a **software package** for developing of 2-Dimensional holographic structures," Photorefractive effects, materials and devices conf., Colorado (1995).

8. S.Samus, and W.Hossack, "Big areas random and structured overlays for pseudo-four level (sandwich) holograms," submitted for publication to Optics Comm.

9. S.Samus, "Visual and other methods of design of continuous holograms for large fan-outs. **A software package to implement principles of visual design,"** submitted to Optics Comm.

10. S.Samus, and W.Hossack "Two algorithms for the fast design of binary phase holograms for analogue weighted fan-outs," submitted to Optics Letters.

11. S.Samus, and W.Hossack, "Combined holograms: Fast calculations of small fan-out holograms using combinations of simple gratings", being prepared for Optics Letters.

References.

1. E.Barnard, "Optimal error diffusion for computer-generated holograms," JOSA, Vol.5 (1988) 1803.

2. N.Barnes, P.Healey, P.McKee, A.O'Neill, M.Rejman-Greene, E.Scott, R.Webb, B.White, D.Wood, "Parallel interconnection and neural network systems employing semiconductor array technology and computer-generated holography," Optical and Quantum Electronics 24 (1992) 505-516.

3. T.H.Barnes, T.Eiju, K.Matsuda, and N.Ooyama, "Phase-only modulation using twisted-nematic liquid-crystal television," Appl. Opt. 28, 4845-4886 (1989).

4. S.Broomfield, M.Neil, E.Paige, and G.Yang, "Programmable binary phase-only optical device based on ferroelectric liquid-crystal spatial light modulators," Electron. Lett. 28, 26-27 (1992).

5. B.Brown and A.Lohmann, "Complex spatial filtering with binary masks", Appl. Opt. 5 (1966) p. 967.

6. D.Burns, "Design and characterisation of a ferroelectric liquid crystal over silicon spatial light modulator," The University of Edinburgh, PhD, (1994).

7. M.Dames, R.Dowling, P. McKee and D. Wood, "Efficient optical elements to generate intensity weighted spot arrays: design and fabrication," Appl. Optics 30 (1991) 121.

8. H.Dammann and E.Klotz, "Coherent optical generation and inspection of two-dimensional periodic structures," Optics Acta 24 (1977) 505.

9. H.Dammann and K.Gortler, "High-efficiency in-line multiple imaging by means of multiple phase holograms," Opt. Comm. 3 (1971) 312.

10. M.Feldman and C.Guest, "Iterative encoding of high efficiency holograms for generation of spot arrays," Opt.Lett. 14, 479-481 (1989).

11. K.M.Flood and J.M.Filnlan, "Collimation of diode laser arrays using etched cylindrical computer generated holograms," Proc. Soc. Photo-Opt. Instrum. Eng. 1052, 186-190.

12. S.Geman and D.Geman, IEEE Trans, Patt, Anan. Mach. Int., PAMI-6 (No. 6), 721-741, Nov. 1984.

13. J.Goodman, A.Dias, and L.Woody, "Fully parallel high-speed incoherent optical method for performing discrete Fourier transforms," Optics Letters, 2 (1978) 1-3.

14. J.Gourlay, S.Samus, P.McOwan, D.G.Vass, I.Underwood, and M.Worboys, "Real-time binary phase holograms on a reflective ferroelectric liquid-crystal spatial light modulator," Appl. Opt. 33, 8251-8254 (1994).

15. J.Gourlay, S.Heddle, A.O'Hara, S.Samus and D.Vass, "Optical interconnect using pixellated spatial light modulators," Opt.Comput.Int.Conf., Edinburgh, 1994.

16. J.Gourlay, "Ferroelectric liquid crystal spatial light modulators: devices and applications," The University of Edinburgh, PhD, (1994).

17. P.Hariharan, "Optical holography. Principles, techniques and applications".

18. R.Hauck and O.Bryngdahl, "Computer holography: review and digressions," J.Opt.Soc.Am. A 1 (1984) 5.

19. H.Herzig, D.Prongue and R.Dandliker, "Design and fabrication of highly efficient fan-out elements," Jap. J. Appl. Physics, Vol. 29, No. 7, (1990) 1307-1309.

20. R.Hoptroff, P.McOwan, T.Hall, W.Hossack and R.Burge, "Two optimisation approaches to cohoe design," Optics Comm. 73 (1989) 188.

21. W.Hossack, P.McOwan and R.Burge, "Computer generated optical fan-out element," Opt.Comm. Vol. 68, No2 (1988) 97-102.

22. M.C.Hutley, "Optical techniques for the generation of microlens arrays," J.Mod.Opt. 37, 253-265 (1990).

23. H.Ichikawa, M.R.Taghizadeh, and J.Turunen, "Noninterferometric fabrication of computer-generated phase holograms on silver halide photographic emulsion," Opt. Eng. 30 (1993) 1869-1877.

24. J.Jahns, M.M.Downs, M.E.Prise, N.Streibl, and S.J.Walker, "Dammann gratings for laser beam shaping," Opt.Eng. 28 (1989) 1267-1275.

25. J.Jahns and S.Walker, "Two-dimensional array of a diffractive microlens fabricated by thin-film deposition," Appl.Opt. 29, 931-936 (1990).

26. B.Jennison, J.Allebach and D.Sweeney, "Iterative approaches to computer-generated holography," Opt.Eng. Vol.28 (1989) 629.

27. K.Johnson, D.McKnight, and I.Underwood, "Smart spatial light modulators using liquid crystals on silicon," J. of Quantum Electronics, vol. 29. No 2, 1993.

28. D.Just and D.Ling, "Neural networks for binarizing computer-generated holograms," Opt. Comm. 81 (1990) 1.

29. A.Kirk, K.Powell, and T.Hall, "A generalisation of the error diffusion method for binary computer generated hologram design," Opt. Comm.92 (1992) 12-18.

30. A.Kirk, W.Crossland, and T.Hall, "A compact and scalable free-space optical crossbar," In proceedings of the Third International Conference on Holographic Systems, Components and Applications, v. 1574, 137-141. IEE, London, Sept. 1991.

31. A.Kirk, S.Jamieson, H.Imam, and T.Hall, "Experimental implementation of an optoelectronic matrix-matrix multiplier which incorporates holographic multiple imaging," in Optical Computing and Processing, 2(4), 293-304, 1992.

32. A.Kirk and T.Hall, "Design of binary computer generated holograms by simulated annealing: coding density and reconstruction error," Opt.Comm. 94 (1992) 491-496.

33. S.Kirkpatrick, C.Gelatt, and J.Vecchi, "Optimisation by simulated annealing," Science 220, 671-680 (1983) .

34. B.Kiselyov, N.Kulakov, A.Mikaelian, "Modification of simulated annealing method for solving combinatorial optimization problems," 120/SPIE Vol. 1773 Photonic Neural Networks (1992).

35. U.Krackhardt, J.Mait, and N.Streibl, "Upper bound on the diffraction efficiency of phase-only fan-out elements," App. Opt. 31 (1992) 27-37.

36. W.Lee, "Computer generated holograms: Techniques and applications," Progr. in Optics XVI Ed E Wolf Nothern Holland 121-232.

37. L.Lesem, P.Hirsch, and J.Jordan, "The kinoform: a new wavefront reconstruction device," IBM J. of Research and Development, 13 (1969) 150-5.

38. J.N.Mait and G.S.Himes, "Computer-generated holograms by means of a magneto-optics spatial light modulator," Appl.Opt. 28, 4879-4852.

39. F.McCormick, "Generation of large spot arrays from a single laser beam by multiple imaging with binary phase gratings," Optical Engineering (1989) Vol. 28 No 4, 299-304.

40. P.McOwan, W.Hossack and R.Burge, "Uses of iterative constraint satisfaction for binary phase detour digital holograms," Opt.Comm. 83 (1991) 21-25.

41. P.McOwan, M.Gordon and W.Hossack, "A switchable liquid crystal binary Gabor lens," Optics Comm. 103 (1993) 189.

42. P.McOwan, "Applications of high resolution computer generated holograms in optical beam shaping and imagte display," PhD, (1990).

43. J.Millar, M.Taghizadeh, N.Ross, E.Noponen, and A.Vasara, "Kinoform array illuminators in fused silica," J.Mod.Opt. 40, 723-732 (1993).

44. R.Morrison and M.Wojcik, "A selective cell-based algorithm for designing high efficiency beam array generators."

45. D.O'Brien, R.Mears, T.Wilkinson, and W.Crossland, "Dynamic holographic interconnects that use ferroelectric liquid-crystal spatial light modulators," Appl. Optics 33 (1994) 2795.

46. D.O'Brien, R.Mears, "Real time holograms using ferroelectric liquid crystal spatial light modulators."

47. A.O'Hara, J.Hannah, I.Underwood, D.Vass, and R.Hlwill, "Mirror quality and efficiency improvements of reflective spatial light modulators by the use of dielectric coating chemical-mechanical polishing," Appl. Optics, 32 (1993) 5549.

48. S.Samus, and W.Hossack, "Combined holograms: Fast calculations of small fan-out holograms using combinations of simple gratings", being prepared for Optics Letters.

49. S.Samus, P.McOwan and W.Hossack, Optics Comm. "An iterative algorithm for connected structure computer generated holograms," Optics Comm. 104 (1994) 266-270.

50. S.Samus, "Visual and other methods of design of continuous holograms for large fan-outs. A software package to implement principles of visual design," submitted to Optics Comm.

51. S.Samus, "Visual aspects of phase holograms design: a software package for developing of 2-Dimensional holographic structures," Photorefractive materials, effect and devices conference, Colorado (1995).

52. S.Samus, and W.Hossack "Two algorithms for the fast design of binary phase holograms for analogue weighted fan-outs," submitted for publication to Optics Letters.

53. S.Samus, and W.Hossack, "Simplified design of binary phase holograms for analogue weighted fan-outs," Photorefractive materials, effect and devices conference, Colorado (1995).

54. S.Samus, and W.Hossack, "Big areas random and structured overlays for pseudo-four level (sandwich) holograms," submitted for publication to Optics Comm.

55. M.Seldowitz, J.Allebach and D.Sweeney, "Synthesis of digital holograms by direct binary search," App. Optics, Vol. 26 (1987) 2788.

56. A.Stevens, W.Hossack, and S.Samus, "Very-large-scale-integration fabrication technique for binary-phase gratings on sapphire," Appl. Optics 34 (1995) 190-193.

57. A.Stevens, J.Gourlay, S.Samus, W.Hossack, D.Vass, and D.Burns, "Experimental investigation of free space optical interconnects," In OSA Technical Digest: "Spatial light modulators and applications." Salt Lake City, UTAH, march 14-16 1995.

58. A.Stevens, "Experimental investigation of free-space optical routing systems using static and dynamic binary holographic elements ," PhD thesis, University of Edinburgh, 1995.

59. M.Styblinski and T.Tang, "Experiments in nonconvex optimization: Stochastic approximation with function smoothing and simulated annealing," Neural Networks, Vol.3. pp 467-483, 1990.

60. H.Szu, "Fast simulated annealing," NRL Invention Patent Case.

61. L.Thompson, C.Wilson and M.Bowden, "Introduction to microlithography," (American Chemical Society, Seattle, 1983).

62. J.Turunen, B.Xingao and J.Guofan, "Optimization of grating multi-beamsplitters," Optica Silica Vol 8, No 10, 1988.

63. I.Underwood, D.Vass, and R.Sillitto, "Evaluation of an nMO VLSI array for an adaptive liquid-crystal spatial light modulator," Proc. Inst. Electr. Eng. Part J, 133, 77-82 (1986).

64. M.Verheijen, "E-beam lithography for digital holograms," J.Mod.Opt. 40, 711-721 (1993).

65. K.J.Weible, H.P.Herzig, "Optical optimization of binary phase fan-out elements," Optics. Comm. 113 (1994) 9-14.

66. S.Weissbach, F.Wyrowski and O.Bryngdahl, "Digital phase holograms: coding and quantization with an error diffusion concept," Opt. Comm. 72 (1989) 37.

67. T.Wilkinson, D.O'Brien and R.Mears, "Dynamic asymmetric binary holograms using a ferroelectric liquid crystal spatial light modulator," Optics Comm. 109 (1994) 222-226.

68. M.Wiltshire, GEC Journal of Research 10 (1993) 119; 9 (1991) 121.

69. E.Wolf, "Optical neural networks: architecture, design and models," Progress in optics XXXII, 1993.

70. F.Wyrowski and O.Bryngdahl, "Iterative Fourier transform algorithm applied to computer holography," J.Opt.Soc.Am. A/Vol. 5, No. 7/July 1988.

71. F.Wyrowski, "Diffractive optical elements: iterative calculation of quantized, blazed phase structures," JOSA, Vol. 7 (1990) 961.

Simplified design of Binary Phase Holograms for Analogue Weighted Fan-Outs.

Sergei S. Samus, William J. Hossack
Department of Physics
The University of Edinburgh
King's Buildings
Edinburgh EH9 9JZ, UK.

ABSTRACT

The algorithm for rapid varying the intensity of output spots by calculation of a synthetic hologram using a small number of precalculated primitive holograms is presented. The results of simulation for 4 point fan-out are given.

SUMMARY

Computer calculated binary holograms are used extensively in optical fan-out. Such holograms can either be static, being fabricated as a transmission and reflective phase grating, [1, 2], or dynamic, being formed by diffraction from a phase modulating SLM [3]. The design of each hologram involves extensive computation, typically involving use of a simulated annealing scheme [2], to form a globally optimal solution. Under these schemes, each fan-out pattern produces a unique hologram, so that even small changes in the output pattern required recalculation of the entire hologram. With the recent availability of high resolution phase modulating SLMs [3], dynamic holograms are becoming practical optical components, and there is a need for rapid calculation schemes to allow rapid update of the output pattern. This paper presents a scheme for varying the intensity of a small number of output spots by taking combinations of primitive holograms with additional filling of the non-overlapped areas.

Section 1. The algorithm for changing the intensity of a single output pixel.

Consider a hologram that splits a beam into n spots. If we wish to vary the intensity of these spots over L output values then, in general we would need L^n individual holographic patterns each designed separately. If n or L are large, this rapidly becomes a computationally impossible task.

Consider the 2 by 2 binary fan-out hologram shown in figure 1. If the hologram is binary phase, then the output pattern will always be symmetric. This hologram has been designed on 64 by 64 pixel grid using simulated annealing, [2], denoted by mask 1. Figure 2 shown a 2 point hologram of the same spacing formed by additional annealing at temperature zero of the mask 1 but with a new target. This is denoted by mask 2. Further we will consider only upper halves of the outputs due to their symmetrical nature. The difference between two outputs is that there is no right spot in the second case. We will call mask 2 a "missing pixel hologram" and mask 1 a "master mask". Figures 3a and 3b show the holograms which are designed to produce two - pixels outputs with different intensities of the right spot. The intensities are respectively 0.4 and 0.8.

Fig. 4 shows masks 1, 2 and 3a added together in a way we would put 3 transparencies on top of each other. We can clearly see that there is a definite link between all of them, in particular mask 3 incorporates the features of mask 1 and mask 2.

Fig. 5 shows the master mask (1) and the missing pixel mask (2) added together in a sequence 1+2+1. The pattern consists of 4 values:

0 - areas where two masks overlap (Black)

1- areas of master mask only (Light grey)

2 - areas which belong only to the missing pixel mask. (Dark grey)
3 - clear areas (White)
shall call 0, 3 'and' areas and 1, 2 'or' areas. The 'or' which is created by the master mask is er because it is overlapped twice. We will call the 'or' areas 'or 1' for master mask and 'or 2' for ing pixel mask. Considering fig. 4a and 4b. We can see that the original holograms for weighted sities pixels change only in 'or' areas. Two extreme cases are our master mask and missing pixel . If we need the solution with the intensity of the right pixel closer to 1 the 'or 1' area will be l more and the 'or 2' area associated with missing pixel mask - less. And the other way round it be for the intensity of the right pixel closer to 0. The "and" areas are not changed at all. Simulation ests that the fraction of area filling is proportional to the intensity of the right pixel. This can be oximated by randomly filling the region 'or 1' proportionally to k and 'or 2' proportionally to 1-k e $0 \leq k \leq 1$. The method works even if the 'or' areas consist of single pixels or small number em. Fig. 6(a,b) shows the final solutions for the synthetic masks which produce 2 pixel output the intensity distributions (1, 0.8) and (1, 0.4). These observations can be generalised, resulting in llowing algorithm for changing the intensity of single output pixel:

. Design a master hologram which produces the required output with intensity of the changeable pixel equal to 1.
. Design a missing pixel hologram which produces the same output with intensity of the changeable pixel equal to 0. The rules for the missing pixel hologram design are:
   a) The starting pattern for the hologram must be its master mask.
   b) The missing pixel mask design must be done using simple error reduction algorithm (the simulated annealing with T = 0).
. Calculate the synthetic hologram using the latter two patterns following the rules:
   a) The pixels with the same phase shift for both masks are not changed.
   b) The pixels with π phase shift for master mask and 0 phase shift for the missing pixel mask are changed to π with the probability k, where $0 \leq k \leq 1$ is the desired intensity coefficient.
   c) The pixels with 0 phase shift for master mask and π phase shift for the missing pixel mask are changed to π with the probability 1 - k.

ion 2. The algorithm for changing the intensity of any output pixel.

possibility to change a single pixel's intensity gives an opportunity to get any distribution of sities of the output pattern. Consider 3 dot fan-out (the top level of the tree on Fig. 8). If we define ighest intensity of central spot to be 1, the intensity distribution can be expressed as (I_1 , 1, I_3). ntensity of dot 3 denoted by I_3 can be controlled by missing pixel pair (I_1 , 1, 1) and (I_1 , 1, 0). mask (I_1 , 1, 1) can be synthesised from two pure holograms: (1, 1, 1) and (1, 1, 0). The other (I_1 , 1, 0) can be calculated using another pair: (1, 1, 0) and (0, 1, 0). Hence for the given em we have to use 4 preinitially designed "pure" holograms. Finally using this method we only to design $2^n - 1$ "pure" or primitive holograms, where n is number of output pixels, in order to the control over any combination of the intensities of the output spots without further design of ologrames with traditional time consuming methods.

on 3. The simulation results.

ccomplished the simulation for three and four pixel task using the described method. The results ombination (0.4, 1, 0.8, I_4) are shown on Fig. 9. The intensities of dots 1, 2, 3 were fixed at the s 0.4, 1, 0.8 using analogically calculated synthetic holograms. And the intensity of the dot 4 ged gradually. The process proved to be very stable and linear as it can be seen from the graph. 3 pixels the number of required pure holograms is 255 which is very small comparing to the

impressive 16 777 216 required to complete the same task using traditional approach for 8 grey levels. Still the number of grey levels is not limited to 8. What becomes a really time consuming task usingthe algorithm is the number of calculations required to achieve the top of the pyramid. For example for 3 spot problem we have to apply the algorithm 3 times. For 4 spots this is 7 times. And for 8 spots it is already 127. The number of calculations is given by $calc=2^n/2-1$ where n is number of output pixels. This means we have to scan through 127 masks for 8 pixels task. But it is not necessary to do all 3 calculations for each particular case. Similarly if we need to change the intensities of only 3 or 2 pixels in 4 pixels set we only have to deal with 3 or 2 pixels computational algorithm.

Conclusion.

The paper presents a scheme that allows efficient calculation of analogue weighted fan-out holograms from a small set of parent holograms. Results for four output fan-outs have been simulated with one output varied over a range 1-99 %.

References.

1. H.Dammann and E.Klotz, Optics Acta 24 (1977) 505.
2. M.Dames, R.Dowling, P. McKee and D. Wood, Appl. Optics 30 (1991) 121.
3. J.Gourlay, S.Samus, P.McOwan, D.G.Vass, I.Underwood, and M.Worboys, Appl. Optics 33 (1994) 8251.

Figures.

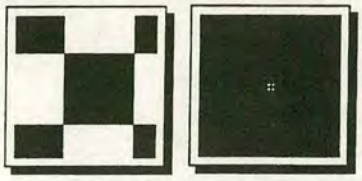

Fig. 1(a,b) 2x2 hologram and its FT.

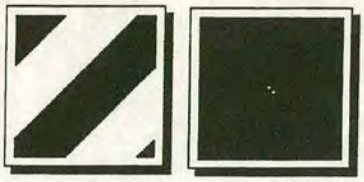

Fig. 2(a,b) missing pixel hologram and its FT.

Fig. 3(a,b) pure holograms for 1&0.8 and 1&0.4 outputs

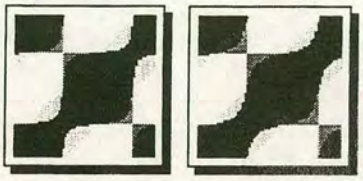

Fig. 4(a,b) added holograms: 1 + 2 + 1 + 3a and 1 + 2 + 1 + 3b.

Fig. 5 added holograms 1 + 2 + 1

Fig. 6(a,b) synthetic holograms which replace 3a and 3b.

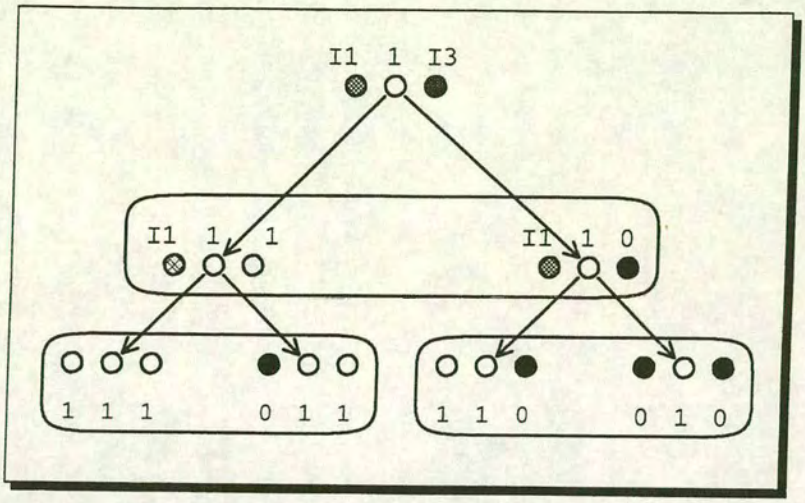

Fig. 8 The tree for the mask of (I_1 , 1, I_3) fan-out. The bottom level consists of "pure" holograms and the second and the top level are synthetic holograms.

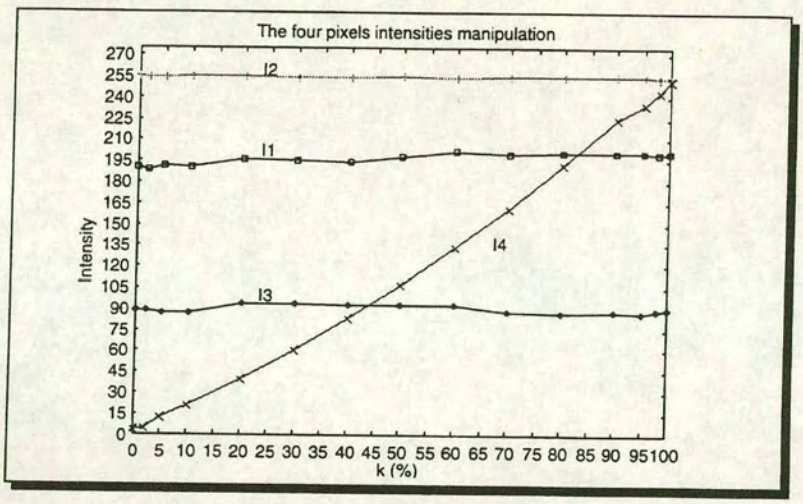

Fig. 9 The simulation results for 4 pixel task (0.4, 1, 0.8, I_4). The intensities of pixels 1, 2 and 3 are fixed at values 0.4, 1, and 0.8 and the intensity of pixel 4 is varied. Note the linearity of the I4 curve and stability of others.

a reprint from Applied Optics

Very-large-scale-integration fabrication technique for binary-phase gratings on sapphire

Andrew J. Stevens, William J. Hossack, and Sergei Samus

An efficient, high-yield process for the production of binary-phase holograms is presented by controlled deposition of silicon nitride over a sapphire substrate with the binary structure formed by plasma etch of the silicon nitride. Optical results are presented for a 16 × 16 transmission fanout element that shows near-optimal performance.

Key words: Phase-only gratings, binary diffractive optics, computer-generated-hologram fabrication, array generators.

Introduction

Binary diffractive optics are important holographic elements in monochromatic optical systems. They are utilized in a range of applications that includes focusing,[1] beam shaping, and fanout.[2] These elements have a high optical efficiency, are easily designed, and are relatively easy to fabricate, and because they operate on axis they are easily incorporated into optical systems. A range of techniques has been used to fabricate binary optics, including controlled exposure and bleaching of photographic materials,[3] lithographic or electron-beam exposure of photoresist,[4] controlled deposition of SiO_2,[5] and controlled etching into solid material. The most successful technique to date appears to be the controlled plasma etching of fused silica.[6,7] This etching technique requires careful calibration of the etch rate, and uniformity across large substrates is difficult. In addition the etched regions tend to be rough, which contributes to light scattering. We present an alternative fabrication technique for binary diffractive optics based on accurately controlled deposition of silicon nitride on a sapphire substrate that is subsequently patterned and etched with the sapphire as an etch stop. This process results in optically smooth transmissive phase gratings with a phase thickness with a maximum variation of 1.5% across a wafer 75 mm in diameter. Results are presented for a 16 × 16 fanout element with an optical transmission of 91.6% and diffraction efficiency of 62.5% compared with a theoretical design efficiency of 64%. All processing operations in this fabrication technique are standard in very-large-scale integrated (VLSI) fabrication, and all patterning and etching were performed with unmodified fabrication facilities normally used for standard 3-μm CMOS (complementary metal-oxide semiconductor) processing.

Materials and Fabrication

Sapphire has optical properties that make it a good substrate for binary holograms; in particular it has a low scatter and absorption in the visible spectrum, is very hard and rigid, can be polished optically flat, and has a low-thermal-expansion coefficient. Its physical properties of a high melting point, zero porosity, and extreme resistance to both wet and plasma etches make it an ideal material for processing. Note, however, that sapphire is a birefringent material with refractive indices of 1.760 and 1.769; so if it is used with polarized illumination, the axis of polarization must be aligned with either the ordinary or extraordinary optical axis. Silicon nitride can be accurately deposited by low-pressure chemical vapor deposition.[8] Typical parameters for deposition are 800 °C with an atmosphere of NH_3 [90 cubic centimeters per minute at standard temperature (SCCM)] and $SiCl_2H_2$ (20 SCCM). Note that the need for high-temperature deposition prevents the use of prepatterned liftoff techniques.[5] With these flow rates the deposited silicon nitride film was measured at 39 Å/min with an index of 2.00. These films were found to be extremely rugged and optically flat, because they do not contain significant quantities of hydrogen that increase porosity. The sapphire substrates, which

The authors are with the Department of Physics, the University of Edinburgh, King's Buildings, Edinburgh, EH9 6JZ, Scotland, UK.

Received 23 November 1993; revised manuscript received 6 July 1994.

0003-6935/95/010190-04$06.00/0.

were in the form of 75-mm-diameter wafers, with a surface flatness of 1/60th of an optical wavelength over a 1-cm^2 region of the wafer, were found to be completely unaffected by this deposition. In addition it was found that the silicon nitride deposition rate was identical to the deposition rate onto bare silicon, which permitted silicon wafers to be used to monitor the film thickness. This permitted standard ellipsometry film thickness monitoring to be used that relies on the film being deposited on an optically reflective substrate.

The deposition technique results in a film of the same thickness being deposited on both sides of the wafers. This film can be easily etched off the unused side.

Diffractive Fanout Elements

The diffractive element chosen for fabrication was a 16 × 16 fanout grating of Dammann and Gortler.[9] The properties of these elements are well known; in particular any errors in phase depth show up as an undiffracted central spot, and these designs are critically dependent on an accurate phase-edge location to obtain good uniformity and diffraction efficiency.[10] The grating design was formed by simulated annealing,[11] and the theoretical diffraction efficiency as calculated for the one-dimensional grating was 79.5% compared with an ideal maximum of 81.1%.[12] The theoretical efficiency of the two-dimensional grating is thus 63.2%, which is typical for such elements. The transition points of a unit cell are in Table 1. The calculated grating transition was used to form a 32 × 32 replicated pattern with Cadence Edge VLSI tools and an industry standard ×10 chromium-on-glass mask with a geometric accuracy of ~0.25 μm. The grating was designed to operate in He–Ne illumination, so a silicon nitride film of 3164 Å is necessary to produce the required phase shift on transmission. This film was produced by two depositions of 30 min and one of 20 min, 8 s. The film thickness was monitored after each deposition by ellipsometry and interferometric thin-film measure of silicon wafers placed adjacent to the sapphire substrate. With this technique it was possible to produce films that were on average within 1% of the required thickness and with a maximum variation of 1.5% across the 75-mm wafer.

Table 1. Binary-Phase Transition Point for a Unit Cell of a 16 × 16 Fanout Element with a Diffraction Efficiency of 79.5% in One Dimension

$0 \rightarrow \pi$ Transition	$\pi \rightarrow 0$ Transition
0.000000	0.039035
0.138932	0.170173
0.224478	0.245961
0.301181	0.361458
0.474307	0.503317
0.538810	0.638775
0.670051	0.720332
0.740412	0.802904
0.858767	0.974260

The wafer was then coated with photoresist and patterned with an Optimetrix ×10 wafer stepper that gave 32 patterned dies of 8 × 8 mm on each sapphire wafer, which gave a unit cell size of 0.25 mm. The wafer was then etched in a Plasma-Therm dry etcher with a hydrogen and CF_4 plasma for 16 min, which etched all the exposed silicon nitride back to the sapphire substrate. Owing to the physical properties of the sapphire, the etching uniformity is not critical, because the sapphire operates as an impervious etch stop. Using this process, we can determine the phase thickness of the holograms by the original wafer scale deposition and not the final etch conditions. The accuracy of 1% that is obtained is comparable with what can be obtained by controlled etching over small areas. Finally the back of the wafer was etched clear of silicon nitride by the above processes, and the back of the wafer was coated with an antireflection coating of MgF for the He–Ne wavelength.

Optical Results

The optical transmission of the wafer was measured at 91.6%. The diffraction pattern from a typical dye is shown in Fig. 1. It was constructed with a 300-mm lens that gave a spot array with a separation of 1.5 mm. The measured spot intensity uniformity is 1.8%, compared with a theoretical uniformity of 0.44%, and the diffraction efficiency is 62.5%, compared with a theoretical efficiency of 63.5%. The undiffracted spot is ~1.5 times that of the diffracted elements. This result is consistent with an error of ~1% in the phase depth.[13] Over the entire wafer of 32 gratings the diffraction efficiency varied by ~1%, and the largest undiffracted central spot was twice that of the diffracted spots, showing a slight lack of uniformity in film thickness across the wafer. All the gratings produced optical fanout elements, putting at least 56% of the total incident laser power into the required 16 × 16 array with an intensity unifor-

Fig. 1. Optical diffraction pattern from a Dammann grating.

nity of better than 2%, which compares favorably vith other fabrication techniques.

Microscopic Examination of the Grating Structure

One of the gratings was coated with 100 Å of gold and examined under scanning electron microscopy. Figure 2 shows a 20° image of a 70 μm × 70 μm region of he grating. It shows that both the silicon nitride urface and the sapphire surface are smooth and here is no granularity or etch attack. The edge rofile is shown in Fig. 3. This profile shows that he silicon nitride has been etched with near vertical dges with little rounding of the top edge and no ndercut. The total edge spread is ~50 nm. Again oth the silicon nitride and the sapphire show no vidence of etch attack and retain their smooth urfaces.

xtension to Multiphase

Jnlike the deposition of SiO_2 at low temperature, vhich can be prepatterned,[5] the silicon nitride is eposited at a temperature at 800 °C, well above the emperature at which photoresists can operate. onsequently conventional multiphase processing annot be applied.

We can, however, extend the technique to four hase levels by using the fact that the same thickness f silicon nitride is deposited on both sides of the afer, which requires an asymmetric deposition with depth of π on one side and $\pi/2$ on the other. Then y patterning and etching both sides, we can obtain our phase levels. The asymmetric deposition can be btained by an initial deposition of $\pi/2$ on both sides. ne side is then etched back to the sapphire to give a ngle-sided deposition of $\pi/2$. A second deposition then performed to lay down a second $\pi/2$ layer, ving the required asymmetric deposition. The resulting four-level hologram would permit asymmetric diffraction patterns but may be limited in space bandwidth because of the diffraction effects between the two faces of the wafer.

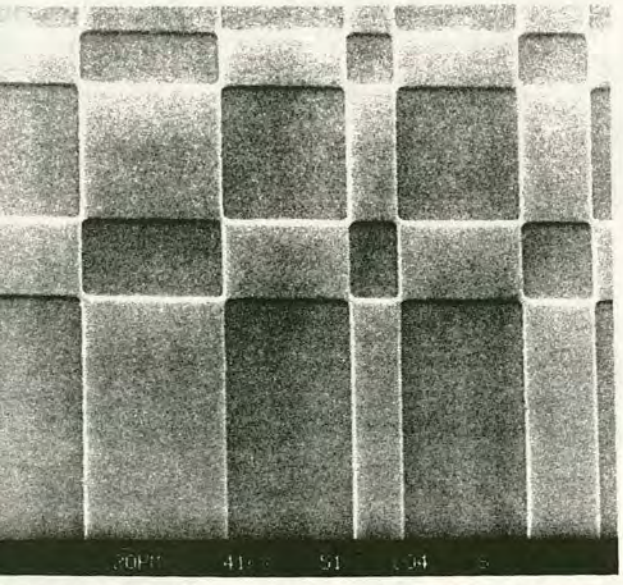

g. 2. Scanning electron micrograph of a coated grating structure.

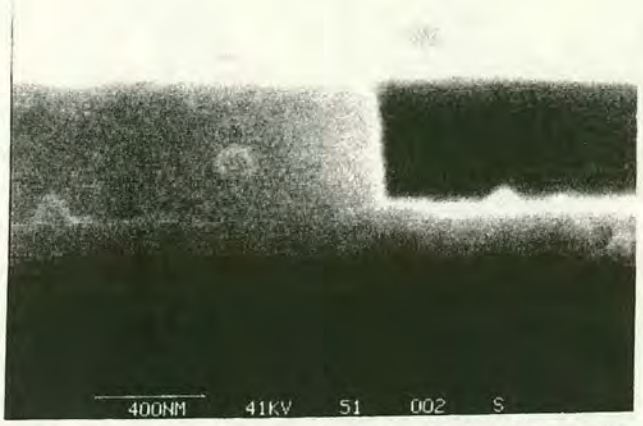

Fig. 3. Scanning electron micrograph showing the edge structure of a grating.

Conclusion

This fabrication technique permits accurate and reproducible production of binary transmission optics with a high yield and excellent uniformity. All processes used are standard in the VLSI production industry and do not require modification of any equipment available in a facility capable of high-resolution CMOS fabrication; in particular the fact that the deposition rates can be monitored on silicon wafers adjacent to the sapphire wafers permits ellipsometry to be used. Because of the birefringence of the substrate, care must be taken when these elements are used in polarized illumination. This restriction can be removed by coating the relief structure in aluminum or silver to form a reflective grating.

This fabrication technique is directly applicable to the fabrication of two-dimensional binary phase structures.[14] These design techniques permit arbitrary symmetric fanouts with diffraction efficiencies as high as 81%. The fabrication of a range of such two-dimensional gratings is currently being undertaken.

The authors thank the staff of the Edinburgh Microfabrication Facility, The University of Edinburgh, for advice and use of equipment. The scanning-electron-microscopy images were prepared by the Faculty Electronmicroscope Unit, The University of Edinburgh. Two authors (A. Stevens and S. Samus) are supported by Science and Engineering Research Council (SERC) studentships, and the research was partially supported under the SERC-

funded SCIOS (Scottish Collaborative Initiative on Optoelectronic Sciences) project.

References

1. T. D. Beynon, I. Kirk, and T. R. Mathews, "Gabor phase plate with binary transmittance values," Opt. Lett. **17,** 544–546 (1992).
2. R. L. Morrison, S. L. Walker, and T. J. Cloonan, "Beam array generation and holographic interconnections in a free-space optical switching network," Appl. Opt. **32,** 2512–2518 (1993).
3. H. Ichikawa, M. R. Taghizadeh, and J. Turunen, "Noninterferometric fabrication of computer-generated phase holograms on silver halide photographic emulsion," Opt. Eng. **30,** 1869–1877 (1991).
4. M. J. Verheijen, "E-beam lithography for digital hologams," J. Mod. Opt. **40,** 711–721 (1993).
5. J. Jahns and S. J. Walker, "Two-dimensional array of a diffractive microlens fabricated by thin-film deposition," Appl. Opt. **29,** 931–936 (1990).
6. J. Jahns, M. M. Downs, M. E. Prise, N. Streibl, and S. J. Walker, "Dammann gratings for laser beam shaping," Opt. Eng. **28,** 1267–1275 (1989).
7. J. M. Millar, M. R. Taghizadeh, N. Ross, E. Noponen, and A. Vasara, "Kinoform array illuminators in fused silica," J. Mod. Opt. **40,** 723–732 (1993).
8. S. M. Sze, *VLSI Technology* (McGraw-Hill, New York, 1988), Chap. 6, pp. 260–262.
9. H. Dammann and K. Gortler, "High efficiency in-line multiple imaging by means of multiple phase holograms," Opt. Commun. **3,** 312–315 (1971).
10. M. R. Taghizadeh, J. I. B. Wilson, J. Turunen, A. Vasara, and J. Westerholm, "Amorphous silicon nitride optical grating beam splitters," J. Non-Cryst. Solids **115,** 165–167 (1989).
11. J. Turunen, A. Vasara, S. Westerholm, G. Jin, and A. Salin, "Optimization and fabrication of grating beam splitters," J. Phys. D **21,** 102–105 (1988).
12. U. Krackhardt, J. N. Mait, and N. Streibl, "Upper bound on the diffraction efficiency of phase-only fanout elements," Appl. Opt. **31,** 27–37 (1992).
13. A. Vasara, M. R. Taghizadeh, J. Turunen, J. Westerholm, E. Noponen, H. Ichikawa, J. M. Millar, J. Jaakkola, and S. Kuisma, "Binary surface-relief gratings for array illumination in digital optics," Appl. Opt. **31,** 3320–3336 (1993).
14. M. P. Dames, R. J. Dowlings, P. McKee, and D. Wood, "Efficient optical elements to generate intensity weighted spot arrays: design and fabrication," Appl. Opt. **30,** 2685–2691 (1991).

Experimental Investigation of Free Space Optical Interconnects.

A.J. Stevens, J. Gourlay, S. Samus, W.J. Hossack,
D.G. Vass, and D.C. Burns.

Applied Optics Group,
Department of Physics,
The University of Edinburgh,
King's Buildings,
Edinburgh,
EH9 3JZ,
Scotland, UK
Phone : +44 (0)31 650 5270.
Email : andy.stevens@ed.ac.uk.

Introduction

Free space optical interconnects have applications in many optical systems such as crossbars, optical neural networks and telecommunications. The interconnect may be implemented in two ways; by the use of static holographic elements to fan out the input channels onto a modulating plane which allows only the only the appropriate channels to propagate[1,2], or by using a dynamic holographic element to provide direct interconnection[3,4]. Ferroelectric liquid crystal over silicon spatial light modulators (FLC/VLSI SLM's) have been demonstrated to be suitable elements as both an amplitude modulating plane addressed by holographic elements, and as a phase modulating plane for encoding dynamic holograms. The aim of this paper is to assess the capabilities of FLC/VLSI SLM's in both these roles using experimental test systems. In order to do this, performance criteria such as scalability, diffraction efficiency, uniformity, contrast ratio, optical throughput, and switching speed shall be considered. Finally, the analysis of these results will provide an insight into the performance of future FLC/VLSI SLM's in optical free space routing systems.

256 Channel Static Hologram Interconnect

The classic matrix-matrix crossbar architecture (fig.1.) consists of an array of $n \times n$ input channels which are fanned out onto an $n^2 \times n^2$ modulating plane, and then fanned back in to an $n \times n$ output array. This allows any input channel to be routed to any output channel, along with broadcast capabilities. With FLC/VLSI SLM's as the modulating plane, each pixel acts as a *transparent window* when turned on (fig.2.), which means that the optical data stream can pass through without the liquid crystal being required to switch at the optical data rate. The pixels only need to switch within the channel reconfiguration time.

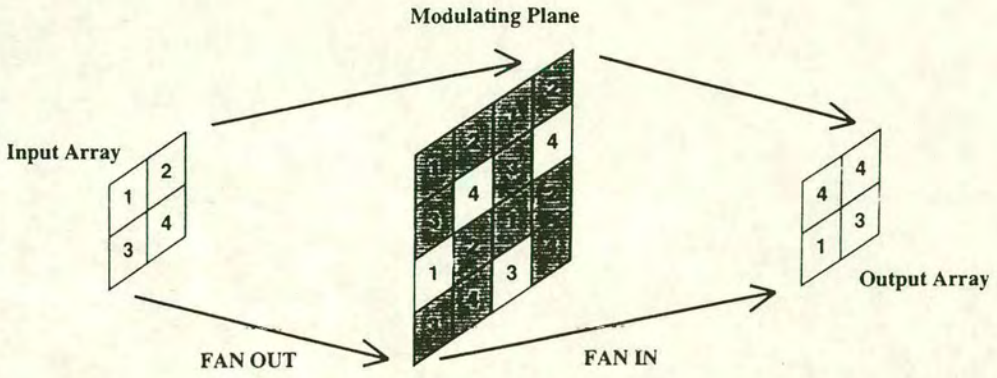

Figure 1: Schematic Model of Matrix-Matrix Crossbar.

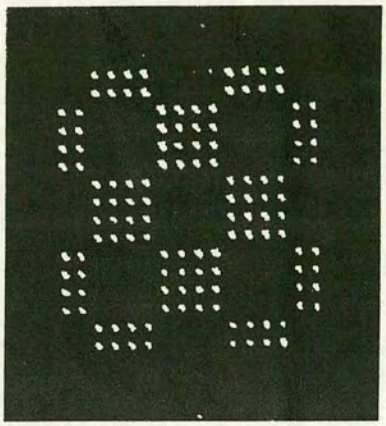

Figure 2: Static Fanout Hologram With 256 Spots Modulated By FLC/VLSI SLM.

In order to assess the performance of FLC/VLSI SLM's in this role, a test system has been constructed[5] (fig.3.). By systematic investigation of the performance of this system we shall address the following; device and system scalability, contrast ratio and uniformity requirements, and space-bandwidth product issues.

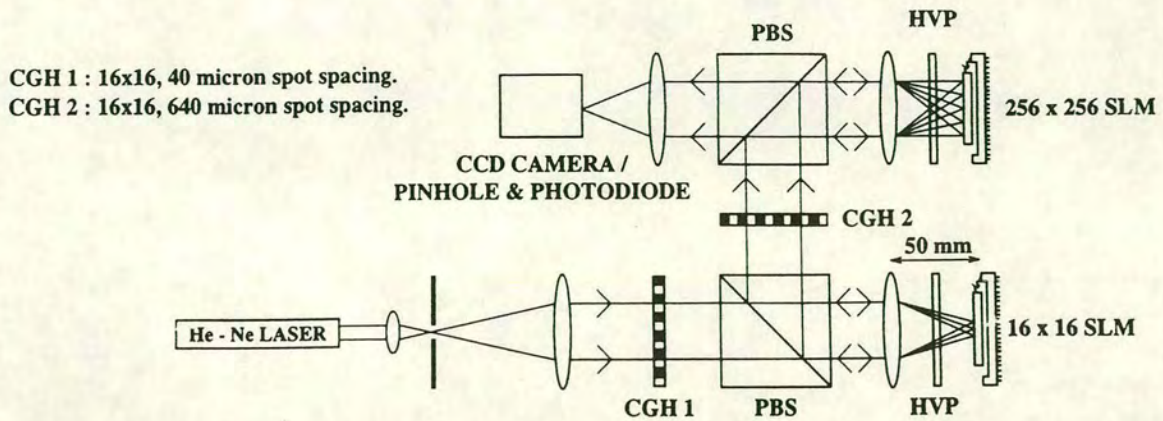

Figure 3: Experimental Test Bed For 256 Channel Interconnect.

Dynamic Holographic Interconnects

Many optical systems require dynamic holographic interconnects for the routing of signals and addressing of optical and electro-optic devices. Such systems require fast reconfiguration times and high diffraction efficiences. It has previously been demonstrated that ferroelectric liquid crystals (FLC's) can be used to provide the 0 to π rad phase modulation required by binary computer generated holograms[6]. Furthermore it has also been shown that FLC/VLSI SLM's are capable of encoding and modulating FLC's so as to produce holographic interconnects[7] (fig.4.). We shall present results of experiments using the test system illustrated in (fig.5.) to give a detailed analysis of the performance of this technology as a means of producing dynamic interconnects.

Finally, we will discuss the feasibility and estimated performance of asymmetric holograms produced by fabricating a $\pi/2$ phase pattern on the SLM coverglass, which, in conjunction with the π phase modulation achievable from the liquid crystal, may be used to produce asymmetric spot arrays.

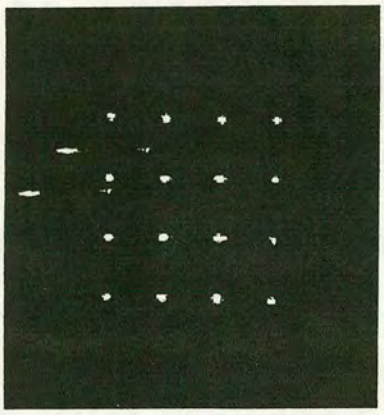

Figure 4: 4x4 Dynamic Holographic Fanout Using A Planarised FLC/VLSI SLM.

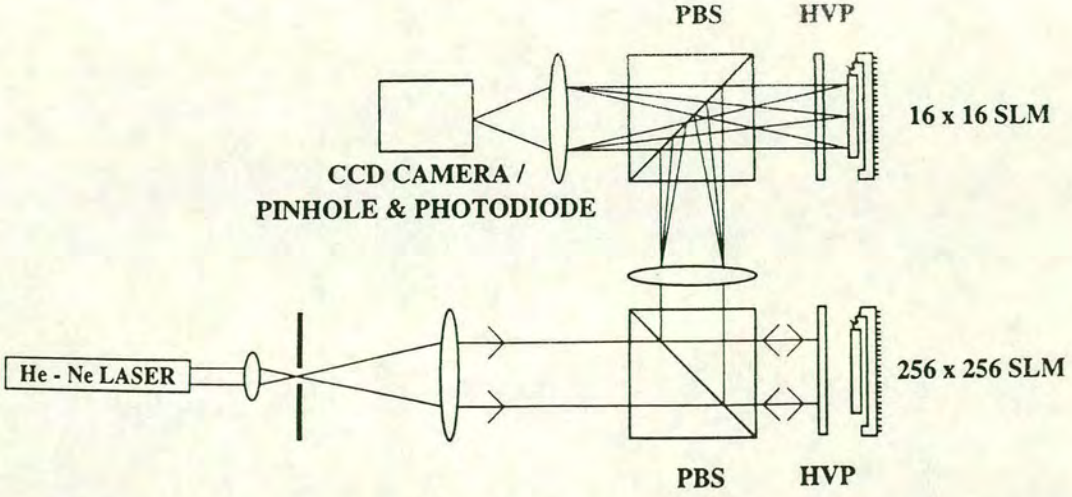

Figure 5: Experimental Testbed For Studying Dynamic Holographic Interconnects.

References

1. A.G. Kirk, W.A. Crossland, T.J. Hall. *A compact and scalable free space optical crossbar.* Proc. SPIE **1574** 137-141 (1991)

2. H.J. White, G.M. Proudly, et al. *Performance of a free space optical crossbar.* Presented at OC'94.

3. D.C. O'Brien, R.J. Mears, T.D. Wilkinson, W.A. Crossland. *Dynamic holographic interconnects that use ferroelectric liquid crystal spatial light modulators.* Applied Optics **33** 2795-2803 (1994)

4. Hirofumi Yamazaki, Masayasu Yamaguchi. *4x4 Free-space optical switching using real-time binary phase-only holograms generated by a liquid crystal display.* Optics Letters. **16** 1415-1417 (1991)

5. F.B. McCormick. *Generation of large spot arrays from a single laser beam by multiple imaging with binary phase gratings.* Optical Engineering **28** 299-304 (1989)

6. S.E. Broomfield, M.A.A. Neil, E.G.S. Paige, G.G. Yang. *Programmable binary phase-only optical device based on ferroelectric liquid crystal SLM.* Electronics Letters **28** 26-28 (1992)

7. J. Gourlay, S. Samus, P. McOwan, D.G. Vass, I. Underwood, M Worboys. *Real-time binary phase holograms on a reflective ferroelectric liquid crystal spatial light modulator.* Accepted for Applied Optics.

8. T.D. Wilkinson, D.C. O'Brien, R.J. Mears. *Dynamic asymmetric binary holograms using a ferroelectric liquid crystal spatial light modulator.* Optics Communications **109** 222-226 (1994)

Inst. Phys. Conf. Ser. No 139: Part II
Paper presented at Opt. Comput. Int. Conf., Edinburgh, 22–25 August 1994

Optical interconnect using pixellated spatial light modulators

J.Gourlay, S.Heddle, A.O'Hara, S.Samus and D.G.Vass
Applied Optics Group, Department of Physics and Astronomy,
The University of Edinburgh, The Kings Buildings, Mayfield Road, Edinburgh EH9 3JZ
tel: 031 650 5270, fax: 031 650 5220, email: jg90@castle.ed.ac.uk

Abstract

Two approaches to optical interconnect using pixellated, electronically addressed spatial light modulators as reconfigurable optical elements are presented: one analytical described using a low resolution device; the other using computer generated holograms and a state-of-the-art planarised silicon backplane device.

1 Introduction

Reconfigurable optical interconnection has been identified as a crucial function in optical computing. One of the more attractive techniques involves the use of an electronically addressed spatial light modulator (EASLM), in a Fourier transform optical system to give holographic routing. For example, the optical information to be routed can be input to a 4-f coherent optical processor, witl the EASLM placed at the Fourier plane and the information destination is at the output plane. By the correct selection of the pattern on the EASLM, the information can be routed to the required regions in the output plane. The patterns on the EASLM are generally gratings, Dammann gratings or computer generated holograms (CGH). A very attractive generic type of EASLM is the Ferroelectric Liquid Crystal over Very Large Scale Intergration (FLC/VLSI) SLM [1]. This device has an FLC cell fabricated on top of a custom designed VLSI silicon backplane. The backplane contains an array of pixel memory elements, pixel mirrors and addressing circuitry. The controllable pixels in the SLM can modulate the relative phase by **exactly** 0 or π due to the switchable uniaxial nature of the FLC structure, as well as perform amplitude modulation. In EASLMs there is a trend towards more pixel complexity and more intelligent modulator arrays, which is the primary advantage of the VLSI backplane based devices. Techniques such as data compression can increase the reconfiguration time, because the main information 'bottleneck' of the EASLM is the transfer of electronic information to the modulator array from 'off-chip' sources.

Generally, pixellation is inherent in spatial light modulators and this has major consequences for their use in Fourier transform optical systems. The pixel transmission function determines the 'sinc' envelope function in the Fourier plane. A 100% fill-factor in the pixel transmission function results in no replication at the Fourier plane, only the zeroth order. Any fill-factor lower than 100% conventionally results in higher order replications. Through planarisation techniques, the pixel fill-factor can be increased towards 100%, but seperation is always required between the pixel modulation elements to avoid inter-pixel cross talk.

2 Manipulation of Replications

The pixellation can be exploited to allow routing through the manipulation of the replicated orders. In a coherent optical processor a conventional pixellated Fourier plane filter will give rise to replication of the information at the output. This is due to the output being equal to the input rotated by 180^0 convolved with the Fourier transform of the filter. Previous work [2] has shown that the delta-function-like spikes in the power spectrum of the filter which give rise to the replication may be attenuated or removed by selection of a specific pixel pitch:size ratio and the introduction of a specific pixel position randomisation scheme which applies a displacement of the pixel centre from its regular position. This generalises the expression for the power spectrum of

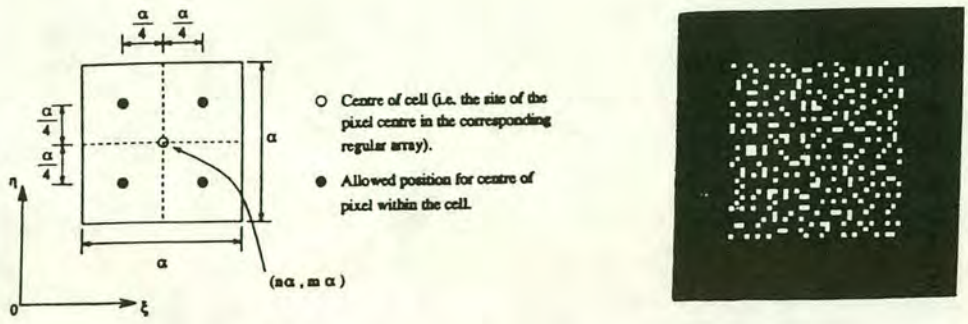

Figure 1: a) Possible pixel positions within $\alpha \times \alpha$ cell b) A resultant 16x16 array of pixels

the Fourier plane filter ($|t_2(x,y)|^2$) with all pixels 'on' to:

$$\langle |t_2(x,y)|^2 \rangle = |P(x,y)|^2 \times Q^2 \left[1 - |\rho(x)|^2 |\rho(y)|^2 + \frac{1}{Q^2} \frac{\sin^2(\pi Q \alpha x)}{\sin^2(\pi \alpha x)} \frac{\sin^2(\pi Q \alpha y)}{\sin^2(\pi \alpha y)} |\rho(x)|^2 |\rho(y)|^2 \right] \quad (1)$$

where $P(x,y)$ is the Fourier transform of the single pixel transmission function, $\rho(x)$ and $\rho(y)$ are the Fourier transforms of the pixel position probability distribution functions, α is the pitch of the underlying regular array, and the array consists of $Q \times Q$ pixels. The spectral orders are placed at $(n/\alpha, m/\alpha)$, $n, m = 0, \pm 1, \pm 2, \ldots$ With square pixels of side $\alpha/2$, $P(x,y) = \frac{\alpha^2}{4} sinc^2(\frac{\alpha}{2}x, \frac{\alpha}{2}y)$ which has zeroes at the positions of all the even numbered spectral orders other than the zero order. Further, choosing $\rho(x) = \cos(\frac{\pi\alpha}{2}x)$ and $\rho(y) = \cos(\frac{\pi\alpha}{2}y)$, we find that the allowed displacements of the pixel from the regular position are such that each pixel can take one of four allowed positions in an $\alpha \times \alpha$ square, (figure 1) and most importantly the odd numbered spectral orders in both x and y directions are eliminated by zeroes of $\rho(x)$ and $\rho(y)$. If however we retain periodicity in either the $x-$direction ($\rho(x) = 1$) and/or the $y-$direction ($\rho(y) = 1$), the first orders on the respective axes will remain. The power in the attenuated orders is redistributed into a diffuse background $\sim 1/Q^2$ times the zero-order intensity ($\sim 0.4/Q^2$ times the first order intensity).

The suggestion here is that a means exists whereby information can be routed via certain of the first order replicas, dependent on the distribution of the transmitting subpixel in each cell of the array- with the discretely randomised array described all first orders would be 'off'; by using arrays with periodicity with respect to the axes the first orders on the x-axis, or y-axis (or both, if the array is regular) would be 'on'. (Figure 2).

There are several points to note. First, the idea lends itself to low resolution SLMs: using the 16x16 silicon backplane SLM designed by Underwood [3], a 2×2 block of pixels could be used to code each of the α by α cells, giving an 8x8 array of cells with one pixel 'on' in each cell. This would then give a background illumination due to the 'off' state of the first order $\sim$ 26 times less than the 'on' state, a difference in states which should be simple to threshold. Further, the SLM would be capable of routing 8x8 pixel arrays when used in the Fourier plane of a 4-f optical processor, offering the benefits of parallelism and a modest degree of image fanout. These properties are scaleable for larger arrays [1], with the added benefit that the signal (intensity of the 'on' first order replicas) to noise (the diffuse background) is proportional to the inverse square of the array size Q. Also, all the 'on' first order replicas have the same intensity regardless of whether there are zero, two or four of them (to a good approximation): this would not be the case if the routing were achieved simply by writing stripe patterns on the SLM to approximate diffraction gratings, as the total number of transmitting pixels would vary depending on the desired number of replicas. Lastly, this process has been described in terms of amplitude modulating SLMs. Phase modulating SLMs are equally applicable and offer the prospect of eliminating the zero order.

3 Computer Generated Holograms

CGHs allow reconfigurable routing within the orders themselves. This is presented using a high performance silicon backplane device, which has been planarised to give a large phase-flat fill-factor. The backplane used is a 176 × 176 pixel DRAM backplane. The pixels have a 30μm pitch and the pixel mirror before planarisation is 14μm × 22μm i.e. $\approx$ 30% fill-factor. The device frame rate is 1kHz, limited by the interfacing electronics. When CGHs were displayed on the device before

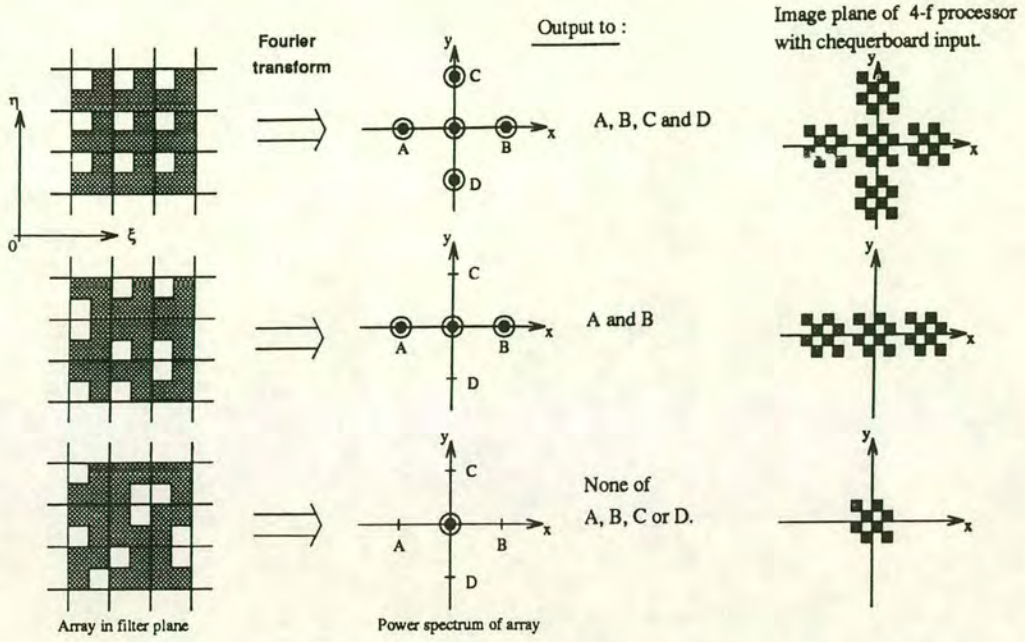

Figure 2: Selective removal of aliasing to provide selective fanout/routing

Figure 3: Diffraction from a simple grating (a) unplanarised EASLM, (b) planarised EASLM.

planarisation, poor results were obtained [4]. This was mainly due to the low pixel fill-factor, but also the poor FLC alignment caused by the low metal quality. The mirrors are fabricated using a standard VLSI aluminium metal layer, so the layer is deposited with electrical conductivity, rather than optical quality, as the main criterion. The mirrors are not optically flat and hence scatter light to give noise in the reconstruction. The rough surface profiles of the mirrors also prevent uniform high quality alignment of the FLC over the array. The low fill-factor resulted in very prominent replicated orders and a very high d.c. spot. Hence, the diffraction efficiency or the quantity of light measured where it was intended, was very low.

Planarisation techniques have been used to overcome the problems associated with the VLSI fabricated circuitry and mirrors by burying them beneath a polished dielectric film, depositing high quality metal mirrors on the surface and providing small interconnection vias through the dielectric layer between the original and new layers [5]. These techniques have been applied to the device described above and have increased the phase-flat fill-factor to 81% [6].

The resulting improvement to the performance of the device in a Fourier transform system was examined. A FLC cell was fabricated on top of a planarised device and a non-planarised device under identical conditions. A simple grating structure (with an 8 pixel pitch) was displayed on both devices and the resulting Fourier transforms are shown in figures 3(a) and 3(b). The planarised device has a very large d.c. term (central peak), very low diffraction peaks and very prominent replications (not shown). The planarised case shows considerable improvement, with the d.c. term much reduced and the diffracted peaks the most prominent.

The display of CGHs on the planarised FLC/VLSI EASLM can produce interconnection or fanout. The CGHs have been designed by simulated annealing to give arrays of spots from a plane

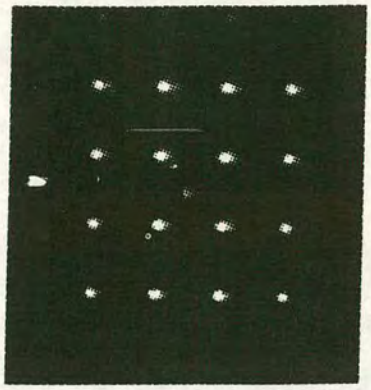

Figure 4: A 4 · 4 fanout pattern produced by a CGH on the EASLM.

wavefront [4]. In the 4-f coherent processor, the input information would be routed to the position of the spots in the output plane. By changing the CGH pattern on the EASLM, the position and number of the spots can be altered and hence route the input information as required by the system. A CGH pattern, designed through simulated annealing to produce a 4 · 4 fanout, was displayed on the EASLM. The resulting fanout obtained after Fourier transformation by a simple lens (f=140mm) is shown in figure 4. The d.c. spot is very low, and the diffraction efficiency (**light in the 16 peaks/total light in the Fourier plane**) is ≈ 65%. Replicated orders are still evident as the pixel function has < 100% fill-factor, but they are very low as the efficiency shows.

The VLSI/SLM is a very attractive device for this application, due to the potential level of addressing complexity available, which allows very high reconfiguration times. Future devices will have smaller pixel pitches (more compact systems), a higher space-bandwidth product (a higher number of pixels) and improved optical quality. There is also the potential for storage of sets of CGH patterns 'on-chip', i.e. designed into the backplane for a specific system requirement, which would increase considerably the reconfiguration time, as only 'local' data transfer need be performed.

4 Conclusions

Both of the techniques are complementary, allowing the manipulation of the replicated orders, and of information inside the orders. The pixellation of the EASLM has been shown to be a very important parameter in terms of both the performance and capabilities. Control of the pixellation is crucial in future devices for high performance in optical computing systems. These conclusions are being considered as the next generation of EASLM devices are being developed.

1 K.M.Johnston, D.J.McKnight and I.Underwood, IEEE Journal of Quantum Electronics, 29, pp699-713, (1993)

2 S.Heddle and R.M.Sillitto, J. Mod. Opt. vol. 40(2), pp299-313 (1993)

3 I.Underwood, D.G.Vass and R.M.Sillito, IEE Proceedings, 133, Pt J, pp77-82, (1986).

4 J.Gourlay, S.Samus, P.McOwan, D.G.Vass, I.Underwood and M.Worboys, Accepted for Appl. Opt

5 A.O'Hara, J.R.Hannah, I.Underwood, D.G.Vass and R.J.Holwill, Appl. Opt., 32, pp5549-5556, (1993)

6 I.Underwood, D.G.Vass, A.O'Hara, D.C.Burns, P.W.McOwan and J.Gourlay, Appl. Opt., 33, pp2768-2774 (1994)

Optics Communications 104 (1994) 266–270
North-Holland

OPTICS
COMMUNICATIONS

An iterative algorithm for connected structure computer generated holograms

S.S. Samus, P.W. McOwan and W.J. Hossack

Department of Physics, The University of Edinburgh, James Clerk Maxwell Building, King's Buildings, Mayfield Road, Edinburgh EH9 9JZ, UK

Received 23 August 1993

An iterative design method for electrically switchable liquid crystal fan-out elements using a constrained growing technique that ensures electrical conductivity is presented. Digital simulations are compared with initial optical results.

1. Introduction

The flexibility of computer generated holograms (CGH) to form arbitrary wavefronts is well established [1]. These synthetic holographic elements have the potential for use in high efficiency, compact, low weight optical systems. Applications exist in such areas as optical telecommunications switching, optical fan-out [2], optical circuit interconnect and optical neural networks [3].

In these applications the system architecture often requires fan-out diffractive elements that produce multiple beams from a single input optical source. There exist a number of proposed methods to make these optical beam routing elements. One area of application for binary phase elements that has received a great deal of attention in the past is the Dammann grating [4,5]. In its generic form these elements are iteratively calculated as one-dimensional phase functions which are then used to define a two-dimensional separable structure. This constraints means that only regular, symmetric, arrays of output spots may be produced. The basic iterative method may be extended to allow the calculation of arbitrary two-dimensional patterns with binary phase [6].

The use of such computer generated gratings may be considerably enhanced if they may be electrically switched. It is possible to make such a device by arranging that the phase modulation is introduced through changing the optical properties of a layer of liquid crystal by applying a spatially modulated electric field. This requires that the phase modulation pattern desired is electrically connected over the spatial extent of the structure.

Electrically switchable liquid crystal lenses using patterned electrodes have been reported [7,8]. The device comprises a liquid crystal cell sandwiched between two glass optical flats. The glass backplane is uniformly coated with a transparent electrode such as indium tin oxide (ITO). The front plate is patterned, again with ITO, with the required connected structure. On application of a potential between front and back plates the liquid crystal undergoes a spatially variant phase modulation corresponding to the patterned front electrode.

In the switchable lens devices various methods have been used to ensure electrical connectivity in the phase pattern required, from a simple bar connecting the rings in a Fresnel zone plate [7], to using the intrinsic connected structure of a binary Gabor zone plate [8]. Such switchable lenses have applications in imaging, scanner systems, detector protection elements and as optical interconnects.

This paper details a new approach to the fabrication of binary phase computer generated holograms where the electrical connectivity requirement is incorporated as a constraint into the iterative algorithm. Liquid crystal devices fabricated using these holographic electrode patterns have the potential for producing high speed switching and the cell struc-

ture allows simple electronic addressing to enable the device. Such pre defined fan-out, switchable, holograms may have applications in systems where a fixed, predefined, set of optical interconnections are required, such as in optical databases, neural networks, and telecommunications. The speed and easier fabrication may make them more attractive than fully reconfigurable CGH, written on spatial light modulators, for some applications.

2. Requirements and implementation of continuity algorithm

The holographic fan-out element consists of spatially varying phase distribution with a specified diffraction pattern, typically a two-dimensional distribution of spots. In this paper we also impose the constraint that the phase distribution is binary so allowing simple fabrication with a patterned liquid crystal cell.

The design approach is based in the two-dimensional iterative scheme proposed by Dames et al. [6]. This, when combined with the binary constraint, allows design of symmetric arbitrary output patterns, being more flexible than the separability condition required for the conventional Dammann grating.

The binary phase hologram is described by a two-dimensional array of N by N pixels constrained to take the values ± 1. The diffracted amplitude is given by

$$F(k,l)=\frac{1}{N^2}\sum_{m=1}^{N}\sum_{n=1}^{N} f(m,n)\exp\left(\mathrm{i}2\pi\frac{mk+nl}{N}\right),$$

where $f(m, n)$ is the transmittance of the pixel (m, n), and the overall phase factor has been ignored. The iterative procedure is performed by changing single pixels in the binary pattern. Dames et al. [6] have shown that it is not necessary to recalculate the full discrete Fourier transform for every change. Instead the change in the reconstructed image, $\Delta F(k, l)$, from changing the phase of a single pixel is given by

$$\Delta F(k,l)=\frac{f'(m,n)-f(m,n)}{N^2}\times\exp\left(-\mathrm{i}2\pi\frac{mk+nl}{N}\right),$$

where $f'(m, n)$ is the new transmittance of the pixel, which for the binary phase hologram takes on the values ± 1.

The minimisation is performed with respect to the cost function,

$$C=\sum_{\text{target points}}\|F(k,l)|-|T(k,l)\|,$$

where $T(k, l)$ is the amplitude of the target output points. To calculate this cost function it is only required to determine the effect of a pixel change at the target spot locations. The converged solution has been found to be independent of the functional form of the cost function, and the above simple cost function has been used for computational simplicity.

The connected structure minimisation is formed by choosing a pixel at random. Then the algorithm tests to see if the pixel could be switched on (set to $+1$) or off (set to -1) by using the following rules:

(i) Switching off the pixel must not break the continuity of the existing pattern. If there are pixels in the neighbourhood of the chosen pixel connected

a) b) c)

Fig. 1. Three examples of pixel transitions. (a) Central pixel is not allowed to be switched off. (b), (c) Allowed pixel transitions.

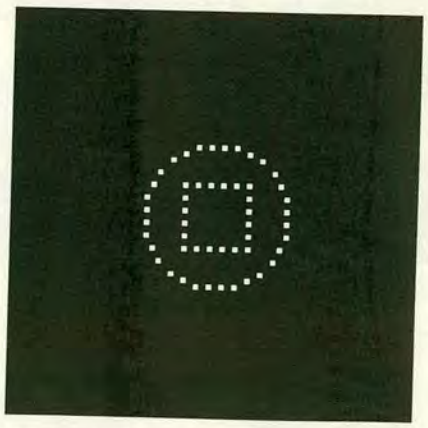

Fig. 2. Target pattern used for simulation.

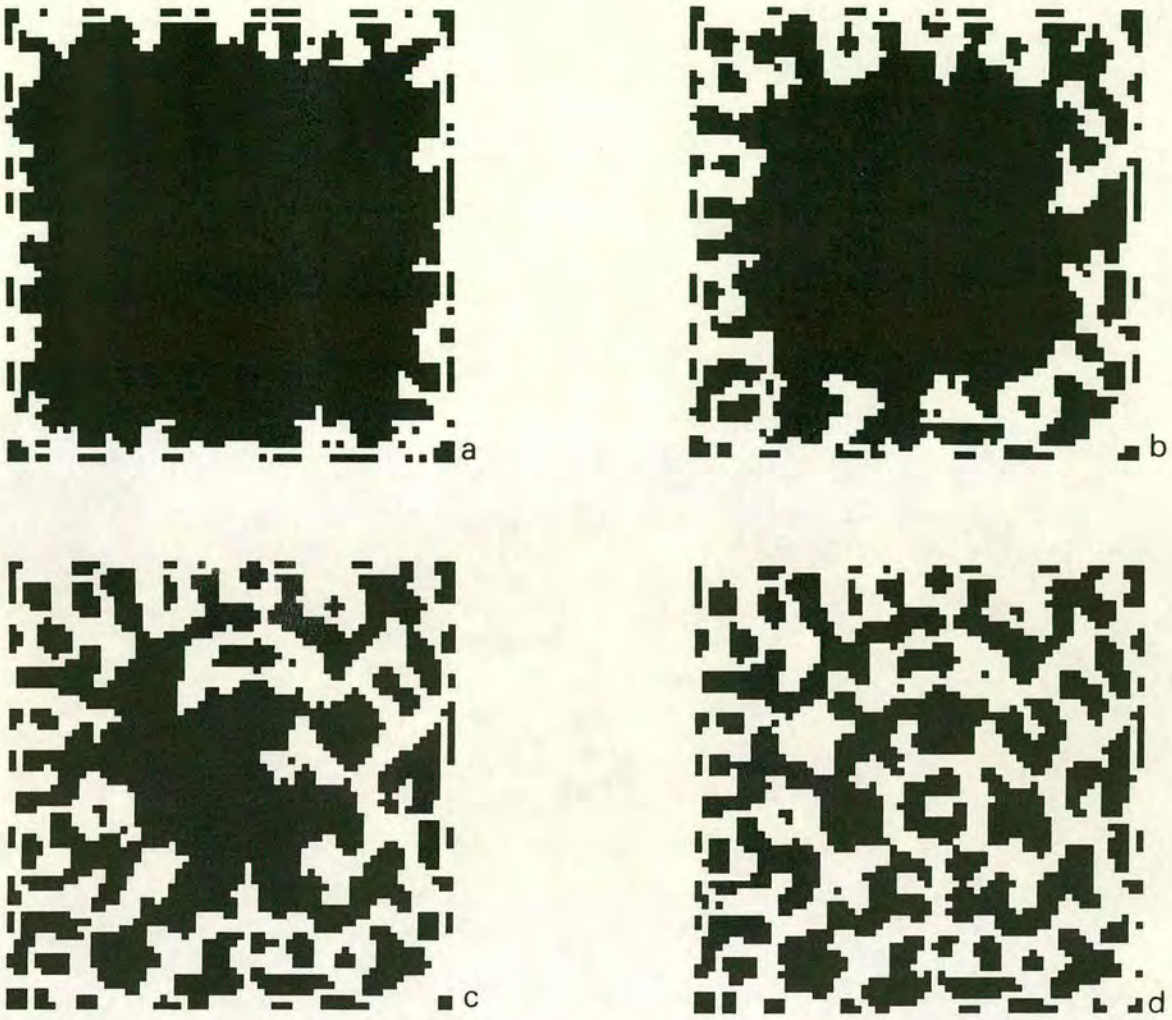

Fig. 3. (a)–(d) "Growing" of the connected pattern from the initial frame. The algorithm progresses (a) through (d).

through this pixel it could only be switched off if there exists an alternative connection in a small neighbourhood between them.

(ii) Switching on the pixel must not lead to appearance of the solitary pixels in the pattern.

(iii) All the solitary pixels are switched off (this constraints allows on-continuous starting patterns).

(iv) When a pixel suitable for flipping is found the cost function C is calculated. If flipping reduces C the change is accepted. If not, the pixel is flipped back.

The algorithm operates with four-pixel connectivity as shown in fig. 1 where examples of allowed and forbidden pixel switching is shown.

The initial starting pattern can in principle be arbitrary since rule (iii) will in general ensure convergence to a connected pattern. In practice, however, good results and rapid convergence have been obtained by starting with a connected pattern, with is then developed by the above iteration. A range of initial structures have been investigated including spirials and frames. All these initial pattern converge to similar solutions. The initial starting point chosen in this work is a frame of one pixel, with the pattern being developed into the centre of the array.

To reduce the computational task, the initial pattern is developed on a course 64 by 64 pixel grid with a search area of 3 by 3 pixels used for rule (i). For the symmetric target pattern shown in fig. 2, four stages of the iteration are shown in figs. 3a–d, show-

Fig. 4. The interpolated 128×128 pattern.

ing the "growing" of the connected pattern from the initial frame. This initial part of the algorithm forms the basic connected structure typically taking 1 minute on a Sparc 2 machine. The pattern is then expanded to 128 by 128 pixels by zero order interpolation, and is then iterated again at this higher resolution. This second stage again takes several minutes of computer time. The final pattern is shown in fig. 4, with an error criteria C of 3%. The digital reconstruction is shown in fig. 5a.

The exact convergence time depends on the number of targets spots in the output pattern. This technique has been found to converge to a good solution for up to 64 target spots in an 8 by 8 grid. For more complex patterns, more pixels are required to specify the phase pattern, with a considerable increase in computational cost.

3. Optical results for continuous diffractive structure

When used optically the structure must be spatially replicated to reduce speckle noise in the reconstruction [9]. Since the above pattern is fully connected starting with a frame, then tiling the pattern edge to edge will also produce a fully connected structure. Initial optical results have been produced by printing a 6 by 6 tiled version on a laser printer and photo-reducing the whole structure to 5 mm by 5 mm. This hologram is binary amplitude, so will have the same reconstruction pattern as the designed binary phase structure, but with the addition of an on-axis dc spot. The optical reconstruction is shown in fig. 5b showing the target distribution as required.

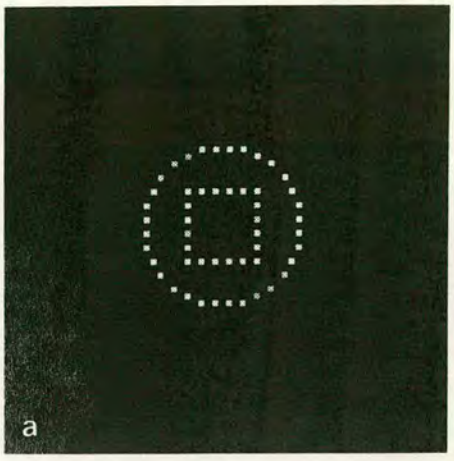

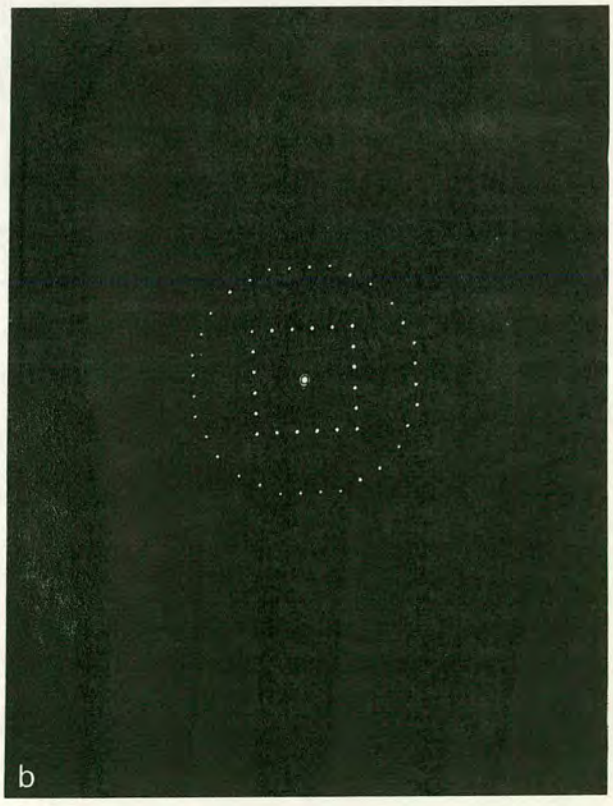

Fig. 5. (a) The digital reconstruction from the structure in fig. 4. (b) The optical reconstruction from a test amplitude connected structure.

4. Conclusion

An iterative constraint satisfaction algorithm has been developed to allow the calculation and fabrication of diffractive structure which is all electrically connected. Digital results showing the evolution of the structure have been presented. An optical reconstruction of the amplitude version of the hologram shows that the algorithm satisfies the constraints in the reconstruction and on the hologram. The structure so defined may be fabricated as a switchable transmission element using a patterned electrode device or form a connected reflecting metal backplane on a liquid crystal over silicon spatial light modulator [10].

References

[1] G. Tricoles, Appl. Optics 26 (1987) 4351.
[2] N. Streibl, J. Mod. Optics 36 (1989) 1554.
[3] A.J. Bostel, P.W. McOwan and T.J. Hall, Opt. Comp. Proc. 1 (1991) 293.
[4] J. Turunen, A. Vasara, J. Westrholm, G. Jin and A. Salin, J. Phys. D 21 (1988) S102.
[5] H. Dammann and E. Klotz, Optics Acta 24 (1977) 505.
[6] M. Dames, R. Dowling, P. McKee and D. Wood, Appl. Optics 30 (1991) 2685.
[7] M.C.K. Wiltshire, GEC Journal of Research 10 (1993) 119; 9 (1991) 121.
[8] P.W. McOwan, M. Gordon and W.J. Hossack, Optics Comm. 103 (1993) 189.
[9] F. Wyrowski, R. Hauck and O. Bryngdal, J. Opt. Soc. Am. A 4 (1978) 694.
[10] K.M. Johnson, D.J. McKnight and I. Underwood, IEEE J. Quantum Electron. 29 (1993) 699.

Real-time binary phase holograms on a reflective ferroelectric liquid-crystal spatial light modulator

J. Gourlay, S. Samus, P. McOwan, D. G. Vass, I. Underwood, and M. Worboys

A ferroelectric liquid-crystal spatial light modulator with an active silicon backplane is used to implement reconfigurable reflective phase holograms. Optical results are presented for an optimized computer-generated Fourier hologram.

Computer-generated holograms (CGH's) are useful components in two-dimensional optical information-processing systems.[1] Applications include array generators for optical interconnection, phase filters for correlation systems, beam shaping, adaptive optical components, and three-dimensional displays. Suitable holographic structures may be designed by a variety of optimization techniques and the computed patterns used with phase modulating spatial light modulators (SLM's) to implement reconfigurable optical elements. Phase modulation has been demonstrated previously with magneto-optic,[2] twisted-nematic liquid-crystal,[3] and transmissive matrix addressed ferroelectric liquid-crystal[4] (FLC) SLM's.

We describe adaptive CGH's displayed on FLC upon very-large-scale-integration (VLSI) silicon backplane SLM's.[5,6] The SLM device used in the experiments has a 176 × 176 pixel backplane designed through the UK Science and Engineering Research Council, Department of Trade and Industry Link, Optoelectronics Programme.[7] The device is electronically addressed and operates in a reflection mode: with the use of reflective SLM's to fold the optical paths, highly compact optical subsystems may be formed. The complementary metal-oxide semiconductor circuitry forms a two-dimensional array of dynamically and randomly addressed memory cells in which metal pads act as both mirrors and the electrodes of the FLC-filled storage capacitors. The aluminum mirrors have size 14 μm × 22 μm and are positioned on a 30-μm pitch, giving a pixel fill factor of ~25% and an overall active area of 5.2 mm × 5.2 mm. The pixels are addressed a row at a time by on-chip shift registers and interfaced to a microcomputer by a custom-designed high-speed frame store. With this interface, frames can be written to the SLM at an image update of 1 kHz, including the complementary voltage balancing frame to avoid electrochemical degradation of the FLC. A surface-stabilized FLC[8] cell, as shown in Fig. 1, was constructed and filled with Smectic C* FLC material (SCE13, Merck-BDH).[9] The thickness of the FLC material was tuned to operate as a switchable half-wave plate on reflection at a wavelength of 633 nm.

Binary phase modulation with the FLC SLM is illustrated in Fig. 2. The stable orientations of the optic axis of the FLC are represented in Fig. 2, indicating that the optic axis switches through an angle θ under the control of the applied voltage signals. The direction of the polarization vector of the incident light is aligned symmetrically between the two directions (separated by θ) of the FLC's switchable optic axis. In the general case, propagation of light through the two liquid-crystal states produces elliptically polarized light (dependent on θ, the cell depth, and the birefringence) from the incident linear polarization. The sense of the polarization depends on which side of the optical axis ($\pm\theta/2$) the polarization vector of incident light falls, i.e., either clockwise or anticlockwise. Light in these two elliptically polarized states then passes through an analyzer, orthogonal to the first polarizer, which reduces the elliptical polarization to a linear polarization exhibiting a relative 0 or π phase difference, independent of switching angle or path length. The director of the FLC material used in the device switches through an angle of θ = 45°; therefore only

J. Gourlay, S. Samus, P. McOwan, and D. G. Vass are with the Applied Optics Group, Department of Physics, University of Edinburgh, Edinburgh EH9 3JZ, UK. I. Underwood is with the Department of Electrical Engineering, University of Edinburgh Edinburgh EH9 3JL, UK. M. Worboys is with the GEC-Marconi Research Centre, Great Baddow, Chelmsford CM2 8HM, UK.

Received 2 December 1994; revised manuscript received 21 June 1994.

0003-6935/94/358251-04$06.00/0.

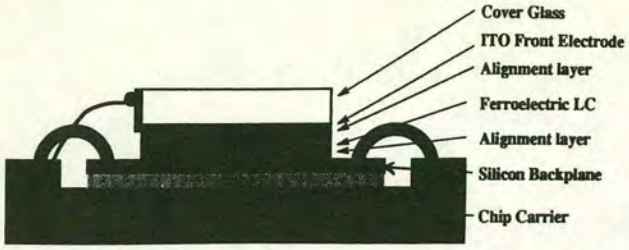

Fig. 1. FLC/VLSI SLM device structure: ITO, indium tin oxide; LC, liquid crystal.

50% of light is transmitted by the analyzer. For 100% transmittance a FLC material switching through an angle of $\theta = 90°$ is required: in this case no analyzer is required, as linearly polarized light is output (but for each state the polarization direction is 180° different, i.e., with 0 or π phase difference). Such suitable material has been developed by Chisso (Chisso 2004).[10]

The optical system used to demonstrate reconfigurable reflection phase holograms with the binary phase-modulation method is shown in Fig. 3. A collimated He–Ne beam is first transmitted through a polarizer to determine the input polarization orientation. A nonpolarizing beam splitter is used to reflect the beam from the SLM. The beam is modulated by the phase pattern written on the SLM. The beam passes through an analyzer. The modulated beam is then Fourier transformed by a lens to form an intensity distribution on a CCD array camera at the back focal plane of the lens. The camera was adjusted to give a linear response to light intensity. An initial assessment of the phase modulator was made by writing a one-dimensional high-frequency binary grating with a period of two SLM pixels. The

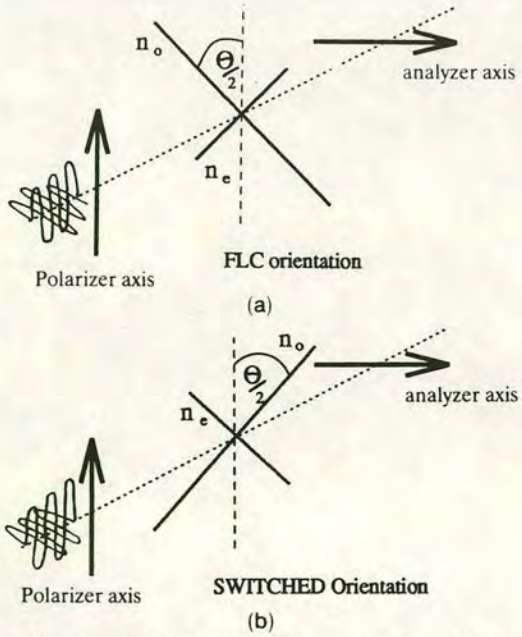

Fig. 2. Phase modulation with FLC modulators: (a) zero relative phase difference, (b) π relative phase difference.

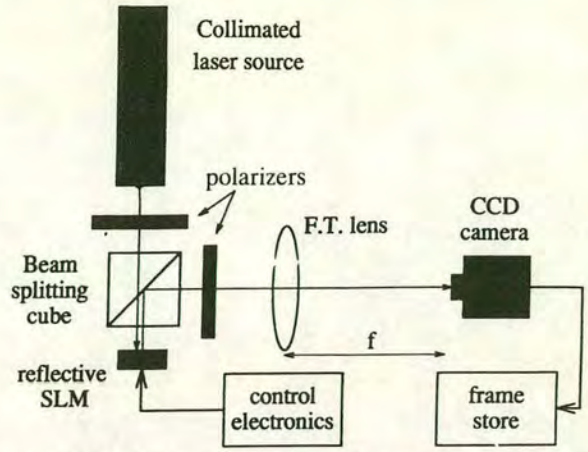

Fig. 3. SLM optical system implementation: F.T. lens, Fourier-transform lens.

resulting Fourier-plane diffraction pattern is shown in Fig. 4.

The reflected diffraction efficiency, the ratio of the total power of light in the two first orders over the total power in the zeroth-order peaks, (ignoring replications), was measured at more than half-maximum intensity at 4.5% ± 0.5% from the digitized CCD camera data. Simulation of the SLM as a binary phase modulator was performed assuming that only 25% of each pixel element could be switched between a relative phase of 0 and π. The other 75% was assumed to have simply a relative phase of 0, although this region has pixel circuitry in the real SLM device. Computer simulations show that the diffraction efficiency should be 11.0% ± 0.1% for a binary grating with 176 × 176 elements and a pixel fill factor of 25%.

CGH's were then designed to perform the function of an array generator to permit the SLM device to be used as an adaptive fan-out element. The phase hologram was designed with a simulated-annealing optimization technique.[11] The hologram pixels are flipped between the phase values 0 or π effectively to

Fig. 4. Resulting diffraction pattern from a fine grating.

reduce an error function specifying the difference between the desired target Fourier-plane reconstruction and the reconstruction achieved by the current state of the hologram. To ensure that the final hologram has the lowest error possible, one may accept changes that increase the error to permit the iteration to escape local minima. Accepting these error-increasing steps is governed by a statistical probability that reduces over time to permit the algorithm to converge to the global error minimum.

A CGH was designed to generate an 8 × 8 array of spots. The theoretical diffraction efficiency was calculated at 81% for this hologram with a 100% fill factor, which reduces to only 5.5% ± 0.1% when simulated with a 25% fill factor at the 176 × 176 elements. Figure 5 shows the holographic phase pattern that was calculated and then displayed on the SLM. The resulting optical transform (i.e., the square of the Fourier transform) obtained at the CCD camera is shown in Fig. 6. The central dc term is very large, as in the case of the grating experiment and in the simulation with a 25% fill factor. The efficiency was measured at 2.5% ± 0.5%, and the peaks were found to vary in intensity by as much as 30%.

The optical results from the grating and the CGH experiments show that the evaluated experimental diffraction efficiency is lower by a factor of ~2 than that expected from the simulations with a 25% fill factor. Also, the large spread of diffracted light around the on-axis dc spot may restrict the use of this SLM device for reflective phase holograms. The origins of these are considered. To display the detail in the regions of low light intensity, we operated the CCD camera at high gain, causing blooming of the high-intensity spot. The light in the dc spot is very high because of the low pixel fill factor, inherent in backplanes fabricated by commercial silicon processing with the microcircuitry located around the mirrors. The mirrors are fabricated, at present, with a standard VLSI aluminum metal layer. This layer is deposited with electrical conductivity rather than optical flatness as the main criterion. The mirrors are not optically flat[12] and hence scatter light to give noise in the reconstruction. The rough-surface profiles of the mirrors also prevent uniform high-quality alignment of the FLC over the array. The FLC misalignments over the active area mean that the amplitude of the light transmitted through the system varies slowly over the SLM. This additional, unwanted, low-frequency amplitude modulation will add to the noise around the dc spot and contribute to the broadening of the peak.

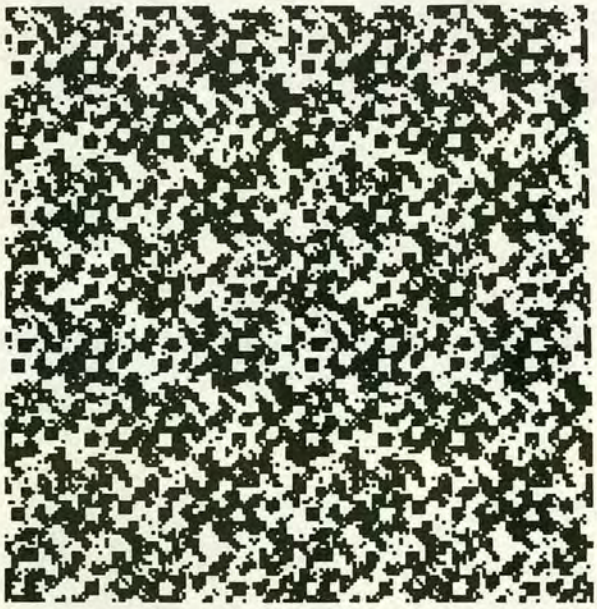

Fig. 5. CGH hologram for display on the SLM device.

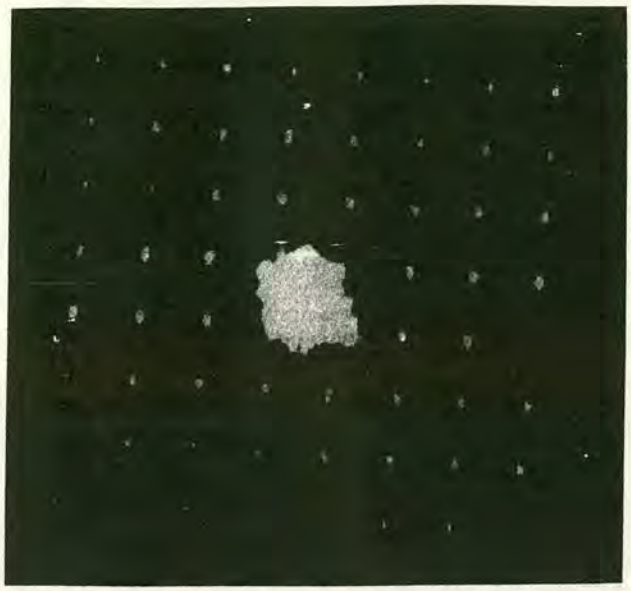

Fig. 6. 8 × 8 array formed from the hologram displayed on the SLM.

In summary, the low values of diffraction efficiency are caused mainly by the low fill factor of the device, but the FLC defect structures, poor mirror reflectivity, and any optical nonuniformity also contribute. We may use planarization techniques to overcome the problems associated with the VLSI fabricated circuitry and mirrors by burying them beneath a polished dielectric film, depositing high-quality metal mirrors on the surface, and providing small interconnection vias through the dielectric layer between the original and the new metal layers.[12] This processing is expected to increase the reflection efficiency of the devices by a factor of ~2 and increase the fill factor to nearly 100%.

The 176 × 176 SLM device has a small space–bandwidth product, the number of pixels forming the hologram, compared with that of a fixed CGH. Techniques may be employed to improve the space–bandwidth product, such as replicating a hologram pattern from an electronically addressed SLM onto an optically addressed SLM device.[13] Another system consideration is that the pixel size should be as small as possible to give the maximum number of line

pairs per millimeter. This determines the separation of the diffractive orders and maximizes the angle of diffraction that may be achieved. The SLM technology employed here will gain from all the improvements in complementary metal-oxide semiconductor silicon processing as smaller circuit geometries become practical; indeed, larger array FLC/VLSI SLM devices are already being designed.[7]

References

1. G. Tricoles, "Computer generated holograms: an historical review," Appl. Opt. **26,** 4351–4360 (1987).
2. J. N. Mait and G. S. Himes, "Computer-generated holograms by means of a magneto-optic spatial light modulator," Appl. Opt. **28,** 4879–4852 (1989).
3. T. H. Barnes, T. Eiju, K. Matsuda, and N. Ooyama, "Phase-only modulation using twisted-nematic liquid-crystal television," Appl. Opt. **28,** 4845–4886 (1989).
4. S. E. Broomfield, M. A. A. Neil, E. G. S. Paige, and G. G. Yang, "Programmable binary phase-only optical device based on ferrolectric liquid-crystal spatial light modulators," Electron. Lett. **28,** 26–27 (1992).
5. I. Underwood, D. G. Vass, and R. M. Sillitto, "Evaluation of an nMO VLSI array for an adaptive liquid-crystal spatial light modulator," Proc. Inst. Electr. Eng. Part J, **133,** 77–82 (1986).
6. K. M. Johnson, D. J. McKnight, and I. Underwood, "Smart spatial light modulators using liquid crystal on silicon," IEEE J. Quantum Electron. **29,** 699–714 (1993).
7. N. Collings, W. A. Crossland, P. J. Ayliff, D. G. Vass, and I. Underwood, "Evolutionary development of advanced liquid-crystal light modulators," Appl. Opt. **28,** 4740–4747 (1989).
8. N. A. Clark and S. T. Lagerwall, "Submicrosecond bistable electro-optic switching in liquid crystals," Appl. Phys. Lett. **36,** 899–901 (1980).
9. J. Gourlay, P. McOwan, D. G. Vass, I. Underwood, and M. Worboys, "Optical engineering aspects of ferroelectric liquid crystal-over-silicon spatial light modulators," in *Proceedings of the Conference on Applied Optics and Opto-Electronics* (The Institute of Physics, Bristol, UK, 1992), pp. 211–213.
10. T. Hatano, K. Yamamoto, H. Takezoe, and A. Fukuda, "Alignment controls and switching characteristics in a ferroelectric liquid crystal," Jpn. J. Appl. Phys. **25,** 1762–1767 (1986).
11. R. Hoptroff, P. McOwan, T. J. Hall, W. Hossack, and R. E. Burge, "Computer-generated optical fan-out element," Opt. Commun. **68,** 97–102 (1989).
12. A. O'Hara, J. R. Hannah, I. Underwood, D. G. Vass, and R. J. Holwill, "Mirror quality and efficiency improvements of reflective spatial light modulators by use of dielectric coatings and chemical-mechanical polishing," Appl. Opt. **32,** 5549–5556 (1993).
13. D. C. O'Brien, W. A. Crossland, and R. J. Mears, "A holographic routed optical crossbar: theory and simulation," Opt. Computer Process. **1,** 233–243 (1991).

Visual Aspects of Phase Holograms Design: A Software Package for Developing of 2-Dimensional Holographic Structures.

Sergei S. Samus
Department of Physics
The University of Edinburgh
King's Buildings
Edinburgh EH9 9JZ, UK.

ABSTRACT

The software package created for the computer generated holograms design is presented. The visual methods of design of binary and multi-phase levels holograms are introduced.

SUMMARY

Computer-generated holograms are important components in two-dimensional optical information-processing systems. Two-dimensional holograms may be used with phase modulating spatial light modulators (SLM's) to implement reconfigurable optical elements [5]. With the introduction of such dynamic holographic structures their importance increased dramatically. These types of holograms are essential for the development of optical switching [5], optical logic and optical neural net systems, since they facilitate the fixed and dynamic beam routing [6]. The number of holograms needed for some of such optical systems can be hundreds or even thousands. In this situation the appropriate tools to design, store and optimise this amount of holographic patterns are needed. We present an advanced software package which serves this purpose.

The phase holograms design program, Holomaster 1 allows interactive design of both binary and multi-level phase holograms. It incorporates most of the known important design techniques used in the calculation of phase only holographic diffractive elements. The main windows of the package are shown on Fig. 1. It can design 5 basic types of 2-dimensional pixelated holograms each of those can produce uniform output or output with weighted intensities.

1. Binary holograms. Introduced by Dames et al [1] in 1991. This basic technique is based on simulated annealing scheme. (See Fig. 2)
2. Four-phase holograms [1]. Calculated using the same principles as binary holograms. (See Fig. 3)
3. Continuous holograms [2]. The electrically switchable holograms designed with a constrained growing technique that ensures electrical conductivity (See Fig. 4)
4. Pseudo four-phase (sandwich) holograms [3]. These are asymmetric binary phase holograms. The symmetry is broken by using a sandwich structure of a random binary fixed hologram overlaying a binary hologram which is calculated in respect of its overlay.
5. Continuous pseudo four-phase holograms [2, 3] incorporate features of continuous and sandwich structures.

The software introduces a new visual approach into the design of holograms. The process of simulated annealing can be observed and controlled dynamically as the designing process is running. The holographic structures can be manually edited with built-in editor program. This feature is especially important for continuous holograms as the continuity constraint can stimulate non-developed patches on the hologram of the large fan-out. In this case the manual bridging technique is very efficient. It is

also essential to be able to check the continuity of the connected hologram. For this purpose the special floodfill feature is implemented which ensures that the replicated version of the hologram is continuous. At the final stage of the design the edge only development technique can effectively reduce the computational time. This feature is also available in the program. It is also easy to design required target patterns with a drawing program and preview the actual symmetrical output of the future hologram. The real strength of Holomaster is that all the design techniques and parameters and even holograms and targets can be changed dynamically during the design process.

Conclusion.

Some modern optical systems require a large number of precalculated holographic structures. We presented a powerful software package for visual design of such structures. The main features of the program are summarised below:

1. Helps the user visualise the whole mask design process
2. Effectively reduces the time of development of multiple holograms.
3. Allows to dynamically change the simulated annealing parameters, masks, targets, overlays
4. Makes much easier file input and storage processes
5. With built-in drawing program allows user to change the masks (especially important with continuous holograms design) and the targets
6. Makes possible the design of the holograms by a non-specialist
7. With the help of Holomaster the user can combine different design techniques and create holograms of better quality.

References.

1. H.Dammann and E.Klotz, Optics Acta 24 (1977) 505.
2. S.Samus, P.McOwan and W.Hossack, Optics Comm. 104 (1994) 266-270.
3. T.Wilkinson, D.O'Brien and R.Mears, Optics Comm. 109 (1994) 222-226.
4. J.Gourlay, S.Samus, P.McOwan, D.G.Vass, I.Underwood, and M.Worboys, Appl.Optics 33 (1994) 8251.
5. D.O'Brien, R.Mears, T.Wilkinson, and W.Crossland, Appl. Optics 33 (1994) 2795.

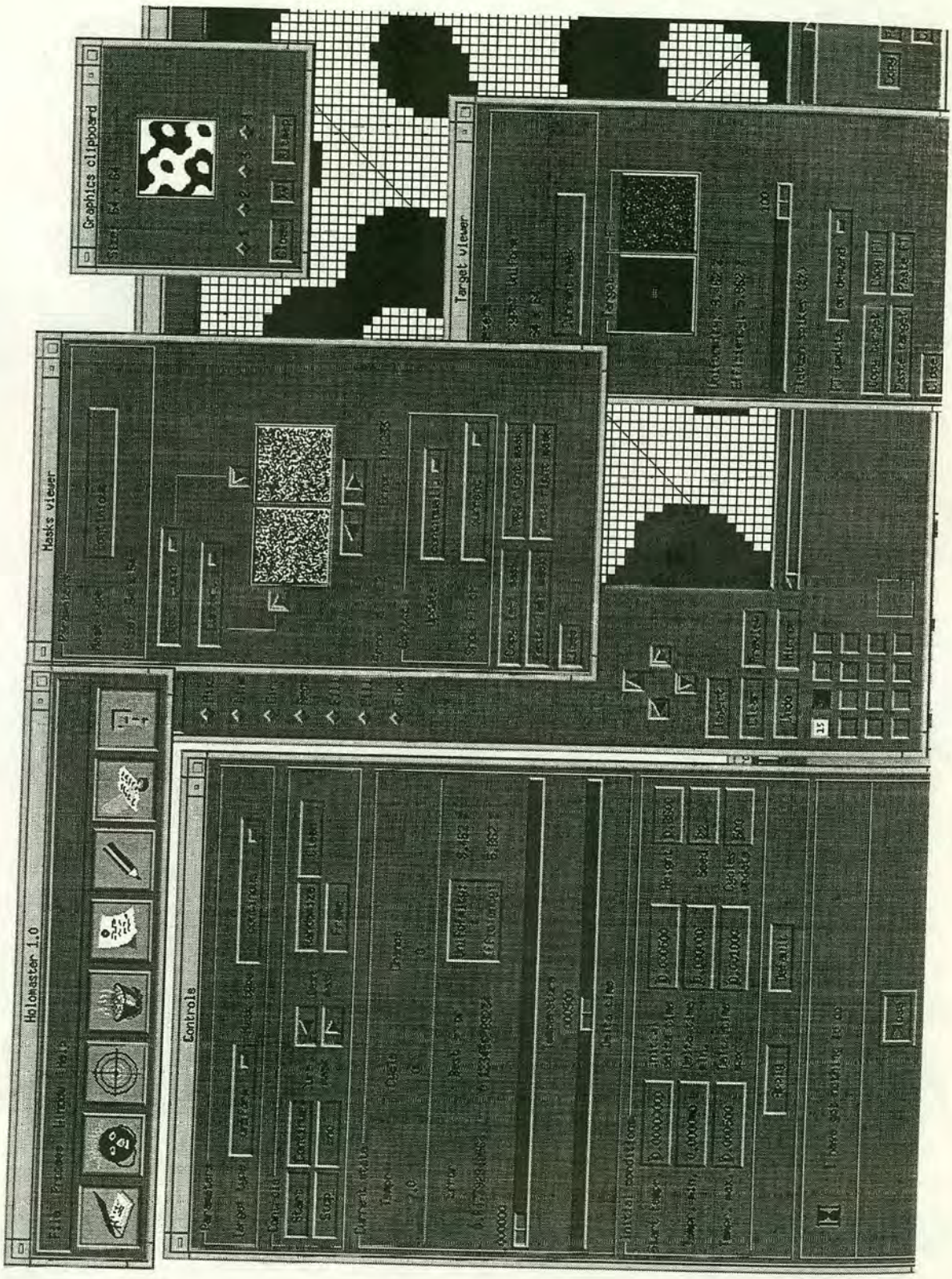

Figure 1: The layout of Holomaster 1

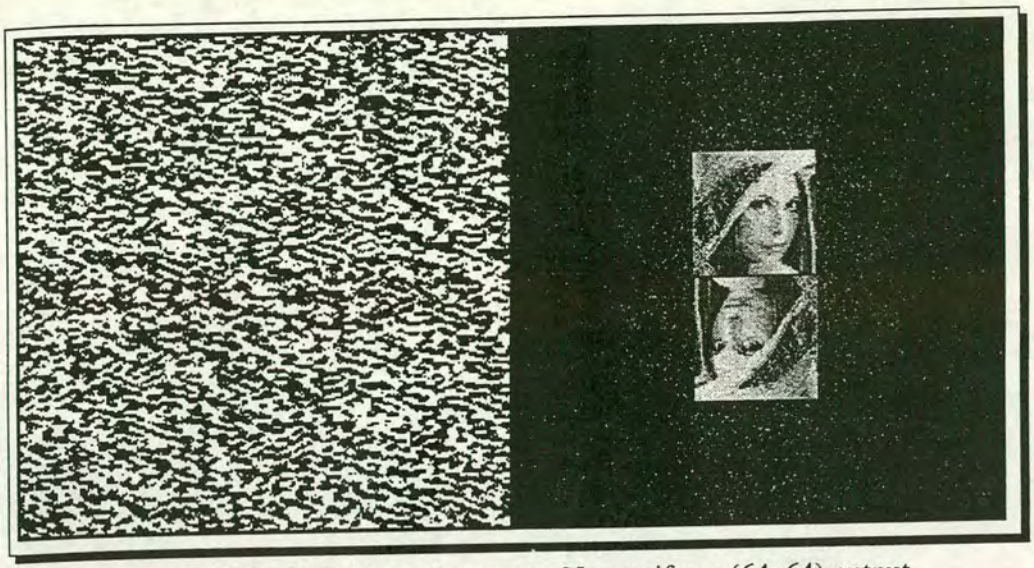

Figure 2: A basic (256x256) binary hologram. Non-uniform (64x64) output.

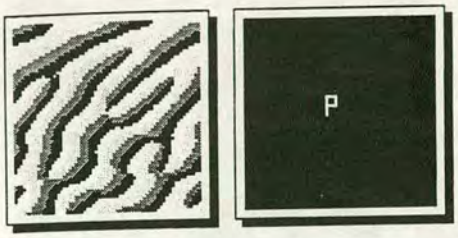

Figure 3: A 4-phase hologram of a letter P. Note non-simmetrical output.

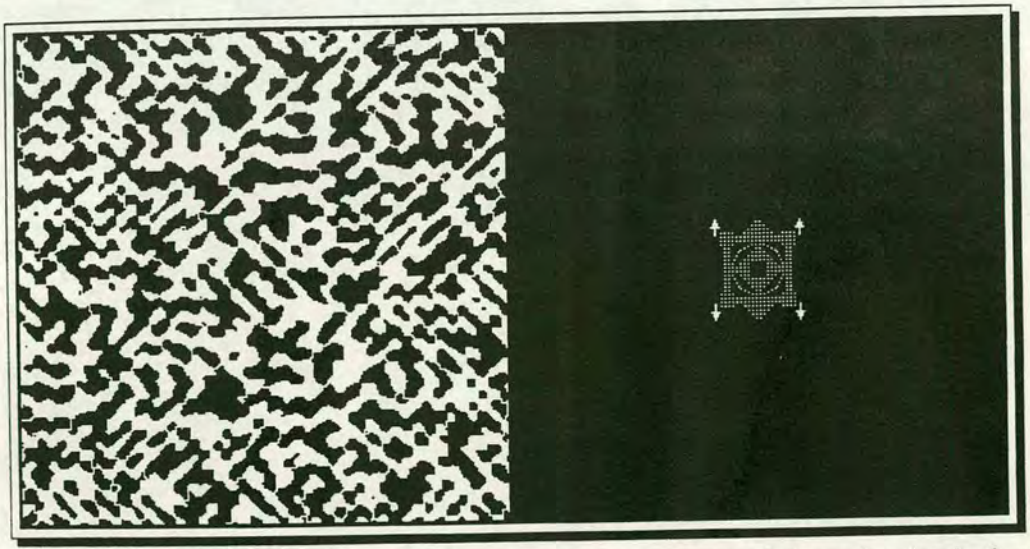

Figure 4: A continuous hologram. All white areas are connected. It can be checked with any drawing program which has floodfill feature. (Consider a one-pixel wide white frame around the mask).